

GEOSCIENCE WISCONSIN

*Associate Editors: Kenneth R. Bradbury
Phillip E. Brown
Charles W. Byers
Lee Clayton
Mark T. Harris*

CONODONTS AND THE CAMBRIAN–ORDOVICIAN BOUNDARY IN WISCONSIN

Brian P. Parsons and David L. Clark

PALEOECOLOGY AND SEDIMENTOLOGY OF THE *PRASOPROA* ZONULE IN THE DUNLEITH FORMATION (ORDOVICIAN), UPPER MISSISSIPPI VALLEY

H.C. Sanders, D.H. Geary, and C.W. Byers

SEDIMENTOLOGY AND SEQUENCE STRATIGRAPHY OF A LOWER ORDOVICIAN MIXED SILICICLASTIC–CARBONATE SYSTEM, SHAKOPEE FORMATION, FOX RIVER VALLEY OF EAST-CENTRAL WISCONSIN

Christopher L. Johnson and J.A. (Toni) Simo

TRACE-ELEMENT SIGNATURES AND TECTONIC AFFINITIES OF PROTEROZOIC A-TYPE GRANITES AND RHYLOLITES IN CENTRAL WISCONSIN

Jennifer M. Wenner and Mindy A. Lloyd

COUPLED MODELING OF GRAVITY AND AEROMAGNETIC DATA TO ESTIMATE SUBSURFACE BASEMENT TOPOGRAPHY IN SOUTHEASTERN WISCONSIN

John D. Skalbeck, James N. Couch, Ryan S. Helgesen, and Daniel S. Swosinski



Published by and available from

Wisconsin Geological and Natural History Survey

3817 Mineral Point Road • Madison, Wisconsin 53705-5100

☎ 608/263.7389 FAX 608/262.8086 www.uwex.edu/wgnhs/

James M. Robertson, *Director and State Geologist*

ISSN: 0164-2049

This report is an interpretation of the data available at the time of preparation. Every reasonable effort has been made to ensure that this interpretation conforms to sound scientific principles; however, the report should not be used to guide site-specific decisions without verification. Proper use of this publication is the sole responsibility of the user.

The use of company names in this document does not imply endorsement by the Wisconsin Geological and Natural History Survey.

Issued in furtherance of Cooperative Extension work, Acts of May 8 and June 30, 1914, in cooperation with the U.S. Department of Agriculture, University of Wisconsin–Extension, Cooperative Extension. University of Wisconsin–Extension provides equal opportunities in employment and programming, including Title IX and ADA requirements. If you need this information in an alternative format, contact the Office of Equal Opportunity and Diversity Programs or the Wisconsin Geological and Natural History Survey (☎ 608/262.1705).

Mission of the Wisconsin Geological and Natural History Survey

The Survey conducts earth-science surveys, field studies, and research. We provide objective scientific information about the geology, mineral resources, water resources, soil, and biology of Wisconsin. We collect, interpret, disseminate, and archive natural resource information. We communicate the results of our activities through publications, technical talks, and responses to inquiries from the public. These activities support informed decision-making by government, industry, business, and individual citizens of Wisconsin.

CONODONTS AND THE CAMBRIAN–ORDOVICIAN BOUNDARY IN WISCONSIN 1

Brian P. Parsons and David L. Clark

PALEOECOLOGY AND SEDIMENTOLOGY OF THE *PRASOPROA* ZONULE IN THE DUNLEITH FORMATION (ORDOVICIAN), UPPER MISSISSIPPI VALLEY 11

H.C. Sanders, D.H. Geary, and C.W. Byers

SEDIMENTOLOGY AND SEQUENCE STRATIGRAPHY OF A LOWER ORDOVICIAN MIXED SILICICLASTIC–CARBONATE SYSTEM, SHAKOPEE FORMATION, FOX RIVER VALLEY OF EAST-CENTRAL WISCONSIN 21

Christopher L. Johnson and J.A. (Toni) Simo

TRACE-ELEMENT SIGNATURES AND TECTONIC AFFINITIES OF PROTEROZOIC A-TYPE GRANITES AND RHYLOLITES IN CENTRAL WISCONSIN 35

Jennifer M. Wenner and Mindy A. Lloyd

COUPLED MODELING OF GRAVITY AND AEROMAGNETIC DATA TO ESTIMATE SUBSURFACE BASEMENT TOPOGRAPHY IN SOUTHEASTERN WISCONSIN 53

John D. Skalbeck, James N. Couch, Ryan S. Helgesen, and Daniel S. Swosinski

CONODONTS AND THE CAMBRIAN–ORDOVICIAN BOUNDARY IN WISCONSIN

Brian P. Parsons¹ and David L. Clark¹

ABSTRACT

For more than 100 years, the Cambrian–Ordovician boundary in the Upper Mississippi Valley, the original type area of the North American Upper Cambrian, has been considered to approximate the contact of the Jordan Formation (Cambrian sandstone) and the Oneota Formation (Ordovician dolomite). Earliest judgments on this sandstone–dolomite systemic contact were based on trilobites, but our recent work with conodonts constrains these earlier determinations. Conodonts that are known to range through several Ibexian (=Early Ordovician) conodont zones are found on either side of the Jordan Formation–Oneota Formation lithologic contact in southern Wisconsin and suggest that no matter which of the four candidates for the international Cambrian–Ordovician boundary (the base of the Cordylodus proavus Zone, the base of the Cordylodus intermedius Zone, the base of the Cordylodus lindstromi Zone, and the base of the Iapetognathus Zone) ultimately is selected, the Cambrian–Ordovician boundary in the Upper Mississippi Valley will lie in the Jordan Formation and its equivalents and not at the younger sandstone–dolomite contact. In addition, the identification of conodont species of similar age that range through several zones in sandstones and dolomites suggests that what has been described as an unconformity at the traditional boundary may be relatively minor, at least in Wisconsin. In other areas, there may be unconformities of greater magnitude or additional unconformities at other horizons in the Jordan.

INTRODUCTION

The contact between the Jordan sandstone and the overlying Oneota dolomite in parts of the Upper Mississippi Valley traditionally has been considered to be a close approximation of the Cambrian–Ordovician boundary. The significance of this assignment relates to the fact that this traditional sandstone–dolomite contact originally served as the reference section for the systemic boundary in North America. However, data concerning the precise nature of the actual systemic boundary are not firm, and the purpose of this study was to use conodonts to more closely define this boundary in southern Wisconsin as well as to comment on the magnitude of the Jordan–Oneota stratigraphic unconformity.

Studies of the formations involved in the systemic boundary definition date back into the nineteenth century, when Winchell (1874) described the Jordan Formation in south-central Wisconsin and in the Minnesota and Mississippi River Valleys. Later, McGee (1891) defined the overlying Oneota Formation as the lower unit of the Prairie du Chien Group in the same general areas where the Jordan was studied. Later

work by Ulrich (1924), Twenhofel and others (1935), Ostrom (1967), Miller and Melby (1971), Odom and Ostrom (1978), Runkel (1994), and Byers and Dott (1995) elaborated on the early definitions and added additional details concerning the two formations. Most recently, Hughes and Hesselbo (1997) have contributed new information regarding the lithologic details of part of this Saukian interval and its importance in understanding the North American type Upper Cambrian.

Ulrich (1924) noted that the Jordan–Oneota contact was unconformable, and much later, Ostrom (1964, 1970) agreed and stressed the relatively minor nature of the unconformity. In spite of the general agreement on the nature of the unconformable contact, recognition of the exact stratigraphic position of the contact between the formations as well as the systemic boundary remained controversial. For example, because the contact at many localities involves sandy dolomite that could not be clearly defined as either Jordan or Oneota, Odom and Ostrom (1978) informally proposed that the transition beds of sandstone and dolomite be called the Coon Valley Member. They assigned the

¹Department of Geology and Geophysics, University of Wisconsin–Madison, Madison, Wisconsin 53706

new member to the Jordan Formation and assumed that this would permit a more consistent stratigraphic definition of the contact. Smith and others (1993) argued with this interpretation and showed that sandy dolomite and sandstone intervals such as that designated as the Coon Valley also are found in younger parts of the Oneota. According to Smith and others (1993), the Coon Valley designation did not solve the problem of providing a uniform stratigraphic horizon for the lithostratigraphic boundary because of the repetitive nature of the Coon Valley lithology in younger horizons of the Oneota. Also, the base of the Coon Valley lithology is an unconformable surface; its top is gradational, with sandstone diminishing in abundance upward. Because of this, Smith and others (1993) reassigned the Coon Valley interval to the lower part of the Oneota. Later, Runkel (1994) reached a similar conclusion. This definition places the unconformity at the base of the redefined Oneota. The Oneota consists of the first major dolomite to appear above the Upper Cambrian sandstone, at least in southern Wisconsin. Because the sandstone and dolomite at the Jordan–Oneota contact have been interpreted to be both gradational and unconformable, the location of the traditional Cambrian–Ordovician boundary becomes a question and results in a more ambiguous definition of the Cambrian–Ordovician boundary in the Upper Mississippi Valley. Was the actual Cambrian–Ordovician boundary within the Jordan sandstone, the Coon Valley mixed lithology, or the Oneota dolomite?

Byers and Dott (1995) addressed the lithostratigraphy of the Jordan Formation, as had Runkel earlier (1994), but they suggested that it is composed of two “coarsening upward” progradational cycles incised by an unconformity at the base of the dolomite of the Oneota. They noted that at some localities an entire Jordan sandstone cycle may be missing because of the unconformity. These observations suggested that the Jordan–Oneota unconformity is more significant than was recognized earlier, but renewed the question of the actual location of the Cambrian–Ordovician boundary within this sequence.

For this study, we relied on the earlier work of Byers and Dott (1995), who studied the Jordan–Oneota relationship in southern Wisconsin. The unconformable contact between these formations is evident at most of the localities we studied and consists of a prominent erosion surface at the top of the Jordan (for example, Byers and Dott, 1995; Miller and Runkel, 1998). The unconformity is evident because the white cross-stratified sandstone of the Van Oser Member is irregularly

cut and filled with the gray, oolitic, intraclastic dolomite of the Oneota (for example, fig. 15 of Byers and Dott, 1995). Although very slightly dolomitic sandstones are known lower in the Jordan, no major dolomites have been observed lower in any of the sections we studied and we agree with the clear definition of this contact as defined by Byers and Dott (1995).

CAMBRIAN–ORDOVICIAN BOUNDARY AND CONODONTS

Byers and Dott (1995) reported that evidence for the Late Cambrian age of the Jordan Formation is based on trilobites identified as *Tellerina strigosa* Ulrich and Ressor, a species found in the *Saukia* Zone underlying the uppermost Cambrian *Eureka apopsis* Zone and restricted to the Late Cambrian. Because specimens of *Tellerina* were not collected from sections showing the complete Jordan–Oneota sequence, the spatial relationship of the several specimens to the base of the Oneota was not determined. However, it is estimated that the specimens, collected in the Madison area, were from a level between 2 and 5 m below the unconformity at the base of the Oneota (R.H. Dott, University of Wisconsin–Madison, verbal communication, 1996). In the flat-lying Cambrian–Ordovician strata in southern Wisconsin, this estimate probably is realistic. The top of the *Saukia* Zone is correlated with the base of the *Cordylodus proavus* conodont zone (fig. 1). Because trilobites from the lower part of the Oneota Formation are identified with the *Symphysurina* Zone of the Early Ordovician (Heller, 1956), the trilobite evidence suggests that the traditional Cambrian–Ordovician boundary approximates the lithologic boundary. However, the absence of trilobites or conodonts in the interval between the highest interval containing *Tellerina* and the Ordovician conodonts in the upper Jordan has not permitted a more precise stratigraphic designation.

Because conodonts have been found in the uppermost beds of the Jordan as well as the basal-most beds of the Oneota (Miller and Melby, 1971; Smith and Clark, 1996), we studied exposures of the Jordan–Oneota contact at eight localities in Wisconsin and Minnesota (fig. 2). At the localities, we observed more or less the same physical relationship as that at our key Miller’s Curve section (figs. 2 and 3), and we believe that the Jordan–Oneota contact was correctly identified. This conclusion is based on examination of all exposures adjacent to the specific localities. We also considered elevations in the relatively flat-lying lower Paleozoic rocks, and, in addition, relied on guidance from those who have worked on the

SERIES	TRILOBITE ZONATION		CONODONT ZONATION	
	STITT (1977)		MILLER (1988)	
	ZONE	SUBZONE	ZONE	SUBZONE
IBEXIAN (part)	Symphysurina	S. woosteri	Rossodus manitouensis	
		Symphysurina bulbosa	Cordylodus angulatus	
			Iapetognathus	
		Symphysurina brevispicata	Cordylodus lindstromi	
	Cordylodus intermedius		Clavohamulus hintzei	Hirsutodontus simplex
		Cordylodus proavus	Clavohamulus elongatus	
	Fryxellodontus inornatus			
	Hirsutodontus hirsutus			
	Missisquoia	Missisquoia typicalis	Cordylodus proavus	Hirsutodontus hirsutus
		Missisquoia depressa		
Eurekia apopsis	Eoconodontus	Cambrooistodus minutus		
Saukiella serotina		Eoconodontus notchpeakensis		
Saukiella junia				
Rasettia magna		Proconodontus muelleri		
CROIXIAN (part)	Saratogia	(UNNAMED)	Proconodontus posterocostatus	
			Proconodontus tenuiserratus	
			No Zonation Established	

Figure 1. Conodont and trilobite zonation of the Late Cambrian and Early Ordovician (adapted from Miller, 1988).

particular outcrops previously. We sampled the rocks immediately adjacent to the contact in greatest detail. Four of the exposures yielded conodonts, two of them (localities 4 and 6, fig. 2) in significant numbers (fig. 4). Samples that did not yield conodonts were primarily sandstone and sandy dolomite, even though several kilograms of each lithologic type were desegregated in the lab. From the productive samples, we made the following conclusions:

1. Conodonts from either side of the Jordan–Oneota unconformity include the same species, with two exceptions. No elements of *Cordylodus lindstromi* were found in the Jordan, and no elements of *Variabiloconus bassleri* were found in the Oneota at our localities. *Variabiloconus bassleri* is known in the Oneota at other localities that were not part of this study (for example, Smith and Clark, 1996), but *C. lindstromi* has not been reported anywhere in the Jordan.
2. The conodonts from the uppermost Jordan and lowermost Oneota are species that range from the Ibexian *Cordylodus proavus* Zone into the Ibexian *Rossodus manitouensis* Zone. If the questionable *Cordylodus proavus* specimen is not considered (fig. 4), the remaining species still range from the upper part of the *Cordylodus intermedius* Zone into the *Rossodus manitouensis* Zone.

This is a range of four conodont zones (fig. 1) in the Early Ordovician Ibexian and is equivalent to the *Symphysurina* trilobite zone of the Early Ordovician. Clearly, the uppermost beds of the Jordan are Early Ordovician and contain the same species (except as noted above) as those in the well established overlying Early Ordovician Oneota Formation.

3. The presence of essentially the same species of conodonts across the lithologic unconformity that separates the Jordan and the Oneota suggests that the unconformity is relatively minor, at least at the several localities where we obtained faunas. Miller and Runkel (1998) reported species of the Cambrian genus *Proconodontus* lower in the Jordan at localities in Minnesota. Unfortunately, no single locality has been identified that yields the Late Cambrian *Proconodontus*, the Late Cambrian trilobite *Tellerina*, and the Ibexian conodonts reported here. However, the several conodont zones apparently missing between Miller’s report of *Proconodontus* in Minnesota and our Ibexian species at the top of the Jordan in southern Wisconsin suggest that there may be multiple unconformities in the upper part of the Jordan in addition to the one at the Jordan–Oneota contact or larger unconformities in Minnesota than in Wis-



Figure 2. Jordan–Oneota boundary sections studied. 1. Boscobel, SW $\frac{1}{2}$, NW $\frac{1}{2}$, section 21, T8N, R3W, Grant County, Wisconsin; 2. Cross Plains East, NW $\frac{1}{2}$, SW $\frac{1}{2}$, sec. 11, T7N, R7E, Dane County, Wisconsin; 3. Denzer, quarry approximately 0.5 mi SE of Denzer, north side of Highway C, NW $\frac{1}{2}$, SE $\frac{1}{2}$, sec. 14, T10N, R5E, Sauk County, Wisconsin; 4. Mazomanie, approximately 3 mi SW of Mazomanie, south side of Highway K, NW $\frac{1}{2}$, NE $\frac{1}{2}$, sec. 31, T8N, R6E, Dane County, Wisconsin; 5. Mendota Station, railroad cut in center sec. 26, T8N, R9E, Dane County, Wisconsin; 6. Miller’s Curve, roadcut approximately 2.5 mi SE of Cross Plains, north side of Highway 14, SW $\frac{1}{2}$, SE $\frac{1}{2}$, section 7, T7N, R8E, Dane County, Wisconsin; 7. Spring Valley, approximately 0.25 mi north of Spring Valley, NW $\frac{1}{2}$, NW $\frac{1}{2}$, sec. 5, T27N, R15E, Pierce County, Wisconsin; 8. Weaver, SW $\frac{1}{2}$, SW $\frac{1}{2}$, sec. 30, T109N, R9W, Wabasha County, Minnesota.

consin. Miller and Runkel (1998, fig. 9) indicated that the major unconformity in the area of Homer, Minnesota, is at the Jordan–Oneota contact, and at that locality as many as eight conodont zones representing the upper Trempealeuan and lower Skullrockian are missing. This suggests that the unconformity at the Minnesota section is more profound and includes part of the Jordan that is present in southern Wisconsin.

Recent studies by the International Working Group on the Cambrian–Ordovician Boundary (IWGCOB) have shown that the Cambrian–Ordovi-

cian boundary has been inconsistently designated at different localities and is not at the same stratigraphic level worldwide. Reasons for this generally reflect the fact that different fossils are used by different investigators in their stratigraphic definitions, and there has not always been a clear understanding of how the different fossil occurrences correlate with each other. The IWGCOB has decided that a standardized international boundary should be based on conodont, graptolite, and trilobite definitions (Miller, 1988).

Conodont-based candidates for the international boundary are 1) the base of the *Cordylodus proavus* Zone; 2) the base of the *Cordylodus intermedius* Zone; 3) the base of the *Cordylodus lindstromi* Zone; or 4) the base of the *Iapetognathus* Zone (Miller, 1988; Ross and others, 1993; Miller and Taylor, 1995) (fig. 1). Assuming that one of these zonal boundaries is selected, it is apparent that the Cambrian–Ordovician boundary is in the Jordan Formation and definitely below the Jordan–Oneota contact as we recognize it in southern Wisconsin, the traditional level.

CONODONTS AND THE JORDAN–ONEOTA INTERVAL

The Ibexian conodonts of the Jordan and lower Oneota (figs. 4 and 5) include species that represent shallow subtidal and possibly supratidal as well as further offshore assemblages. We interpret the *Teridontus* and

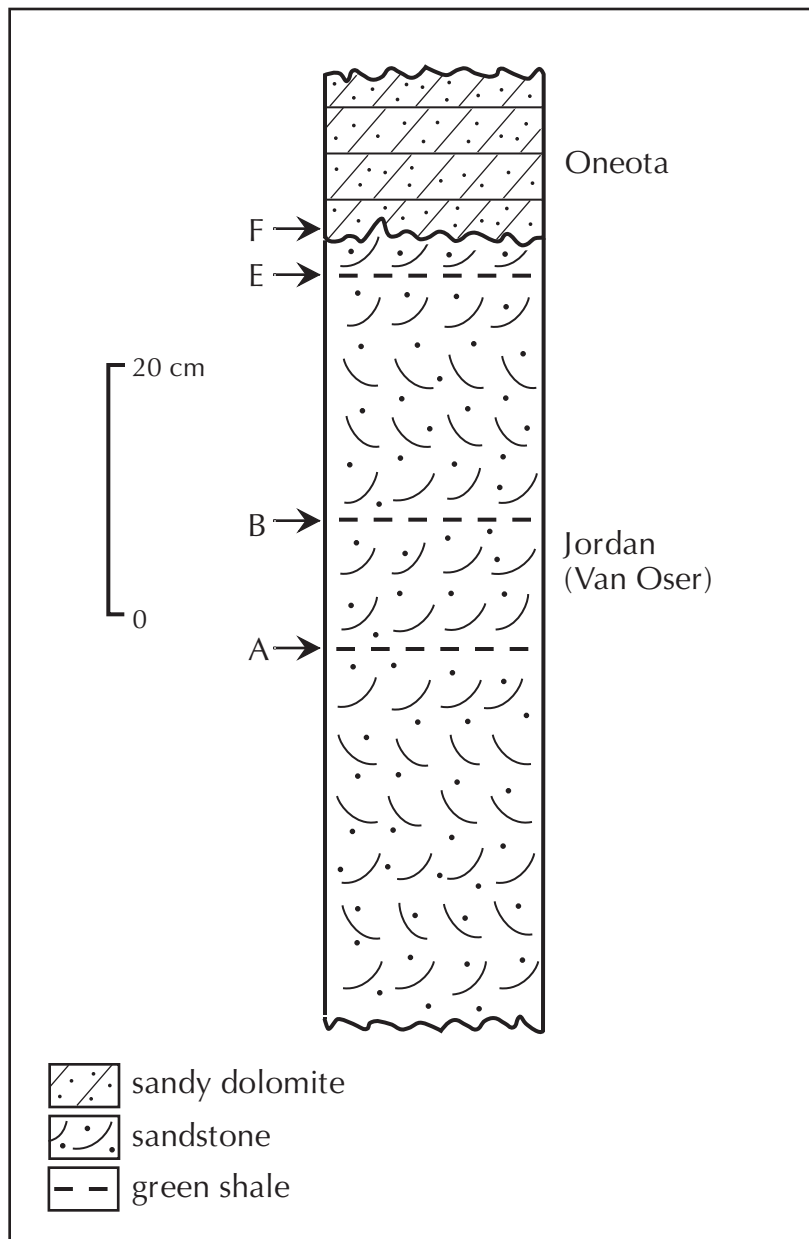


Figure 3. Oneota–Jordan relationship at Miller’s Curve (locality) a few miles west of Madison. Letters and arrows indicate important samples that yielded conodonts (fig. 4). Essentially, the same relationship of lithostratigraphic units shown here for Miller’s Curve is found at each of the other localities studied (fig. 2).

Species	Locality 6 Samples						Locality 3	Locality 4	Locality 7
	A	B	C	D	E	F	G	H	I
Acanthodus uncinatus Furnish		3	6	15	6	4		6	
Aloxoconus sp.					3	7		5	
Aloxoconus iowensis (Furnish)			8	9	7	3		4	
Aloxoconus propinquus (Furnish)	1		12	8	1	2		2	1
Aloxoconus staufferi (Furnish)			4	2	2			4	
Cordylodus lindstromi Druce and Jones						4			
Cordylodus proavus Müller	1?								
Oneotodus simplex (Furnish)			29	61	34	13	1	44	
Teridontus nakamurai (Nogami)		1	55	131	71	78	3	107	1
Variabiloconus bassleri (Furnish)			5	6			2	1	

▲ **Figure 4.** Conodonts from the Jordan–Oneota contact area, Wisconsin. Samples A–F are from locality 6 (figs. 2 and 3), G, H, and I are from localities 3, 4, and 7 (fig. 2). A. Lower shale of Van Oser Member of Jordan Formation, 30 cm above base of Van Oser, center of roadcut. B. Intermediate shale of Van Oser Member of Jordan Formation, 40 cm above base of Van Oser, center of roadcut. C. Same as A, west end of roadcut. D. Same as A, east end of roadcut. E. Uppermost green shale of Van Oser Member of Jordan Formation, 61 cm above base of Van Oser, 3 cm below Jordan–Oneota contact, center of roadcut. F. Base of lowermost dolomite of Oneota Formation, center of roadcut. G. Locality 3, green shale lenses of Van Oser Member, 20 cm below Jordan–Oneota contact. H. Locality 4, green shale lenses of Van Oser Member, 10 cm below Jordan–Oneota contact. I. Locality 7, green shale lenses of Van Oser Member, 9 cm below Jordan–Oneota contact. All shale samples were treated in water; dolomites and sandy dolomite were treated with acetic and/or formic acid. Residues were washed on a 120 mesh screen and were concentrated in tetrabromoethene. As much shale as could be sampled was taken at each outcrop (up to 1 kg), and up to 5 kg of the dolomites and sandy dolomites were sampled.

► **Figure 5.** Conodonts from the Jordan–Oneota contact area in Wisconsin. All specimens are $\times 100$, except as indicated. Specimens are in the Museum of the Department of Geology and Geophysics of the University of Wisconsin–Madison, UW1904.

1–5, *Aloxoconus propinquus* (Furnish), 1–3, posteriolateral views, 1, sample D, locality 6, UW1904/15, 2, sample C, locality 6, UW1904/16, 3, sample F, locality 6, UW1904/17; 4–5, posterior and enlargement ($\times 1000$) showing microstriations, sample C, locality 6, UW1904/18.

6–7, *Aloxoconus staufferi* (Furnish), 6, posterior, sample C, locality 6, UW1904/13, 7, lateral, sample H, locality 4, UW1904/14.

8–9, *Aloxoconus iowensis* (Furnish), 8, lateral, sample D, locality 6, UW1904/12, 9, posterior, sample H, locality 4, UW1904/11.

10–11, *Variabiloconus bassleri* (Furnish), 10, posteriolateral, sample D, locality 6, UW1904/7, 11, lateral, sample C, locality 6, UW1904/8.

12–16, *Acanthodus uncinatus* Furnish, 12, lateral, sample D, locality 6, UW1904/20, 13, lateral, sample B, locality 6, UW1904/9, 14, posteriolateral, sample H, locality 4, UW1904/7, 15, posterior and 16, basal cavity showing lamellae, $\times 500$, sample H, locality 4, UW1904/10.

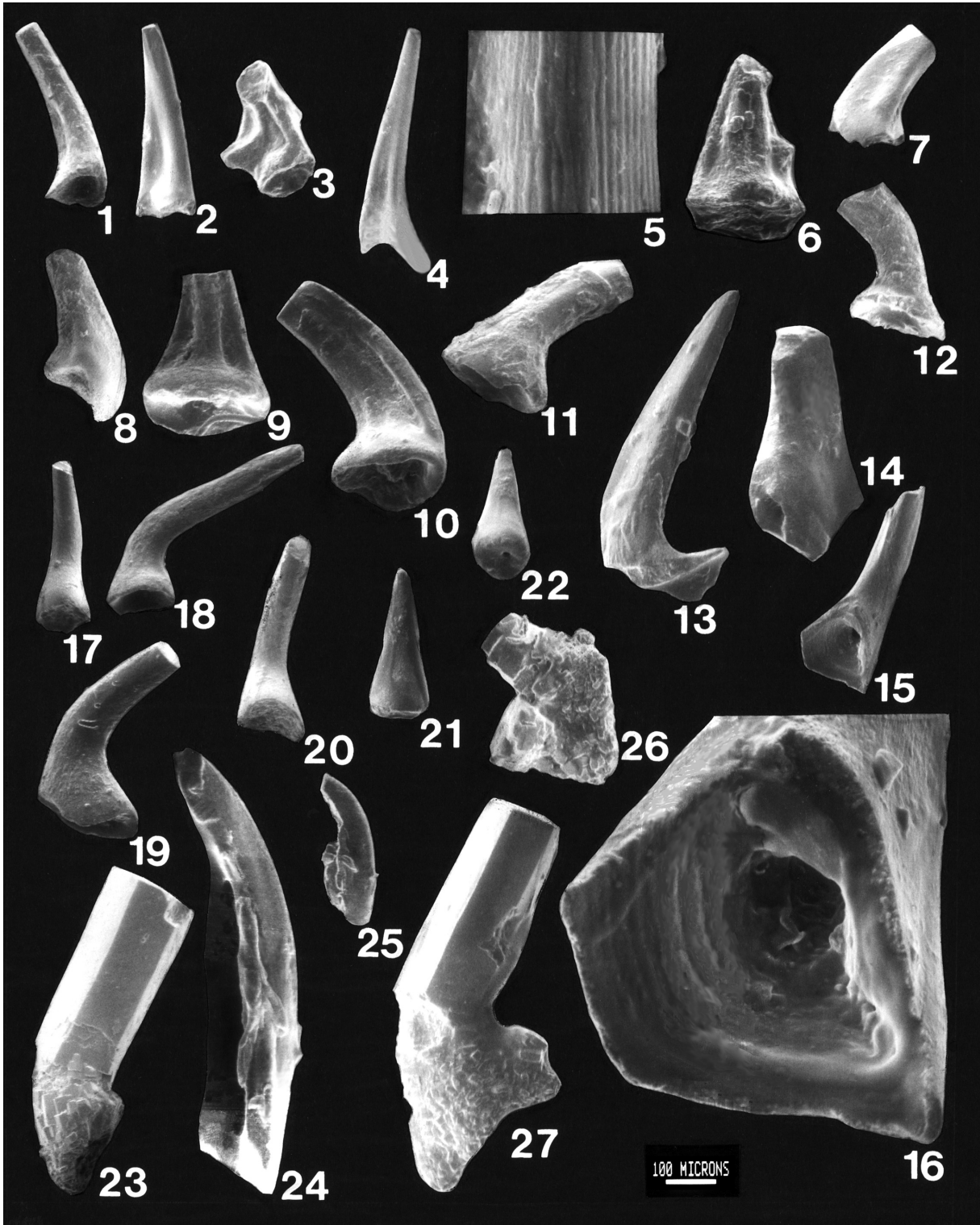
17–18, 23, *Teridontus nakamurai* (Nogami), 17, posterior, sample E, locality 6, UW1904/6, 18, lateral, sample D, locality 6, UW1904/5, 23, lateral showing apatite overgrowth on cusp, sample B, locality 6, UW1904/2.

19–20, *Oneotodus simplex* (Furnish), 19, lateral, sample D, locality 6, UW1904/2, 20, posterior, sample H, locality 4, UW1904/3.

21–22, *Aloxoconus* sp. ?, 21, posterior and 22, basal, sample H, locality 4, UW1904/23.

24–25, *Cordylodus proavus* Müller?, 24, posterior-lateral, X300, and 25, lateral, sample A, locality 6, UW1904/22.

26–27, *Cordylodus lindstromi* Druce and Jones, 26, specimen with projection of basal cavity into first broken denticle base (not shown), sample F, locality 6, UW1904/19, 27, specimen with main cusp recrystallized, sample F, locality 6, UW1904/1.



Variabiloconus–*Aloxoconus* assemblage of the Jordan to represent the shallow subtidal to intratidal environment. In contrast, the conodont assemblage of the Oneota may represent a slightly deeper subtidal facies. This interpretation is consistent with recent work with the Lower Ordovician St. George Group of western Newfoundland (Ji and Barnes, 1994) that included many of the same species as our Upper Mississippi Valley section.

The conodonts from the Jordan were recovered primarily from centimeter-scale shale partings in a sandstone matrix (for example, fig. 3). These very thin shale intervals are discontinuous laterally, never more than 1 cm thick, and their relationship to the enclosing sandstone must be considered. We believe that these tiny shale partings represent tidal deposits of the fine-grained material carried to the site of deposition by tidal surges and then deposited during time of slack tide, similar to the earlier interpretations of Runkel (1994) and Byers and Dott (1995). During the succeeding tidal surges, most of the fine-grained material was probably removed. This explains the very thin and discontinuous nature of the shales. The

only fine-grained sediment remaining was that which was trapped in the more protected parts of the undulating sand bottom. Conodonts living in this shallow zone also left a record in the fine-grained sediment. Analogous sedimentation has been described for other parts of the Upper Mississippi Valley Cambrian sediment (Dott and others, 1986; Haddox and Dott, 1990) and is consistent with more recent interpretations of the Jordan (Byers and Dott, 1995). This suggests to us that the unconformity at the Jordan–Oneota contact is relatively minor and was produced by subaerial erosion during hundreds or thousands of years, or perhaps during an even shorter interval. Additional unconformities probably exist lower in the section (fig. 6), at least in Minnesota if the interpretation of Miller and Runkel (1998, fig. 9) is accepted.

As interpreted, the most significant difference between the conodonts of the uppermost Jordan and the lowermost Oneota may have been environmental. There are not significant faunal differences.

SUMMARY

The nearshore region of the epeiric sea surrounding the North American cratonic interior was a sand shoal during the Late Cambrian and Early Ordovician. The shallow water sands prograded over the deeper water sands at least twice during deposition of the Jordan. The Jordan–Oneota unconformity which has been considered to represent the Cambrian–Ordovician boundary probably is relatively minor in southern Wisconsin, as suggested from the conodonts that range across it. However, there are localities where the unconformity cuts down into the sands of the Jordan Formation to varying degrees, in some places possibly eliminating an entire progradational cycle (Byers and Dott, 1995) or several Late Cambrian–Early Ordovician conodont zones (Miller and Runkel, 1998). This may have occurred during a relatively short time interval. There may be other unconformities lower in the Jordan as well (fig. 6). The sea level fall and its subsequent rise were rapid and occurred during the time of formation of one or several of the closely related Ibexian conodont intervals (fig. 1). Although the amount of time represented by the conodont ranges or the zones is not known with precision, it probably does not represent more than a few hundred thousand years. The similarity of conodonts of the uppermost Jordan and the lowermost Oneota constrains the magnitude of the unconformable lithologic contact to the range of the several species reported here, but probably does not represent a major interval of geologic time. The late Cambrian trilobite *Tellerina strigosa* of the upper Jor-

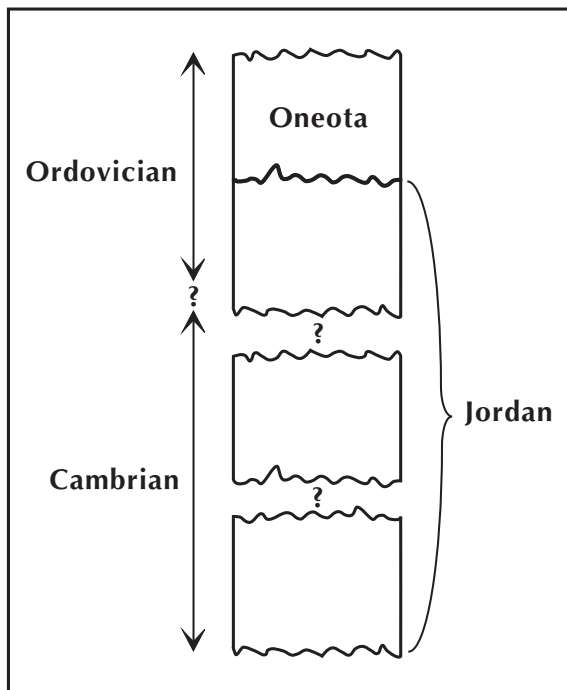


Figure 6. Cambrian–Ordovician relationship of the Oneota and Jordan. Major unconformities may be present lower in the Jordan and would account for the missing conodont zones suggested by Miller and Runkel (1998) in Minnesota.

dan (uppermost *Saukia* Zone) has been found only a few meters below the Ibexian conodonts of the Jordan. This indicates that the uppermost Jordan, at least in southern Wisconsin, is Ordovician (figs. 1 and 6) according to any of the possible boundaries that might be selected by the IWGCOB. If our interpretation is correct, the Cambrian–Ordovician boundary in this part of the Upper Mississippi Valley is lower than the Jordan–Oneota lithologic contact.

ACKNOWLEDGMENTS

C.W. Byers, University of Wisconsin–Madison, assisted in the field and lab as well as in preparation of the manuscript. R.H. Dott, Jr., University of Wisconsin–Madison, assisted in stratigraphic discussions. J.F. Miller, Southwest Missouri State, and A.C. Runkel, Minnesota Geological Survey, made helpful comments concerning the manuscript, although this does not indicate agreement with our conclusions. Mary Diman, University of Wisconsin–Madison, prepared the figures.

REFERENCES

- Byers, C.W., and Dott, R.H., Jr., 1995, Sedimentology and depositional sequences of the Jordan Formation (Upper Cambrian), Northern Mississippi Valley: *Journal of Sedimentary Research*, B, v. 65, p. 289–305.
- Dott, R.H., Jr., Byers, C.W., Fielder, G.W., Stenzel, S.R. and Winfree, K.E., 1986, Aeolian to marine transition in Cambro–Ordovician cratonic sheet sandstones of the northern Mississippi Valley, U.S.A.: *Sedimentology*, v. 33, p. 345–367.
- Haddox, C.A., and Dott, R.H., Jr. 1990, Cambrian shoreline deposits in northern Michigan: *Journal of Sedimentary Petrology*, v. 60, p. 697–716.
- Heller, R.L., 1956, Status of the Prairie du Chien problem, in G. M Schwartz, ed., Geological Society of America Guidebook for Field Trips, Trip 2, p. 29–40.
- Hughes, N.C., and Hesselbo, S.P., 1997, Stratigraphy and sedimentology of the St. Lawrence Formation, Upper Cambrian of the northern Mississippi Valley: Milwaukee Public Museum Contributions in Biology and Geology, no. 91, 50 p.
- Ji, Z., and Barnes, C.R., 1994, Conodont paleoecology of the Lower Ordovician St. George Group, Port au Prince Peninsula, western Newfoundland: *Journal of Paleontology*, v. 68, p. 1368–1383.
- McGee, W.J., 1891, The Pleistocene history of north-east Iowa: U.S. Geological Survey Eleventh annual Report, p. 187–577.
- Miller, J.F., 1988, Conodonts as biostratigraphic tools for redefinition and correlation of the Cambrian–Ordovician boundary: *Geological Magazine*, v. 125, p.349–362.
- Miller, J.F. and Melby, J.H., 1971, Trempealeuan conodonts, in Clark, D.L., ed., Conodonts and biostratigraphy of the Wisconsin Paleozoic: Wisconsin Geological and Natural History Survey Information Circular 19, p. 4–9.
- Miller, J.F. and Taylor, M.E., 1995, Biostratigraphic significance of *Iapetognathus* (Conodonts) and *Jujuyaspis* (Trilobites) in the House Limestone, Ibex area, Utah, in Cooper, J.D., Droser, M.L., and Finney, S.C., eds., Ordovician Odyssey: Short papers for the Seventh International Symposium on the Ordovician System: Book 77, Pacific Section of the SEPM, p. 109–112.
- Miller, J.F. and Runkel, A.C., 1998, Biostratigraphy of conodonts from Jordan Sandstone and Lowermost Oneota Dolomite near Homer, Minnesota, in Institute on Lake Superior Geology, 44th Annual Meeting Field Trip Guidebook, May, p. 119–120.
- Odom, I.E. and Ostrom, M.E., 1978, Lithostratigraphy, petrology, sedimentology and depositional environments of the Jordan Formation near Madison, Wisconsin, in Lithostratigraphy, Petrology, and Sedimentology of Late Cambrian–Early Ordovician Rocks near Madison, Wisconsin: Wisconsin Geological and Natural History Survey Field Trip Guide Book 3, p. 23–45.
- Ostrom, M.E., 1964, Pre-Cincinnatian Paleozoic cyclic sediments in the Upper Mississippi Valley: A discussion: Kansas Geological Survey Bulletin 169, v. II, P. 381–398.
- Ostrom, M.E., 1967, Paleozoic stratigraphic nomenclature for Wisconsin: Wisconsin Geological and Natural History Survey Information Circular 8.
- Ostrom, M.E., 1970, Lithologic cycles in Lower Paleozoic rocks of western Wisconsin, in Field Trip Guide Book for Cambrian–Ordovician Geology of Western Wisconsin: Wisconsin Geological and Natural History Survey Information Circular 11, p. 10–34.
- Ross, R.J. Jr., Hintze, L.F., Ethington, R.L., Miller, J.F., Taylor, M.E., and Repetski, J.E., 1997, The Ibexian, Lowermost Series in the North American

- Ordovician: U.S. Geological Survey Professional Paper 1579-A, 50 p.
- Runkel, A.C., 1994, Deposition of the uppermost Cambrian (Croixan) Jordan Sandstone and the nature of the Cambrian–Ordovician boundary in the Upper Mississippi Valley: *Geological Society of America Bulletin*, v. 106, p. 492–506.
- Smith, G.L., Byers, C.W., and Dott, R.H., Jr., 1993, Sequence stratigraphy of the Lower Ordovician Prairie du Chien Group on the Wisconsin Arch and in the Michigan Basin: *American Association of Petroleum Geologists Bulletin*, v. 77, p. 49–67.
- Smith, G.L. and Clark, D.L., 1996, Conodonts of the Lower Ordovician Prairie du Chien Group of Wisconsin and Minnesota: *Micropaleontology*, v. 42, p. 363–373.
- Twenhofel, W.H., Raasch, G.O., and Thwaites, F.T., 1935, Cambrian strata of Wisconsin: *Geological Society of America Bulletin*, v. 46, p. 1687–1743.
- Ulrich, E.O., 1924, Notes on new names in the table of formations and on physical evidence of breaks between Paleozoic systems in Wisconsin: Wisconsin Academy of Science, Arts, and Letters, Transactions, v. 21, p. 71–107.
- Winchell, N.H., 1874, The geology of the Minnesota Valley, Part E, The Jordan Sandstone: Geological and Natural History Survey of Minnesota, Second Annual Report, p. 147–152.

PALEOECOLOGY AND SEDIMENTOLOGY OF THE *PRASOPORA* ZONULE IN THE DUNLEITH FORMATION (ORDOVICIAN), UPPER MISSISSIPPI VALLEY

H.C. Sanders^{1,2}, D.H. Geary¹, and C.W. Byers¹

ABSTRACT

The dome-shaped bryozoan *Prasopora* and its accompanying fauna display distinct distributional patterns in Middle to Late Ordovician epeiric sea deposits of the Galena Group in the Upper Mississippi Valley. These rocks consist of interbedded carbonates and siliciclastics, and *Prasopora* is abundant in some intervals, but absent in others. *Prasopora* is most abundant in the widely recognized *Prasopora* zonule in the Dunleith Formation of the Galena Group.

We studied the *Prasopora* zonule and surrounding beds at an outcrop south of Guttenberg, Iowa. Point counts showed distinct vertical changes in faunal composition and sedimentology. Where *Prasopora* abundance is high, so is that of other bryozoans, but brachiopod abundance is low. Carbonate mud content is lowest where *Prasopora* and other bryozoans dominate and highest where brachiopods dominate. We considered taphonomic, ecological, and environmental explanations for these faunal and sediment distribution patterns. Statistical analyses of fossil-size differences among the units studied did not show evidence of taphonomic sorting due to storm currents. At Guttenberg, brachiopod and bryozoan abundances appear to be associated with the change in carbonate mud content at the onset of the zonule as well as the zonule's position at the transition from a shallowing-upward cycle to the beginnings of a transgressive systems tract.

INTRODUCTION

Rock layers rich in the bryozoan genus *Prasopora* are found sporadically within the Galena Group (Ordovician, Trentonian Stage) of the upper Midwestern United States, including much of southern and central Wisconsin (fig. 1). *Prasopora* is particularly abundant in one interval in the Dunleith Formation of the Galena Group. Although this "*Prasopora* zonule" has been widely recognized (Kay, 1929; Sloan, 1956; Rose, 1967; Levorson and Gerk, 1972–1973; Willman and Kolata, 1978; Delgado, 1983), controls on the abundance of *Prasopora* in the Galena Group have not been investigated previously. The purpose of our study was to determine controls on *Prasopora* concentration through consideration of sedimentology, paleoecology, and taphonomy.

GEOLOGIC SETTING

Galena Group

Stratigraphic nomenclature for Trentonian Stage deposits varies slightly among states of the Upper Mid-

west. Herein we employ the group, formation, and member names of Levorson and others (1987) still commonly used in Iowa. According to that system, the Galena Group contains the Spechts Ferry, Guttenberg, Dunleith, Wise Lake, and Dubuque Formations (fig. 1). The Galena Group extends through parts of Iowa, Minnesota, Illinois, and much of southern Wisconsin. Most of the beds in Wisconsin, however, are heavily dolomitized because post-depositional phreatic water influence was greater toward the Wisconsin Arch. Therefore, we have chosen an undolomitized outcrop containing well preserved fossils in northeastern Iowa for the focus of this study. Because of regional horizontal continuity of strata, we assume that conclusions about the *Prasopora* zonule in Iowa hold true for that of Wisconsin.

The sedimentology, biota, and geometry of Galena Group rocks are typical of the storm-swept interior seaway that characterized the upper Midwest during the Middle and Late Ordovician. Episodic storm-event indicators include bioclastic grainstones that pinch and swell laterally; some show graded bed-

¹Department of Geology and Geophysics, University of Wisconsin–Madison, Madison, Wisconsin 53706

²Now at Department of Geology, Pomona College, Claremont, California 91711

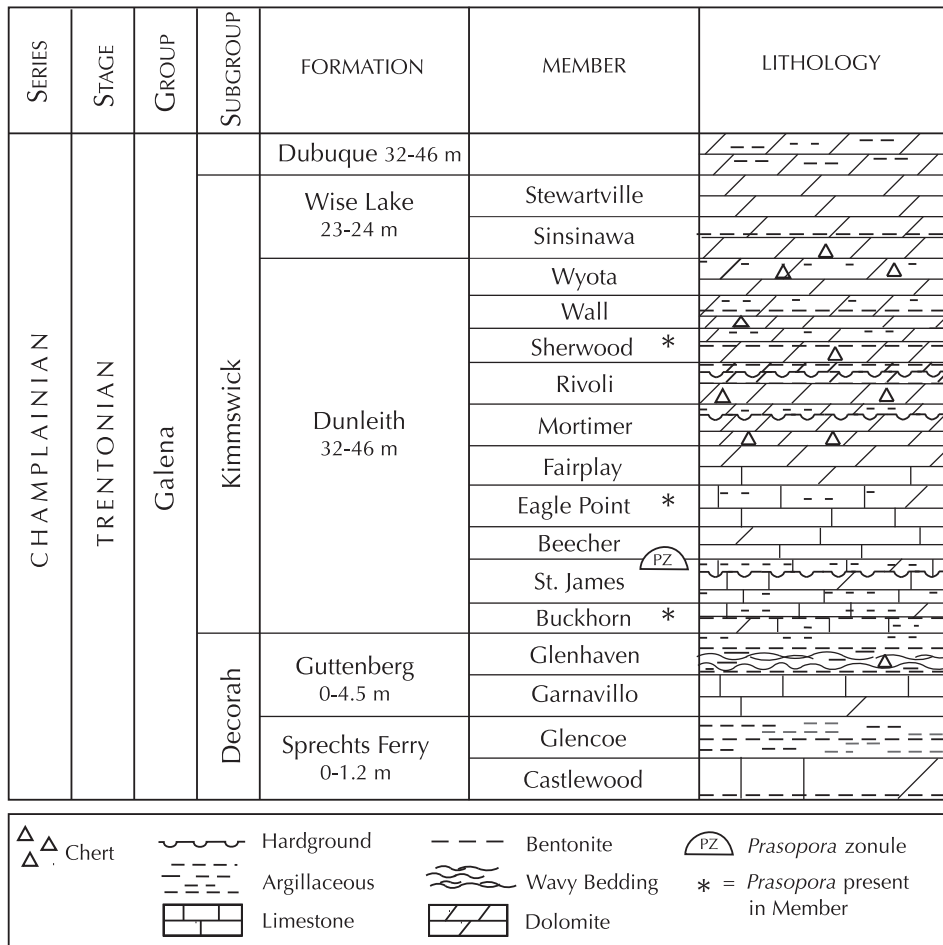


Figure 1. Stratigraphic column of the Galena Group (after Levorson and others, 1987). The *Prasopora* zonule is at the St. James–Beecher Member contact. Other *Prasopora*-bearing beds are marked. Hardgrounds are common throughout the Galena Group; the most prominent ones are indicated here.

ding, although it is commonly obscured as a result of bioturbation. Rocks of the Galena Group are made up of partially to completely dolomitized carbonate mud and fossil debris. Small amounts of terrigenous silt are present, probably derived from the Transcontinental Arch to the northwest (Willman and Kolata, 1978). Several bentonite layers derived from volcanoes of the Taconic Uplands have been documented (Kolata and others, 1986). A striking feature of Galena Group stratigraphy is the presence of numerous hardgrounds (previously termed corrosion zones), which represent depositional hiatuses and intervals of submarine cementation (Delgado, 1983). Early diagenetic processes of the Galena Group strata include submarine dissolution of aragonite, submarine cementation forming numerous hardgrounds and nodules, and some submarine dolomitization within filled burrows (Delgado, 1983).

Later diagenetic processes include silicification of biotites, formation of chert nodules, dolomite mottling, and regional dolomitization, which is more prevalent in outcrops east of the Mississippi River. The regional post-depositional, mesogenetic dolomitization probably resulted from the mixing of fresh and marine phreatic water during the worldwide eustatic drawdown at the end of the Ordovician Period (Delgado, 1983). The Wisconsin Arch was exposed and receiving fresh-water recharge at this time, which explains why the dolomitization is more prevalent eastward toward the arch (Delgado, 1983).

A lack of shoreline or nonmarine sedimentary features, in conjunction with the broad, laterally continuous sedimentary units within the Galena Group, suggests that deposition occurred on an extensive platform or ramp. Indicators of intertidal or supratidal en-

vironments are absent; no stromatolites, mudcracks, hummocky cross-bedding, or fenestral porosities have been observed. Modern day analogues for the Galena platform include the cool water Lacepede shelf off Australia (James, 1990) and the Bahama Bank (Kolata, 1975; Arens and Cuffey, 1989).

The fossils of the Galena Group consist mainly of benthic biota, including brachiopods, crinoids, gastropods, and bryozoans.

Prasopora

Prasopora colonies are distinct among Galena Group fossils because of their relatively large, domal form (fig. 2). The hemispheres of the colonies are generally 2 to 4 cm in diameter and contain thin-walled, elongate zooecial tubes with widely spaced diaphragms and intervening special support structures (mesopores and acanthopores; Bassler, 1953; Cuffey, 1997). *Prasopora* belongs to the class Stenolaemata, the dominant bryozoan class of the Ordovician (McKinney and Jackson, 1989). *Prasopora*-bearing strata in eastern North America have been the subject of several previous investigations (Sparling, 1964; Arens and Cuffey, 1989; Cuffey, 1997).

***Prasopora* zonule**

Centimeter-scale concentrations of *Prasopora* have been recognized in the Decorah Subgroup and in the Buckhorn, St. James, Beecher, Eagle Point, and Sherwood Members of the Dunleith Formation (Sloan, 1956, 1987; Delgado, 1983; Kolata, 1987; Leverson and others, 1987). The most impressive concentration of *Prasopora* is a particular zonule around the St. James–Beecher Member boundary (fig. 1). This zonule is visible in outcrops throughout the Upper Mississippi Valley, even in regions where dolomitization is pervasive. The approximately 45 cm thick *Prasopora* zonule is predominantly carbonate with shale partings, similar to that of other Galena Group sediments.

We studied a locality south of Guttenberg, Iowa (fig. 3), where the Galena Group strata are especially well exposed. We divided the lower Beecher and upper St. James Members into six units (A–F) on the basis of lithology and fossil content (figs. 4 and 5; Sanders, 1996). Units A and B lie within the upper St. James Member, below the *Prasopora* zonule. A prominent bedding plane between them marks the change from the less resistant unit A to more resistant unit B. Unit B is distinguished from unit A by having less carbonate mud. The *Prasopora* zonule comprises three distinct units (C, D, and E). Units C and



Figure 2. A colony of the bryozoan *Prasopora* (approximately 2.5 cm wide) is indicated by a white outline in this photograph taken at the outcrop. Scale bars are in millimeters.

D are within the St. James Member and unit E is in the Beecher Member. A prominent hardground lies at the base of the lowest unit of the zonule, unit C. This 12.5 cm thick unit (and the non-zonule subjacent unit B) consists of a calcareous packstone with grainstone-rudstones pinching and swelling laterally. Unit D above, approximately 9 cm thick, is a thinly bedded, fissile packstone. The top of this fissile unit marks the St. James–Beecher contact. The third and topmost unit of the *Prasopora* zonule (unit E) is a poorly stratified wackestone, approximately 23 cm thick, at the base of the Beecher Member. Above the zonule is unit F, a resistant carbonate separated from the zonule by a distinctive, non-scoured hardground surface.

MATERIALS AND METHODS

We obtained lithologic and faunal composition data by point counting sediment grains and fossils in thin sections and polished slabs (table 1; fig. 6). We measured the sizes of fossil fragments to determine the extent of breakage indicating taphonomic reworking in each layer (table 2; fig. 7). The longest axis of each fossil grain in thin section was measured using a digital image processor. Also, the extent of burrowing, abrasion, and the position relative to life-position of fossil bodies was examined.

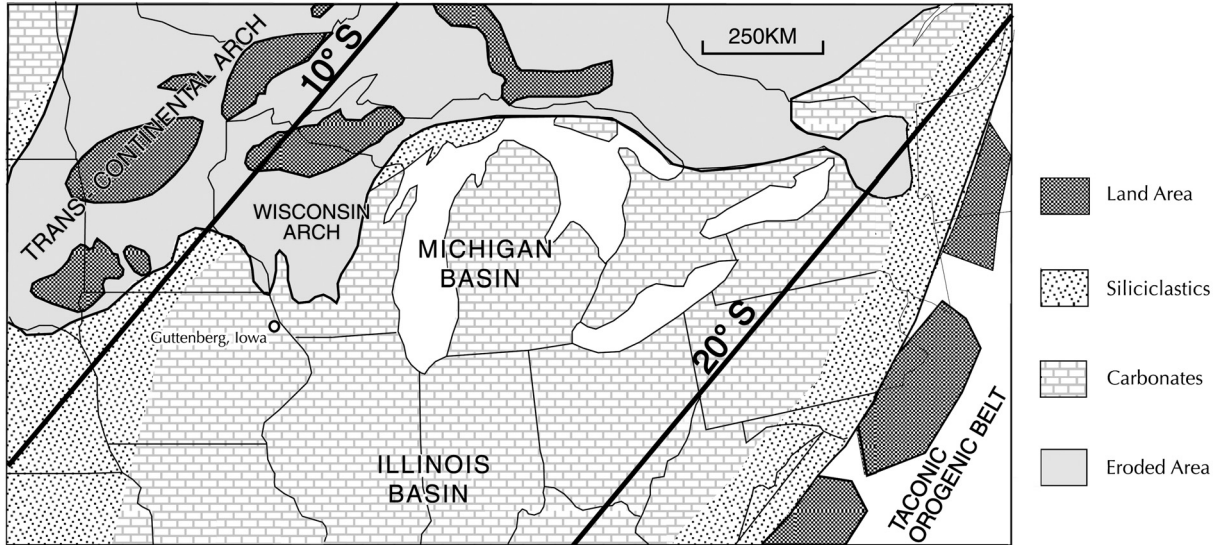


Figure 3. Map indicating the interpreted paleogeography of the study region (compiled from Witzke, 1980 and Choi, 1995). Structural highs (the Transcontinental and Wisconsin Arches) and basins (Illinois and Michigan) are indicated along with paleolatitudes. Guttenberg, Iowa, is indicated. The outcrop discussed in this paper is a roadcut on the west side of Iowa State Highway 52, 0.5 km south of Guttenberg.

We took lithologic point counts from thin sections viewed with a petrographic microscope (1.5x) connected to a video screen. Each centimeter on the screen represented 1.0 mm on the thin section. One 2.5 by 5 cm thin section was used for every 5 cm of vertical thickness of outcrop section. A grid divided into 20 points placed 5 cm apart was overlaid on the image. The lithology under each point on the grid was placed into one of these categories: mud (mud-sized particles that appeared to be carbonate in composition), dolomite crystals, fossils, calcite cement crystals, silt, and other. (“Other” refers to trace elements and unidentified grains.)

Faunal frequency measurements come from polished slabs viewed under a dissecting microscope (1.5x). A 4 cm² frame was moved across the slab at regular intervals. At each interval, the fossils that fell within the square were classified into the following categories: brachiopod, non-prasoporan bryozoan, *Prasopora*, or other. (The faunal category “other” refers to the fossils that had such low abundances that their counts were insignificant: trilobites, gastropods, crinoids, and bivalves.) If a fossil spanned two squares, it was counted only once. *Prasopora* colonies were considerably larger than other fossils, so their relative frequencies appeared low even where they are highly visible in outcrop.

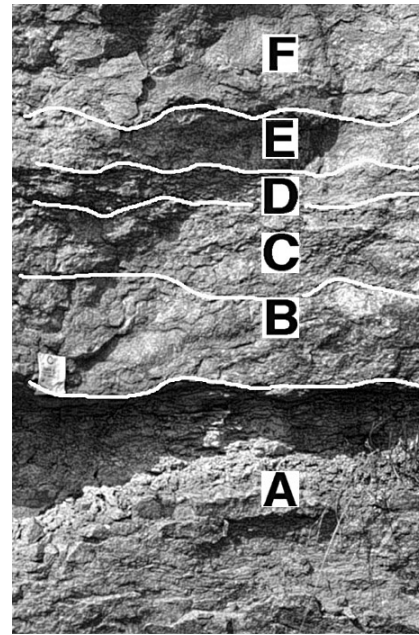


Figure 4. Photograph of units A–F taken at the Guttenberg outcrop.

RESULTS

Most of the fossils of units A–F were fragmented and did not appear to be in life position. *Prasopora* colonies were nearly whole and only slightly abraded. They were not in life position and exhibited no preferred orientation. Physical and biological reworking obscured the nature of the attachment surface of *Prasopora* and other invertebrates.

The faunal and lithological distributions in units A–F are shown in table 1 and figure 6. Of the points counted from unit A, 39 percent were carbonate mud. Unit A has the highest proportion of carbonate mud of any unit as well as a large proportion of brachiopods (76%) and a relatively small proportion (17%) of non-prasoporan bryozoans (fig. 6; table 1). Unit B, which lies directly below the zonule, is like unit A in that it is relatively high in the percentage of brachiopods (77%) and low in the percentage (18%) of non-prasoporan bryozoans (fig. 6; table 1). In addition to the presence of a prominent (conformable) bedding plane between the two units (figs. 2 and 3), unit B is distinguished from unit A by having less carbonate

mud (fig. 6; table 1). Unit C, the lowermost *Prasopora* zonule unit, marks the shift from brachiopod-dominated to bryozoan-dominated fauna and also shows a drop in mud content. The bar graph in figure 6 demonstrates the large increase in non-prasoporan bryozoans in unit C (up 30% from unit B). At this point there is also a drop in brachiopod percentage (from 77% to 39%). Unit C also has the lowest percentage of carbonate mud (20%) of all units (fig. 6; table 1). A Z-test on the distribution of mud percentages in units A–C shows that unit C's mud content falls outside the 94 percent confidence interval ($Z = 1.558$). This is the only unit in which mud content is significantly lower. Above this initial unit of the zonule, mud levels rise again (27%, 33%, and 30% in units D, E, and F, respectively). The highest proportion of *Prasopora* (10%) is in unit D, a fissile layer, composed mainly of dolomite and fossils (fig. 6; table 1). Unit E is in the topmost *Prasopora* zonule unit. The carbonate mud content is 6 percent higher than that of unit D. In the Beecher Member above the zonule, unit F has the lowest percentage of fossils (21%) overall, but a high-

Figure 5. Cartoon of units A–F, Guttenberg outcrop. Lithologies are indicated in boxes. The zonule is bounded by two prominent hardgrounds, indicated by the wavy contact lines. *Prasopora* fossils are most abundant in unit D, the thin, fissile layer. The other two zonule units are more massively carbonate, similar to the rest of the Beecher Member. Unit C contains grainstone lenses.

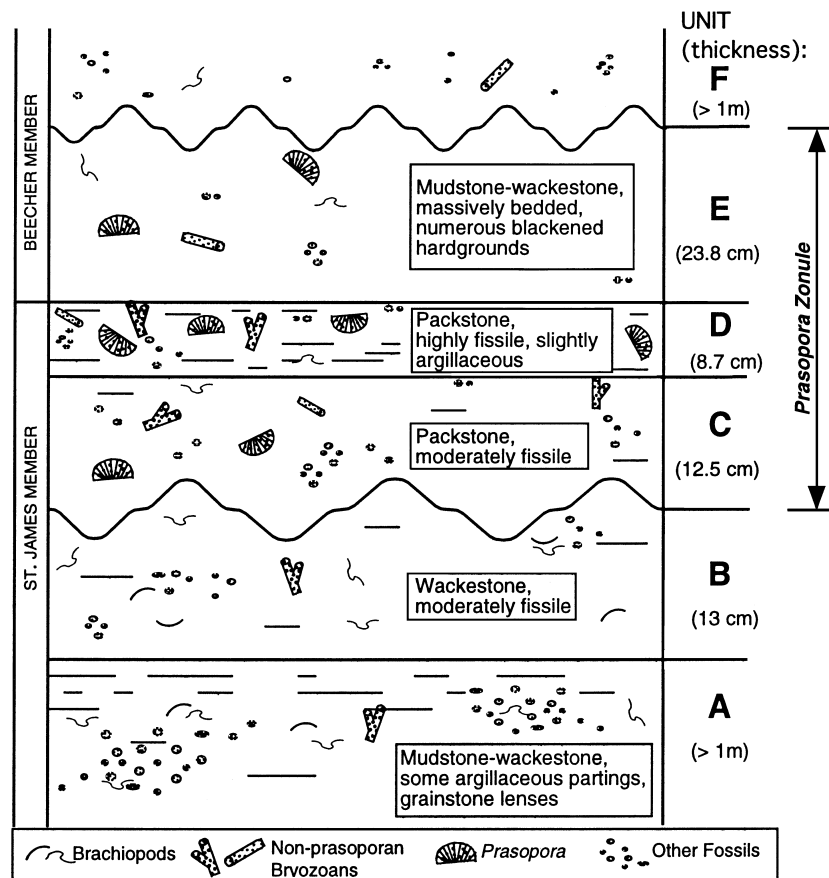


Table 1. Point count data (n = number of points; percent = percent within unit). Refer to figure 6 for graph.

FAUNAL DISTRIBUTION

Unit	Brachiopods		Non-prasop. bryoz.		Prasopora		Other	
	n	percent	n	percent	n	percent	n	percent
A	290	76	65	17	1	~0	28	7
B	430	77	102	18	2	~0	25	5
C	130	39	162	48	25	8	18	5
D	67	47	45	32	14	10	15	11
E	135	45	109	37	16	5	37	13
F	90	57	37	23	3	2	28	18

LITHOLOGIC DISTRIBUTION

Unit	Mud		Dolomite		Fossils		Calcite		Silt		Other	
	n	percent	n	percent	n	percent	n	percent	n	percent	n	percent
A	2109	39	1790	33	1175	22	138	3	184	3	4	~0
B	1283	30	1659	38	1112	26	133	3	117	3	4	~0
C	488	20	1002	41	762	32	41	2	124	5	0	~0
D	990	27	1128	31	1131	31	199	6	170	5	8	~0
E	1015	33	251	8	936	30	883	28	25	1	10	~0
F	2500	30	3456	42	1720	21	604	7	27	~0	9	~0

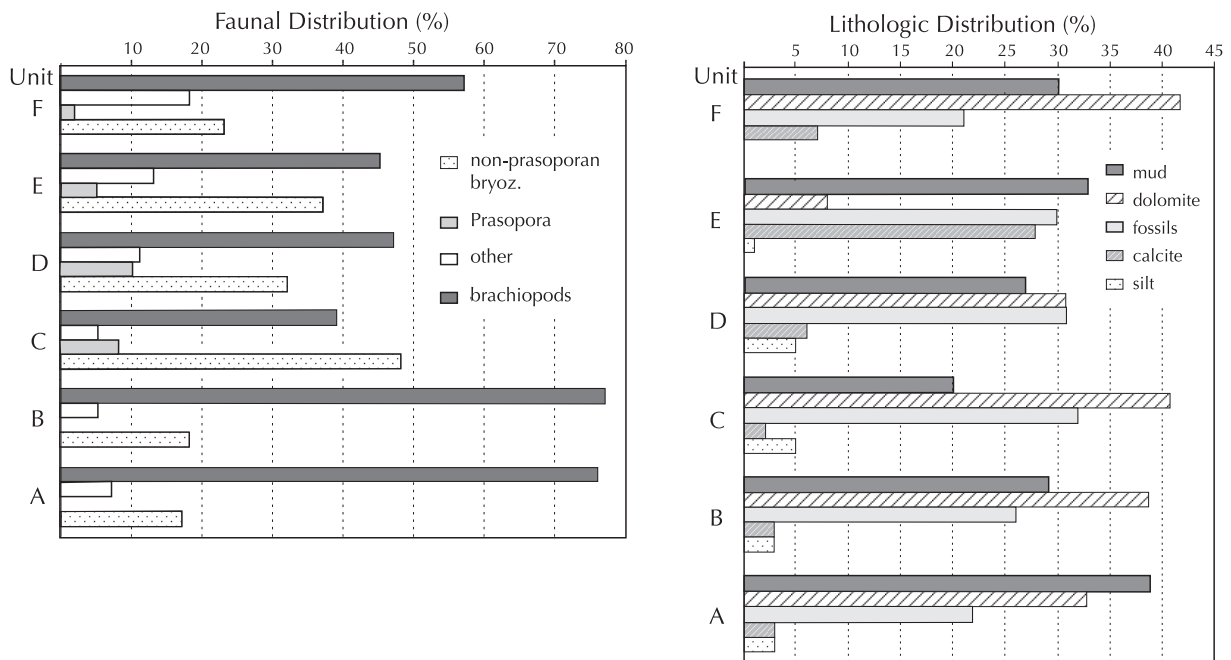


Figure 6. Percentages of faunal and lithological types within each unit, Guttenberg outcrop. See table 1 for point count data; refer to text for point-counting methods.

er proportion of other fossils (18%; fig. 6; table 1).

To test for consistent differences among units in the size of fossil fragments, we performed a Kolmogorov–Smirnov test on brachiopod and non-prasoporan bryozoan size data (Sokal and Rohlf, 1981). These

analyses indicated that the size of fossils inside versus outside of the zonule is not significantly different (p [the Kolmogorov–Smirnov probability statistic] = 0.730 for brachiopods; p = 0.383 for non-prasoporan bryozoans). For 726 brachiopods, mean sizes were

Table 2. Size of fossils, Guttenberg outcrop, in millimeters. s = standard deviation, n = number of points. Refer to figure 7 for graph.

Unit	Brachiopods			Non-prasoporan bryozoans			Prasopora			Other		
	mean	s	n	mean	s	n	mean	s	n	mean	s	n
A	115.0	116.0	193	169.7	89.9	12	—	—	0	66.4	52.7	51
B	144.5	120.3	150	188.7	115.6	13	228.0	0.0	1	95.1	50.2	37
C	91.0	83.0	211	240.2	158.8	58	426.2	121.2	11	104.1	95.0	25
D	157.0	122.9	122	227.1	122.4	31	91.5	31.8	2	66.2	37.8	51
E	189.9	102.1	23	234.6	184.1	13	160.0	84.9	2	113.4	80.3	14
F	66.3	57.3	247	234.6	160.1	9	328.0	0.0	1	58.7	52.2	93

1.41 mm (s [standard deviation] = 1.33) outside the zonule and 1.36 mm (s = 1.20) in the zonule. For 154 non-prasoporan bryozoans, mean sizes were 2.33 mm (s = 1.38) outside the zonule and 2.72 mm (s = 1.68) inside the zonule.

Brachiopod fragment sizes coarsen upward from zonule layer C to zonule layer E and from non-zonule unit A to non-zonule unit B (fig. 7, table 2). Average sizes of non-prasoporan bryozoan fragments exhibit no such trends within or outside of zonule layers, but fluctuate erratically upward (fig. 7; table 2).

DISCUSSION

The most striking feature of the faunal data is the inverse relationship between the abundances of brachiopods and bryozoans (including *Prasopora* and other bryozoans). The most prominent feature of the lithologic data is the decrease in mud content from unit B to unit C at the base of the *Prasopora* zonule. This coincides with a decrease in brachiopods and an increase in bryozoans. To shed light on these observations, we considered a variety of sedimentologic, taphonomic, and paleoecologic factors.

Rock type does not change much from unit to unit. All units are calcareous with small amounts of silt and argillaceous material. Bioturbation obscures other sedimentary structures. Dolomitization is variable (for instance, unit E is mostly undolomitized), but does not appear to be related to the presence or absence of the zonule in the units. Sedimentary texture varies among units (units C and D are packstone and the rest are mudstone–wackestone). Particularly noticeable is the decrease in proportion of finer-

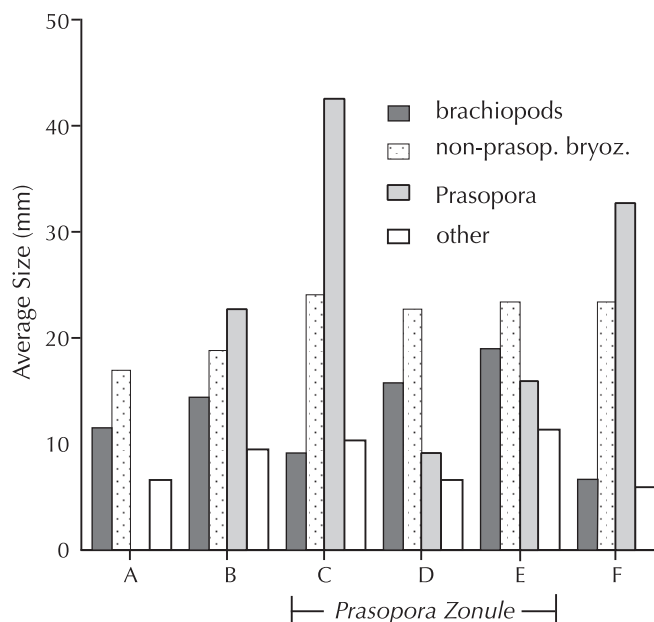


Figure 7. Size of fossils, Guttenberg outcrop. The longest axis of each fossil grain in thin section was measured using a digital image processor. See table 2 for size measurements.

grained sediments at the base of the zonule; a shift back to higher proportions of fine sediment is evident upward and out of the zonule. This variation in sedimentary texture likely represents a change in paleoenvironment (substrate or environmental energy).

We considered hydraulic sorting as a taphonomic explanation for the observed faunal patterns. Alternating environmental energies inside and outside the zonule could result in differential breakage of fossil types, ultimately affecting abundances observed from point counts; however, we have no evidence supporting this. Measurements of the fossil groups show no trends in size with respect to position in relation to the

zonule. Because sedimentary structures other than burrows are absent, it is difficult to determine the extent of reworking by waves and currents. That the *Prasopora* colonies in the zonule are not in life position, do not exhibit a preferred orientation, and are unfragmented with only slight abrasion suggests that the colonies were swept up, tumbled around, and redeposited near where they had grown. Evidence of long-distance transport or repetitive wave action is lacking.

Repeated scouring of the submarine surface appears to have occurred in the Galena sea, as evidenced by the many hardgrounds. These hardgrounds have been interpreted as cemented submarine erosion surfaces because signs of subaerial exposure, such as mudcracks and evaporites, are absent. Hardgrounds could have served as colonization surfaces for brachiopods and bryozoans. Studies of microhabitat partitioning and colonization of hardgrounds show that shallow, stormy shelf environments can contain series of living communities overlying dead, cemented ones (Palmer and Palmer, 1977; Brett and Liddell, 1978; Arens and Cuffey, 1989; Wilson and others, 1992). However, our examination of thin sections as well as outcrops revealed no evidence of *Prasopora* or other bryozoans cementing themselves to the hardground surface or to brachiopod shells in units A–F.

The alternation of brachiopod and bryozoan abundances around the *Prasopora* zonule may reflect differential tolerances of these organisms to environmental conditions or substrates. Many of the brachiopods that characterize the Galena Group (for example, *Sowerbyella* and *Rafinesquina*) are those that used their broadness and flatness to create a snowshoe effect that allowed them to rest on soft bottoms and keep their shell margins above the sediment-water interface (Rose, 1967; Thayer, 1975; Lehman and Pope, 1989). The Dunleith Formation's branching and fan-shaped bryozoans, such as *Batostoma* and *Hallopora*, could not have remained upright and functional on a mud substrate as easily as the broad, flat brachiopods. At Guttenberg, the non-zonule layers might represent times when an abundance of carbonate mud prevented bryozoans from colonizing as rapidly as brachiopods. Then, perhaps when sediments more suitable for attachment were available, as in unit C, bryozoans could dominate the substrate and remain even as carbonate mud content rose again.

The shift in dominant grain size at the start of the zonule could account for the alternating abundances of brachiopods and non-prasoporan bryozoans, but it

does not explain the concentration of *Prasopora* in the zonule. In Dunleith-equivalent rocks elsewhere, *Prasopora* is found in shale. On the eastern edge of the North American craton, where orogenic activity and delta formation occurred, *Prasopora* is found most commonly in siliciclastic shales or carbonate mudstones and shaly mudstones (Sparling, 1964; Ross, 1967; Arens and Cuffey, 1989). To the north of Guttenberg, nearer the Transcontinental Arch, zonule-equivalent outcrops near Decorah, Iowa, and Spring Grove, Minnesota, consist primarily of siliciclastic shale (Levorson and Gerk, 1972–1973). Elsewhere in the Decorah area, *Prasopora* has been collected from fine-grained carbonate and shale layers of the Decorah Subgroup (Delgado, 1983; Sloan, 1987). Thus, the presence of *Prasopora* is not limited to a particular lithologic facies.

The St. James–Beecher transition is an important interval in the Dunleith Formation because not only is the *Prasopora* zonule a prominent feature, but a change in the sedimentology and other biota is also evident. The St. James–Beecher contact is widely recognized in the Upper Mississippi Valley as marking a shift from relatively shaly carbonate in the Buckhorn and St. James Members to relatively pure carbonate sediment above (Templeton and Willman, 1963; Willman and Kolata, 1978). The amount of shale present varies with proximity to the Transcontinental Arch (fig. 3). In southeastern Minnesota, the Buckhorn–St. James interval is sometimes referred to as nearly pure shale, and the overlying Beecher equivalent (Cummingsville Formation) is a shaly limestone (Witzke, 1987; Sloan, 1997). Despite lithostratigraphic name changes, the boundary between the shalier interval (below) and the more carbonate-rich interval (above) is traceable on a regional basis. The *Prasopora* zonule is present at this boundary, regardless of the particular lithofacies present. Witzke and Bunker (1996) placed the entire lower Dunleith in one depositional cycle (number 5A in their terminology) and indicated that it was apparently subdivided into finer-scale cycles (fig. 2 of Witzke and Bunker, 1996). They regarded the presence of shale as a progradational indicator and purer carbonates as showing deepening. The sharpness of the St. James–Beecher boundary and the presence of numerous hardground surfaces in the Beecher suggest an abrupt increase in water depth, which shut off clastic influx and winnowed the seafloor. The *Prasopora* zonule would thus mark the final shoaling stage of the St. James sequence and the initial stage of transgression in the Beecher sequence.

CONCLUSIONS

The most striking features of our data are the alternating abundances of brachiopods and bryozoans in Guttenberg units A–F and the drop in mud content in the first zonule layer. The *Prasopora* zonule, which on a regional scale marks an important lithologic transition, appears to record an environmental or ecological change. The results of lithologic and faunal counts from the Guttenberg outcrop rule out taphonomy, environmental energy shifts, or sediment composition (meaning mineralogy, not texture) as explanations for the abundance of *Prasopora* in the zonule. The abundance of fine sediment (carbonate mud) is related to the proportion of bryozoans (*Prasopora* and non-*Prasopora*) in some of the Guttenberg units A–F. Thus, although the exact significance *Prasopora* concentrations in the Dunleith Formation is still unclear, sedimentary texture appears to be a controlling factor in the alternating abundances of brachiopods and bryozoans in the Guttenberg units.

ACKNOWLEDGMENTS

We thank Roger Cuffey for providing extremely helpful bryozoological information and insightful discussion, without which this study could not have been completed. We also thank Dianna Padilla for her input and Norlene Emerson for her help scouting localities. In addition, we thank the reviewers, whose comments greatly improved this manuscript. The Paleontological Society and the Department of Geology and Geophysics at the University of Wisconsin–Madison provided funds for this project.

REFERENCES

- Arens, N.C., and Cuffey, R.J., 1989, Shallow and stormy: The Middle Ordovician paleoenvironments in central Pennsylvania: *Northeastern Geology*, v. 11, no. 4, p. 218–224.
- Bassler, R.S., 1953, Part G, Bryozoa in Moore, R.C., ed., *Treatise on Invertebrate Paleontology*: University of Kansas Press and Geological Society of America, Lawrence, Kansas, p. G1–G23.
- Brett, C.E., and Liddell, W.D., 1978, Preservation and paleoecology of a Middle Ordovician hardground community: *Paleobiology*, v. 4, no. 3, p. 329–348.
- Choi, Y.S., 1995, Stratigraphy and sedimentation of the Middle Ordovician Sinnipee Group, eastern Wisconsin: M.S. thesis, University of Wisconsin–Madison.
- Cuffey, R.J., 1997, *Prasopora*-bearing event beds in the Coburn Limestone (Bryozoa; Ordovician; Pennsylvania) in Brett, C.E. and Baird, G.C., eds., *Paleontologic Events: Stratigraphic, Ecological, and Evolutionary Implications*: Columbia University Press, New York, p. 110–130.
- Delgado, D.J., ed., 1983, Ordovician Galena Group of the Upper Mississippi Valley—Deposition, diagenesis, and paleoecology, Great Lakes SEPM 13th Annual Field Conference Guidebook, 135 p.
- James, N.P., 1990, Cool water carbonate sediments: Viable analogues for Paleozoic limestones? in The 13th International Sedimentological Congress: International Association of Sedimentologists, Comparative Sedimentology Division, Utrecht, Netherlands, p. 245–246.
- Kay, G.M., 1929, Stratigraphy of the Decorah Formation: *Journal of Geology*, v. 32, p. 639–670.
- Kolata, D.R., 1975, Middle Ordovician echinoderms from northern Illinois and southern Wisconsin: Paleontological Society Memoir 7, 74 p.
- Kolata, D.R., 1987, Lithostratigraphy of the Platteville, Galena, and Maquoketa Groups in Northern Illinois in Sloan, R.E., ed., Middle and Late Ordovician lithostratigraphy and biostratigraphy of the Upper Mississippi Valley: Minnesota Geological Survey Report of Investigations 35.
- Kolata, D.R., Frost, J.K., and Huff, W.D., 1986, K-Bentonites of the Ordovician Decorah Subgroup, Upper Mississippi Valley: Correlation by chemical fingerprinting: Illinois State Geological Survey Circular 537, 30 p.
- Lehman, D., and Pope, J.K., 1989, Upper Ordovician tempestites from Swatara Gap, Pennsylvania: Depositional processes affecting the sediments and paleoecology of the fossil faunas: *Palaios*, v. 4, p. 553–564.
- Levorson, C.O., and Gerk, A.J., 1972–1973, A preliminary stratigraphic study of the Galena Group of Winneshiek County, Iowa: Proceedings: Iowa Academy of Science, v. 79, nos. 3–4, p. 111–122.
- Levorson, C.O., Gerk, A.J., Sloan, R.E., and Bisagno, L.A., 1987, General section of the Middle and Late Ordovician strata of northeastern Iowa in Sloan, R.E., ed., Middle and Late Ordovician lithostratigraphy and biostratigraphy of the Upper Mississippi Valley: Minnesota Geological Survey Report of Investigations 35, p. 25–39.

- McKinney, F.K., and Jackson, J.B.C., 1989, *Bryozoan Evolution*: University of Chicago Press, Chicago, 238 p.
- Palmer, T.J., and Palmer, C.D., 1977, Faunal distribution and colonization strategy in a Middle Ordovician hardground community, *Lethaia*, v. 10, no. 3, p.179–199.
- Rose, J.N., 1967, The fossils and rocks of eastern Iowa: Iowa Geological Survey, Educational Series I, 147 p.
- Ross, J.P., 1967, Evolution of ectoproct genus *Prasopora* in Trentonian time (Middle Ordovician) in northern and central United States: *Journal of Paleontology*, v. 41, no. 2, p. 403–416.
- Sanders, H.C., 1996, Distribution and Paleocology of *Prasopora* in the Galena Group (Ordovician) of the Upper Mississippi Valley: M.S. thesis, University of Wisconsin–Madison.
- Sloan, R.E., ed., 1956, Lower Paleozoic of the Upper Mississippi Valley in Schwartz, G.M., ed.: Guidebook for Field Trips, Minneapolis Meeting, Geological Society of America.
- Sloan, R.E., ed., 1987, Middle and Late Ordovician lithostratigraphy and biostratigraphy of the Upper Mississippi Valley: Report of Investigations 35, Minnesota Geological Survey, 232 p.
- Sloan, R.E., 1997, Middle Ordovician carbonate stratigraphy of the type Chatfieldian and biostratigraphy of a recovery from a mass extinction: Guidebook for the 27th Annual Field Conference, GLS-SEPM, p. 1–35.
- Sokal, R.R., and Rohlf, F.J., 1981, *Biometry: The Principles and Practice of Statistics in Biological Research*: W.H. Freeman and Co., San Francisco, 859 p.
- Sparling, D.R., 1964, *Prasopora* in a core from the Northville area, Michigan: *Journal of Paleontology*, v. 38, no. 6, p. 1072–1081.
- Templeton, J.S., and Willman, H.B., 1963, Champlainian Series (Middle Ordovician) in Illinois: Illinois State Geological Survey Bulletin 89, 260 p.
- Thayer, C.W., 1975, Morphologic adaptations of benthic invertebrates to soft substrata: *Journal of Marine Research*, v. 33, no. 2, p. 177–189.
- Willman, H.B., and Kolata, D.R., 1978, The Platteville and Galena Groups in Northern Illinois: Illinois State Geological Survey Circular 502, 75 p.
- Wilson, M.A., Palmer, T.J., Guensburg, T.E., Finton, C.D., and Kaufman, L.E., 1992, The development of an Early Ordovician hardground community in response to rapid seafloor calcite precipitation: *Lethaia*, v. 25, no. 1, p. 19–34.
- Witzke, B.J., 1980, Middle and Upper Ordovician paleogeography of the region bordering the Trans-Continental Arch, in Fouch, T.D. and E.R. Magathan, eds.: Paleozoic Paleogeography of the West-Central United States: Rocky Mountain Paleogeography Symposium I, SEPM Rocky Mountain Section, p. 1–18.
- Witzke, B.J., 1987, Middle and Upper Ordovician stratigraphy of the Iowa subsurface, in Sloan, R.E., ed., Middle and Late Ordovician lithostratigraphy and biostratigraphy of the Upper Mississippi Valley: Minnesota Geological Survey Report of Investigations 35, p. 40–41.
- Witzke, B.J., and Bunker, B.J., 1996, Relative sea-level changes during middle Ordovician through Mississippian deposition in the Iowa area, North American craton, in Paleozoic sequence stratigraphy: Geological Society of America Special Paper 306, p. 307–330.

SEDIMENTOLOGY AND SEQUENCE STRATIGRAPHY OF A LOWER ORDOVICIAN MIXED SILICICLASTIC–CARBONATE SYSTEM, SHAKOPEE FORMATION, FOX RIVER VALLEY OF EAST-CENTRAL WISCONSIN

Christopher L. Johnson¹ and J.A. (Toni) Simo^{1, 2}

ABSTRACT

The mixed siliciclastic–carbonate facies of the Shakopee Formation in east-central Wisconsin were deposited in a peritidal setting in two depositional sequences separated by a previously undocumented intra-Shakopee unconformity. The intra-Shakopee unconformity is regionally continuous in the study area and is characterized by 8 m of vertical erosional relief in an incised valley network. The incised valley has a channel-like morphology and contains deformed deposits consisting of a thick wedge of siliciclastics and multiple meter-scale, angular, carbonate blocks that dip into the center of the valley. We interpreted the intra-Shakopee unconformity to be a subaerial exposure surface because of the erosional relief, normal faults, and tilted strata; we interpreted the tilted strata and normal faults to have been caused by cave collapse from karstification. Deformation of the siliciclastics and carbonates in the incised valley was probably caused by differential compaction resulting from differential lithification rates of carbonates in relation to siliciclastics. The tilted blocks are truncated by a near-horizontal surface with incised valleys.

The two sequences are 1 and 2, oldest to youngest. The intra-Shakopee unconformity is the upper bounding surface for sequence 1 and the lower bounding surface for sequence 2. The exposed part of sequence 1 consists of a highstand systems tract. Sequence 2 contains a lower transgressive systems tract and an upper highstand systems tract. The highstand system tracts consist of mixed siliciclastic–carbonate facies in meter-scale, shallowing-upward (coarsening-upward) cycles. The cycles are not regionally continuous and in many places are bounded by erosional surfaces. The cycle facies variability suggests an autocyclic peritidal island facies model. The transgressive systems tract consists of deformed siliciclastics that fill the incised valley, which is overlain by a marine flooding surface.

Facies-defining cycles are divided into grainy carbonate, muddy carbonate, sandstone, shale, and stromatolitic–algal mat boundstones. The grainy carbonate facies is further subdivided into quartz sand grainstones, oolitic grainstones, and peloidal grainstones. The grainy and stromatolitic–algal boundstone facies were deposited in a subtidal to supratidal environment. The muddy dolostone, sandstone, and shale facies were deposited in a subtidal environment.

INTRODUCTION

The purpose of this study was to document the previously undocumented intra-Shakopee unconformity associated with an incised valley system as well as the anomalous dips of the strata first recognized by Chamberlin (1877) within the Shakopee and Platteville Formations of east-central Wisconsin. The incised valley contains siliciclastic facies similar to those of the St. Peter Formation, but stratigraphic relationships indicate that it is in the Shakopee Formation. In this study we reconstructed the sequence stratigraphy and the depositional environments of the Shakopee Forma-

tion east of the Wisconsin Dome. Because of the discontinuity of the St. Peter Formation in this area, the basal unconformity of the St. Peter and the Platteville Formations is collectively called the post-Shakopee unconformity in this paper.

The Lower Ordovician Shakopee Formation is a mixed siliciclastic–carbonate peritidal part of the Prairie du Chien Group that crops out around the Wisconsin Dome and in parts of Minnesota, Iowa, and Illinois (fig. 1). The Shakopee Formation was deposited in a shallow-water cratonic epeiric sea that flooded North America and consists of heterogeneous litholo-

¹Department of Geology and Geophysics, University of Wisconsin, Madison, Wisconsin 53706

²Now at ExxonMobil, URC GW3 908B, P.O. Box 2189, Houston, Texas 77252

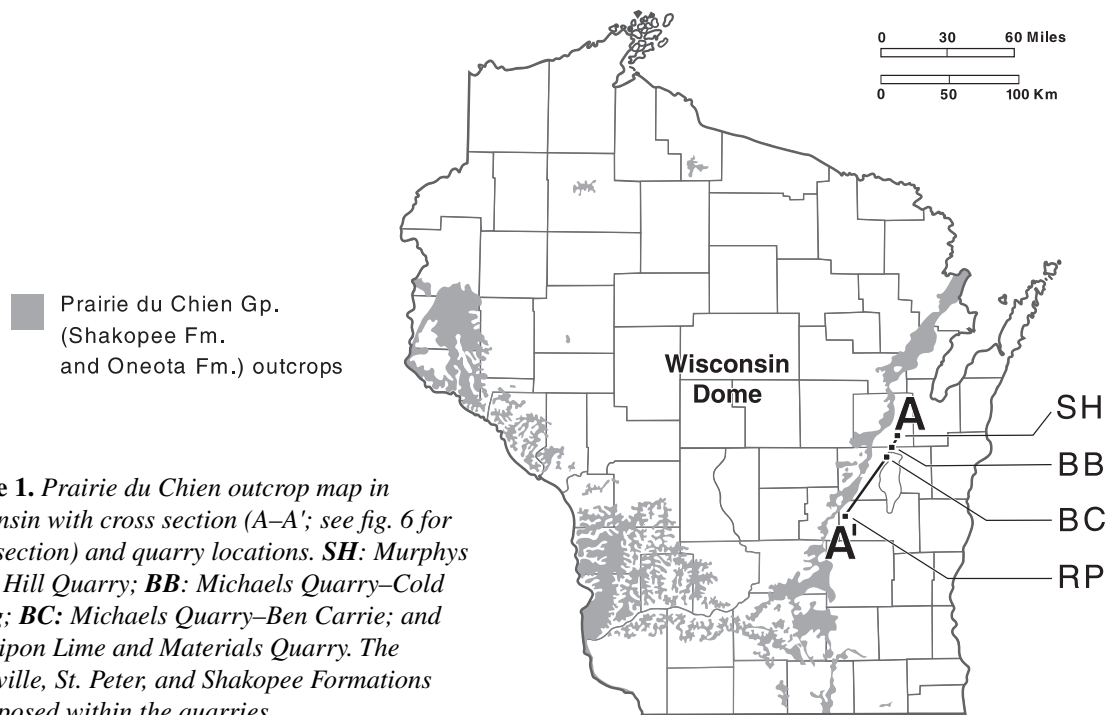


Figure 1. *Prairie du Chien outcrop map in Wisconsin with cross section (A–A’; see fig. 6 for cross section) and quarry locations. SH: Murphys Skunk Hill Quarry; BB: Michaels Quarry–Cold Spring; BC: Michaels Quarry–Ben Carrie; and RP: Ripon Lime and Materials Quarry. The Platteville, St. Peter, and Shakopee Formations are exposed within the quarries.*

gies and shallowing-upward cycles; stromatolites and gastropods indicate a peritidal depositional environment (this study; Davis, 1966; Smith and others, 1993, 1996). Our paper is the result of a senior thesis at the University of Wisconsin–Madison (Johnson, 1998).

Previous work

The Prairie du Chien Group is divided into the Oneota and Shakopee Formations (Ulrich, 1911, 1924). The Shakopee Formation consists of the New Richmond and Willow River Members. Early regional studies of the Shakopee Formation in the Mississippi River Valley in western Wisconsin were conducted by Winchell (1874), Wooster (1882), and Chamberlin (1877). Ulrich (1911, 1924) was the first to recognize the Shakopee and Oneota Formations as unconformity bounded units.

More recent studies were conducted by Davis (1966) on the Willow River Member of the Shakopee Formation in western Wisconsin and by Smith (1991) and Smith and others (1993, 1996) on the Prairie du Chien Group in Wisconsin and Michigan. Davis (1966) described the depositional environments as current dominated, open marine, wave dominated, shallow marine, and intertidal. Davis’ interpretation showed a general deepening and decreasing of energy upward throughout the Willow River Member. Davis (1966) suggested that the Wisconsin Dome emerged

at the end of the Lower Ordovician. The studies of Smith (1991) and Smith and others (1993, 1996) suggested that eustasy, rather than tectonics, controlled depositional packaging during the time when the Prairie du Chien was deposited. Figure 2 illustrates the regional sequence stratigraphic interpretation adapted from Smith and others (1993, 1996). The unconformity between the Oneota and Shakopee Formations is an emergent sequence boundary. The Willow River Member is capped by an emergent sequence boundary, ending the Sauk Sequence (Smith and others, 1993, 1996). Smith (1991) compared the shoaling-upward sequences in the Shakopee Formation to the “low energy intertidal stromatolite sequences” of James (1984).

METHODS

We developed our descriptions of the strata by measuring detailed stratigraphic sections, sketching cross sections, and mapping three-dimensionally important surfaces with a total station, an infra-red laser distance-measurement device. All percentage measurements in the study are field approximations. The quarries studied (fig. 1) are 1) Ripon Lime and Materials Quarry in Ripon, Wisconsin (Highway 151 north to Highway 49 north to Liberty Road west); 2) Michaels Quarry–Ben Carrie, Neenah, Wisconsin (Highway 151 north to Highway 41 north to Highway

PERIOD	FORMATION	WEST WISCONSIN DOME - MICHIGAN BASIN		CONTINENT WIDE	EAST-CENTRAL WI DOME
		SMITH AND OTHERS, 1996		SHUTTER 1992	THIS STUDY
M. ORDOVICIAN	PLATTEVILLE	X		X	PLATTEVILLE
	ST. PETER	TONTI	mfs, TST, TS	TIPPECANOE A	ST. PETER
L. ORDOVICIAN	PRAIRIE DU CHIEN GP. SHAKOPEE	IV	WILLOW RIVER	HST	SAUK C 2.3
		III	NEW RICHMOND	TS / SB / mfs	SAUK C 2.2
		II	HAGER CITY	TS / SB	SAUK C 2.1
		I	STOCKTON HILL	TS / SB / mfs	SAUK C 1.2
				TS / SB	SAUK C 1.1
U. CAMB.	JORDAN	VAN OSER	HST	SAUK B	NOT EXPOSED IN STUDY AREA

Figure 2. Formations and sequence stratigraphic interpretations of the Lower Ordovician in Wisconsin (after Smith and others, 1996; Shutter, 1992) compared to this study. HST: highstand system track, TST: transgressive system track; LSW-ivf: incised valley fill of lowstand system wedge; mfs: maximum flooding surface; TS: transgressive surface; SB: sequence boundary; ivf: incised valley fill. Sequence numbers from Schutter (1992).

114 west to Tular Lane north); 3) Michaels Quarry–Cold Spring, Neenah, Wisconsin (Highway 151 north to Highway 41 north to Highway BB west to Cold Spring south); and 4) Murphys Skunk Hill Quarry (Highway 151 north to Highway 41 north to Highway E north to Highway C north).

The basis of the sequence stratigraphic interpretation was the regional correlation of the intra-Shakopee and post-Shakopee unconformities between all four quarries in east-central Wisconsin. We applied sequence stratigraphic concepts and terminology from Van Wagoner and others (1988) to the sequence stratigraphic interpretations. We classified dolostone facies according to Dunham's (1962) textural classification scheme; bedding, according to Ingram (1954).

RESULTS

Facies description

The Shakopee Formation is characterized by a heterogeneous lithology composed of carbonates and siliciclastics on the bedform and bedset scale. Our study showed that the five major facies, in order of decreasing abundance, are 1) grain-supported dolostone (grainy facies); 2) matrix-supported dolostone

(muddy facies); 3) sandstone; 4) green shale; and 5) stromatolitic boundstone that contains gastropod and shell-fragment-rich grainstone. The grainy facies is subdivided into quartz sand, oolitic, and peloidal sub-facies because of the complexity and abundance of this facies in the Shakopee Formation.

Grain-supported dolostone facies

The grainy carbonate facies are dark gray, medium- to thin-bedded dolostones with moderately well preserved grainstone to packstone textures. Skeletal components are whole-shell gastropods and unidentified shell fragments; non-skeletal components are quartz sand grains, ooids, peloids, and dolostone intraclasts. Sedimentary structures are imbricated flat pebble conglomerates or breccias, oblate to irregularly shaped vugs, mudcracks, shale intercalations (<3 mm), thick high-angle planar cross-beds (approximately 30 cm), and symmetrical ripples that have a 10 to 30 cm wavelength, burrow mottling, and chert nodules.

The following grainy subfacies are listed in order of decreasing abundance:

Quartz sand grainy subfacies. A medium-grained, well rounded quartz sand is in thin cross-bedded layers (2–20 mm), patches, lenses, and along ripple crests.

The concentration of quartz grains ranges from 0 to 50 percent, usually approximately 10 to 25 percent. Vugs, mudcracks, and breccia beds are common. We classify a facies that has greater than 50 percent quartz grains as a sandstone.

Oolitic grainy subfacies. Ooids are the major component (>10%) of this subfacies. Minor components (<10%) are medium-grained quartz sand (not in grain to grain contact), whole-shell gastropods, and other unidentified shell fragments. The ooids are identified by their size and spherical shape; their internal structure was destroyed by dolomitization.

Peloidal grainy subfacies. This subfacies appeared matrix-supported in the field, but thin sections revealed rounded, well sorted, medium-grained peloids. The peloids are structureless spheres of fine-grained dolomite that occur as matrix-supported individuals and in flocculent coalesced clots. Peloid preservation is poor and identification difficult in the field due to dolomitization.

Matrix-supported dolostone facies

The muddy carbonate facies is light gray to light brown, massive to thinly bedded and has moderately well preserved mudstone and packstone textures. Sedimentary structures include plane beds, wavy lamination, thin laminae of clay, thin beds of siltstone, and burrow mottling. Non-skeletal grains are lenses of quartz sand and rare mudstone intraclasts. Skeletal grains are absent.

Sandstone facies

This facies is a white, massive, thickly to thinly bedded, well rounded to subrounded, medium-grained sandstone consisting of mostly quartz grains (>90%) containing minor proportions of subrounded pebbles of mudstone-textured dolostone intraclasts and thin shale intercalations. In one location, angular cobble-size dolostone intraclasts were found. This facies may be well lithified by a calcareous matrix or poorly cemented. Bedding at quarry scale is continuous with minor lateral pinch out. Sedimentary structures are high (approximately 25°) and low (approximately 10°) planar cross-bedding and low amplitude (5-10 cm), wide (approximately 50 cm) basal scours. In one locality, this facies is a thick (approximately 8 m), wide (approximately 50 m) wedge that contains irregularly and thinly layered red chert and undulating shale (approximately 30 cm thick). Dipping dolostone blocks overlie this sandstone wedge, which is located in the incised valley described below.

Green shale facies

This facies is a thinly bedded green shale containing thin lenses of siltstone and sandstone. Beds greater than approximately 5 cm are laterally continuous in places and are recessive in outcrop.

Stromatolitic–algal mat boundstones facies

Stromatolitic heads are approximately 30 to 50 cm wide and thick and commonly are separated by approximately 10 to 50 cm wide areas filled with gastropod and shell-fragment-rich dolostone. In this study, algal mats are distinguished from stromatolites by their flat, wavy laminations. This facies is easily recognized in outcrop and is laterally continuous in places.

Description of stratal geometries

Faulting and stratal tilting

Underneath the post-Shakopee unconformity, the Shakopee Formation exhibits normal faulting and irregular tilting of strata. Four high-angle normal faults are present at the Ripon Lime and Materials Quarry in Ripon, Wisconsin (fig. 3A). The faults are truncated above by the intra-Shakopee unconformity. The dips on these faults range from 55° to 85° in the north, southeast, and southwest directions. Beds less than 1 m from the faults appear deformed in the direction of movement with approximately 10 to 50 cm of displacement (fig. 3A). The entire Shakopee Formation shows local tilting in the study area. These stratal undulations appear to have no preferred direction (Simo and others, 1996). Two types of tilted strata are in the area: strata truncated by the intra-Shakopee unconformity (fig. 3A, right side), and strata above and below the intra-Shakopee unconformity (fig. 3A, left side).

Valley fill and associated deformation

Convolute siliciclastic beds and many dipping dolostone blocks compose the thick sandstone wedge (referred to in the *Sandstone facies* section above). This wedge fills an incised valley cutting into beds in the underlying dolostone at Michaels Quarry–Ben Carrie (fig. 4A and 4C). The incised valley fill has a basal drape of shale that has thin lenses of sandstone. Figure 5 illustrates the shape, thickness, and orientation of the incised valley fill. The axis of the incised valley fill is oriented east–west. The facies in the incised valley are truncated above by an erosional surface and are bound below by an erosional surface with a minimum of 8 m of vertical relief. Some shale beds are truncated by the upper erosional surface, some are truncated by the dolostone blocks, and others have a

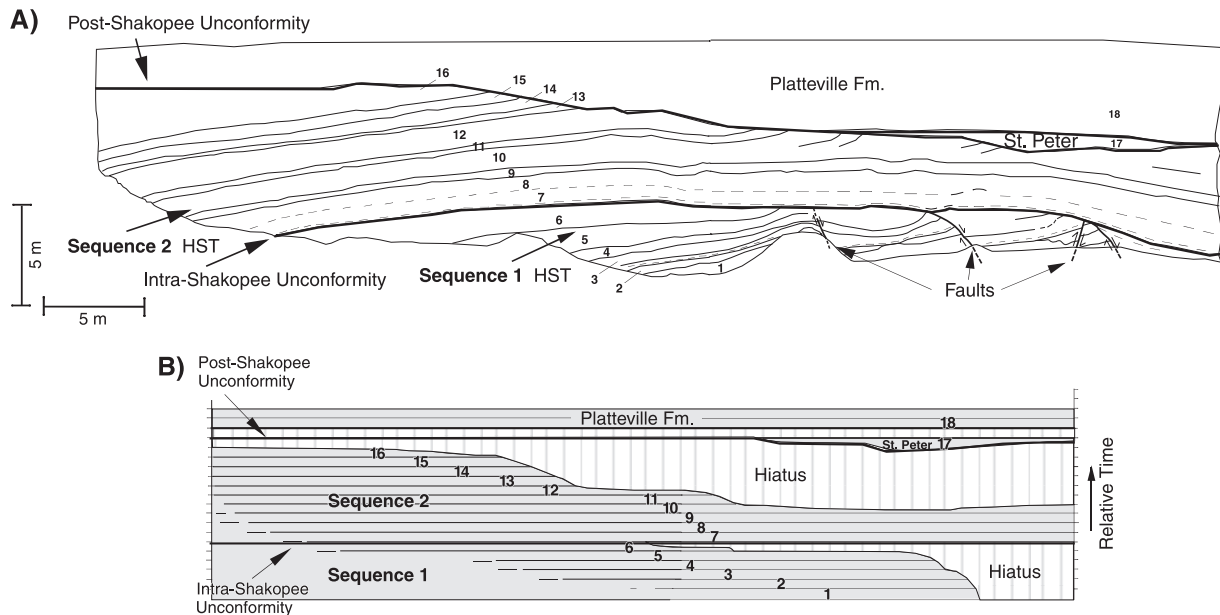


Figure 3. Cross section and Wheeler diagram from Ripon Lime and Materials Quarry. **A.** Cross section illustrating the unconformities, strata, truncation, congruent and incongruent tilting, and normal faulting. **B.** Wheeler diagram illustrating depositional sequences 1 and 2, hiatus periods of no deposition, and the two unconformities.

conformable contact with the dolostone blocks (fig. 4A and 3C). We did not determine whether the surface between the siliciclastics and dolostone blocks was erosional or non-erosional. The dolostone blocks are 3 to 20 m wide, angular with broken surfaces oriented perpendicular to bedding, and preferentially dip 4° to 30° into the center of the incised valley from both sides (fig. 4C). The facies of the dolostone blocks is grainy dolostone.

Unconformity surfaces

Two unconformity surfaces are recognized in the Shakopee Formation in the study area: the regionally recognized post-Shakopee unconformity, which is the boundary between the Sauk and Tippecanoe Supersequences of Sloss (1963), and a previously undocumented intra-Shakopee unconformity (figs. 3, 4, and 5).

The post-Shakopee unconformity is the upper bounding surface of the entire Shakopee Formation. This unconformity is characterized by a sharp lithologic contact between the Shakopee and St. Peter or Platteville Formations. The St. Peter Formation is absent in two of the four quarries in the study area and apparently pinches out from paleo-topographic highs on the Prairie du Chien Group (Simo and others,

1996). This surface is flat and laterally continuous; however, it undulates 1.5 m down into the incised valley fill of the Shakopee Formation below (fig. 5A).

The intra-Shakopee unconformity is characterized by the following:

- 8 m of erosional relief truncating dolostone beds below (fig. 4A);
- high-angle normal faults truncated by the unconformity above (fig. 3A);
- a regionally laterally continuous shale drape on the erosional surface; and
- a thick sandstone wedge that fills an incised valley above the intra-Shakopee unconformity. Figure 5 illustrates the features of the incised valley.

Regional correlation of the intra-Shakopee unconformity and post-Shakopee unconformity was possible because both were found at all four quarries in the study area. We did not observe the basal Shakopee unconformity (Shakopee–Oneota contact) in any of the quarries (fig. 6).

DISCUSSION

Depositional environment

The Shakopee Formation is a mixed siliciclastic–

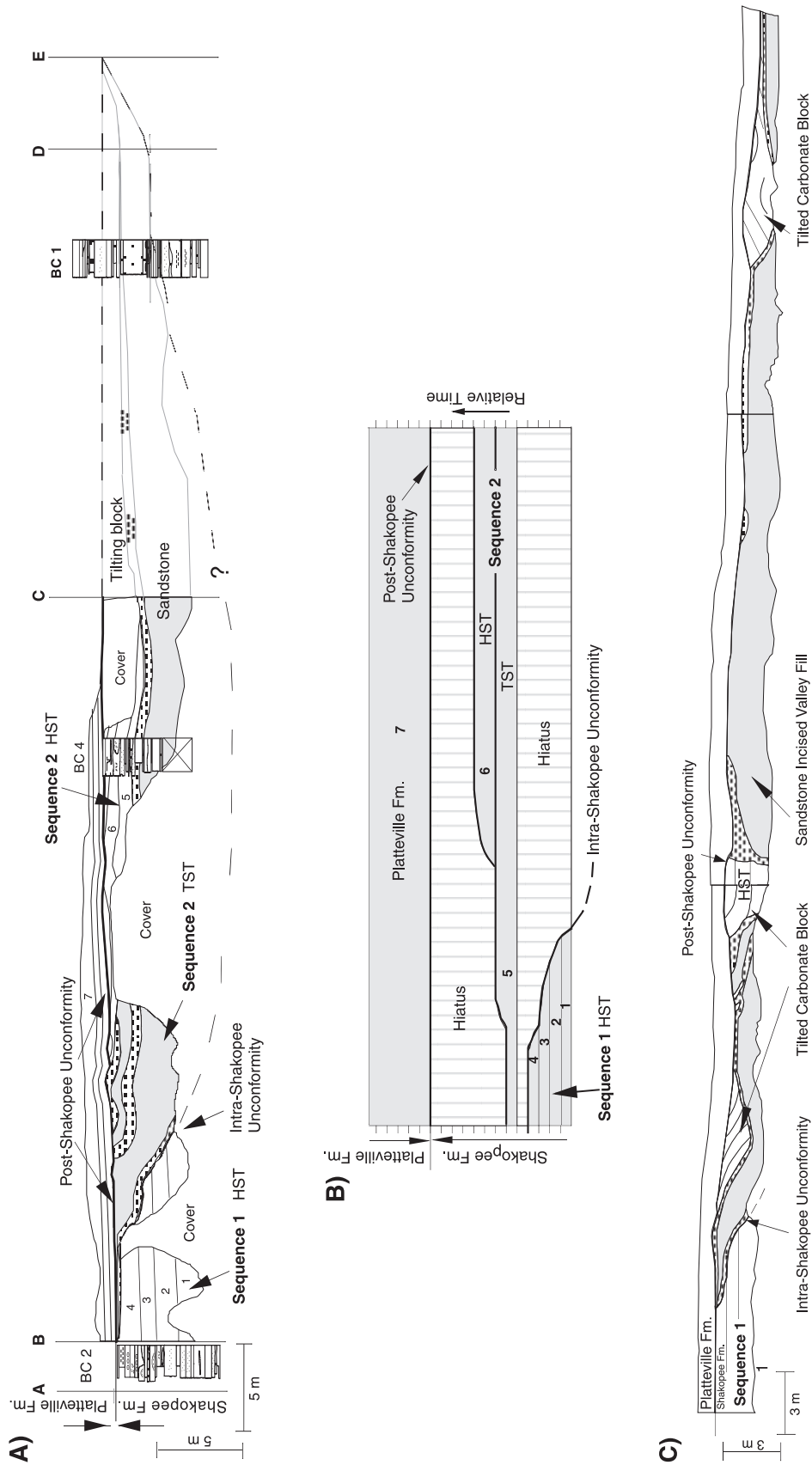


Figure 4. Cross sections and Wheeler diagram from Michaels Quarry–Ben Carrie. **A.** Cross section with stratigraphic sections illustrating the west axis of the incised valley system. **B.** Wheeler diagram illustrating depositional sequences 1 and 2, hiatus periods of no deposition, and the two unconformities. **C.** Cross section illustrating east axis of the incised valley, tilted carbonate blocks, and convoluted shale beds.

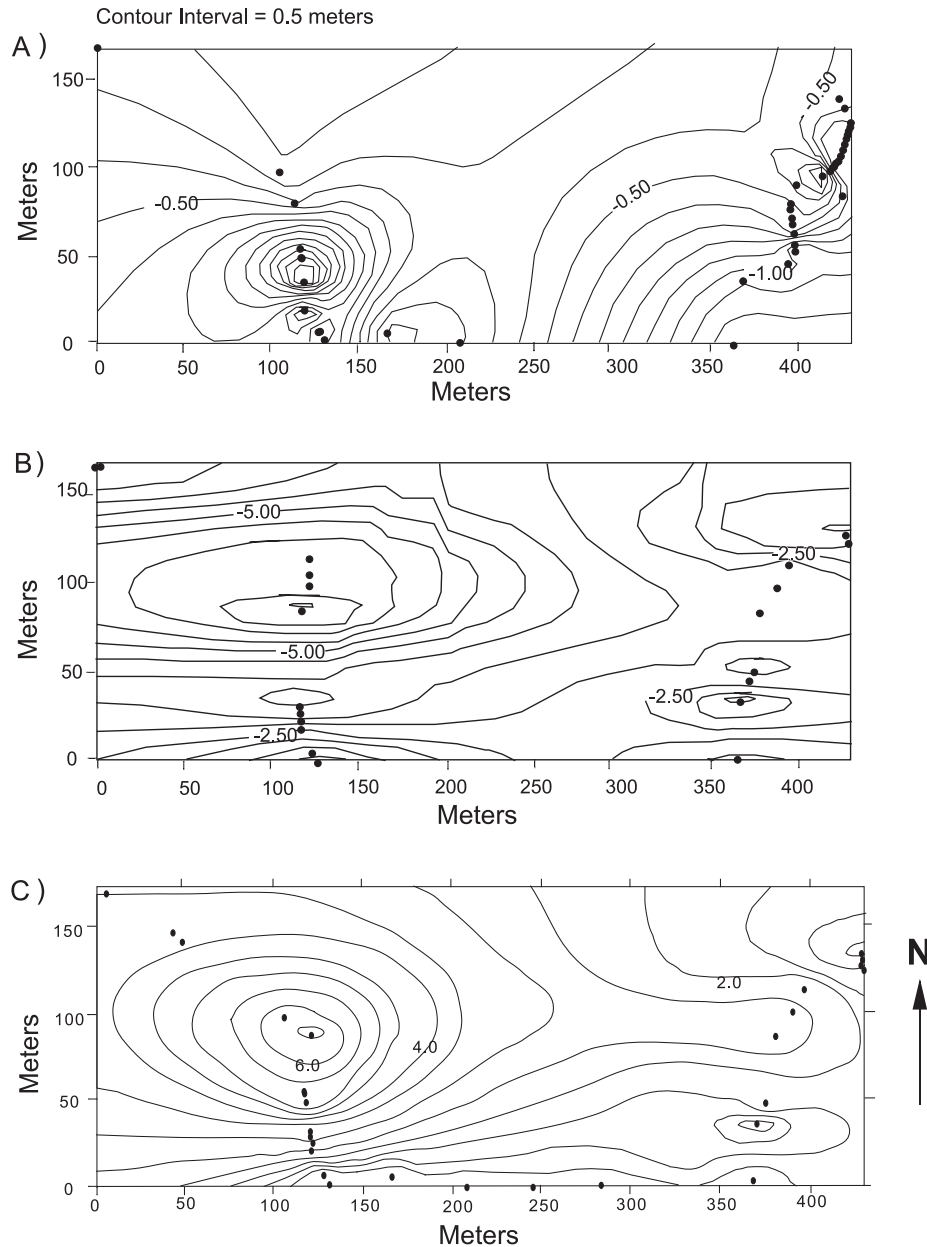


Figure 5. Contour and isopach maps created with a total station at Michaels Quarry-Ben Carrie. **A.** Contour map of St. Peter-Platteville unconformity. **B.** Contour map of the intra-Shakopee unconformity, illustrating the east-west axis orientation of the incised valley. **C.** Isopach map of sequence 2, illustrating the shape of the incised valley fill.

carbonate system deposited in a restricted, peritidal environment that was punctuated by erosion and incision of a valley network. This incised valley filled with siliciclastics and later carbonates. The grainy and stromatolitic-algal boundstone facies were deposited in a subtidal to supratidal environment (fig. 7). The muddy dolostone, sandstone, and shale facies were

deposited in a subtidal environment.

The features of the grainy dolostone facies indicative of a subtidal environment are the presence of a small amount of carbonate mud, which suggests winnowing by waves (Enos, 1983), and the presence of peloids, bioturbation, mottled textures, and fossils, which suggest the ability to sustain life (Shinn, 1983;

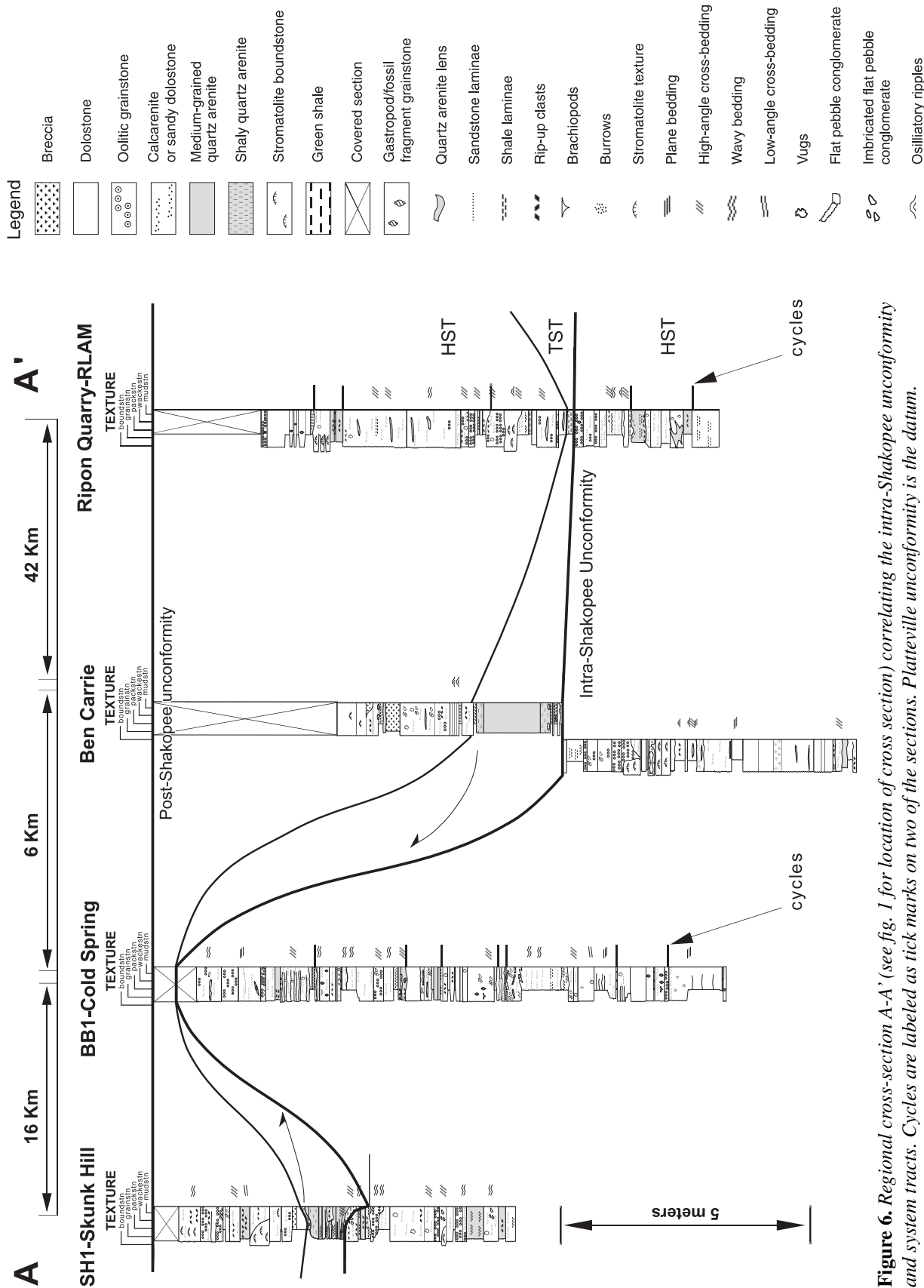


Figure 6. Regional cross-section A-A' (see fig. 1 for location of cross section) correlating the intra-Shakopee unconformity and system tracts. Cycles are labeled as tick marks on two of the sections. Platteville unconformity is the datum.

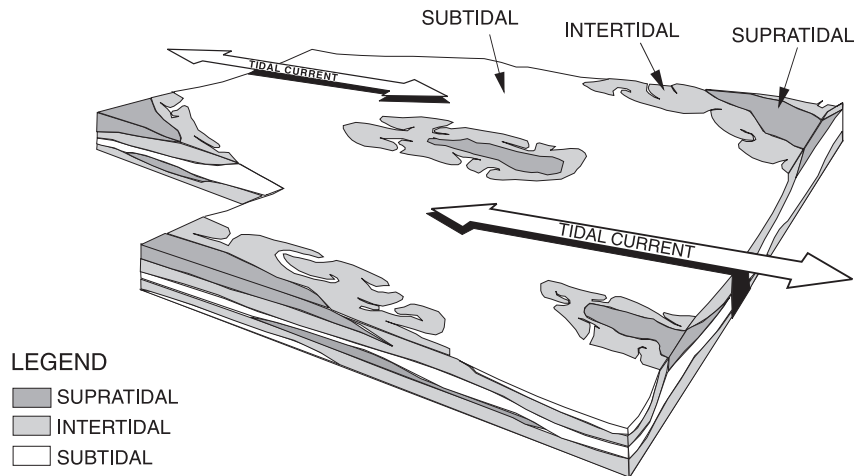


Figure 7. Hypothetical block diagram of the peritidal island facies model of Pratt and James (1986), showing an epeiric sea and laterally discontinuous sub-, inter-, and supratidal deposits.

Enos, 1983; James, 1984). The presence of ooids suggests constant wave agitation, which is common in the shallow subtidal realm (Enos, 1983). Features of the stromatolitic boundstone and grainy facies that suggest an intertidal setting are stacked hemispherical stromatolites that have generous spaces between hemispheres (Logan and others, 1964; Ginsburg, 1975), algal mats, preserved sedimentary structures, and mudcracks (Shinn, 1983).

The features of the muddy dolostone, sandstone, and shale facies indicative of a subtidal environment are siliciclastic and carbonate fines, which suggest little winnowing by waves, and massive textures, which indicate profuse bioturbation (Enos, 1983). Restrictive, highly saline, marine conditions are supported by the presence of stromatolites and gastropods (Enos, 1983), the location far inland on a shallow epeiric sea, and the presence of a facies mosaic (Laporte, 1967).

The small size of the incised valley, its channel-like shape, steep flanks, orientation perpendicular to the paleoshoreline, and location on the inner shelf of a wide epeiric sea suggest that it was eroded by fluvial processes. The siliciclastic facies filling the incised valley lack fluvial indicators such as a basal conglomerate and traction bedforms. The deposit has a basal shale drape and massive texture in the sandstones, suggesting the deposits are marine in origin. The shale was probably deposited as the relative sea level rose and a reworking surface removed fluvial deposits.

The source of the quartz sand in the Shakopee Formation probably was the emergent Wisconsin Dome because the sand decreases in abundance from

the Wisconsin Dome to the Michigan Basin (Smith, 1991). Davis (1966) interpreted the shale to be from granite on the Wisconsin Dome. This concentration of sand in the Wisconsin Dome in relation to that of the Michigan Basin implies that the sand source is older Wisconsin Dome Paleozoic sandstone (Davis, 1966; Mai and Dott, 1985; Smith and others, 1993, 1996). The Shakopee, Oneota, and Jordan Formations show formation-scale thinning toward the Wisconsin Dome from the Michigan Basin and Minnesota (Ahlen, 1952; Smith, 1991; Smith and others, 1993, 1996; Starke, 1949). This thinning suggests that the Wisconsin Dome was a topographically positive structure and siliciclastic source in the Lower Ordovician.

Cyclicality

Meter-scale, mixed siliciclastic–carbonate, shallowing-upward (coarsening-upward) cycles are exposed in Ripon Lime and Materials Quarry in Ripon and Michaels Quarry–Cold Spring. Similar cycles have been described in the literature (Smith, 1991; Smith and others, 1993, 1996; James, 1984). The cycle boundaries are recognized on the basis of erosional surfaces evidenced by a sharp lithologic contact of contrasting facies. These surfaces are recessive and in places laterally continuous in outcrop.

The cycles are defined by a basal erosional surface overlain by shale or sandstone that has a gradational contact upward to muddy carbonate facies. The middle section is dominated by oolitic, peloidal, and quartz-sandstone grainy carbonate subfacies with lesser amounts of the muddy carbonate facies. The lower

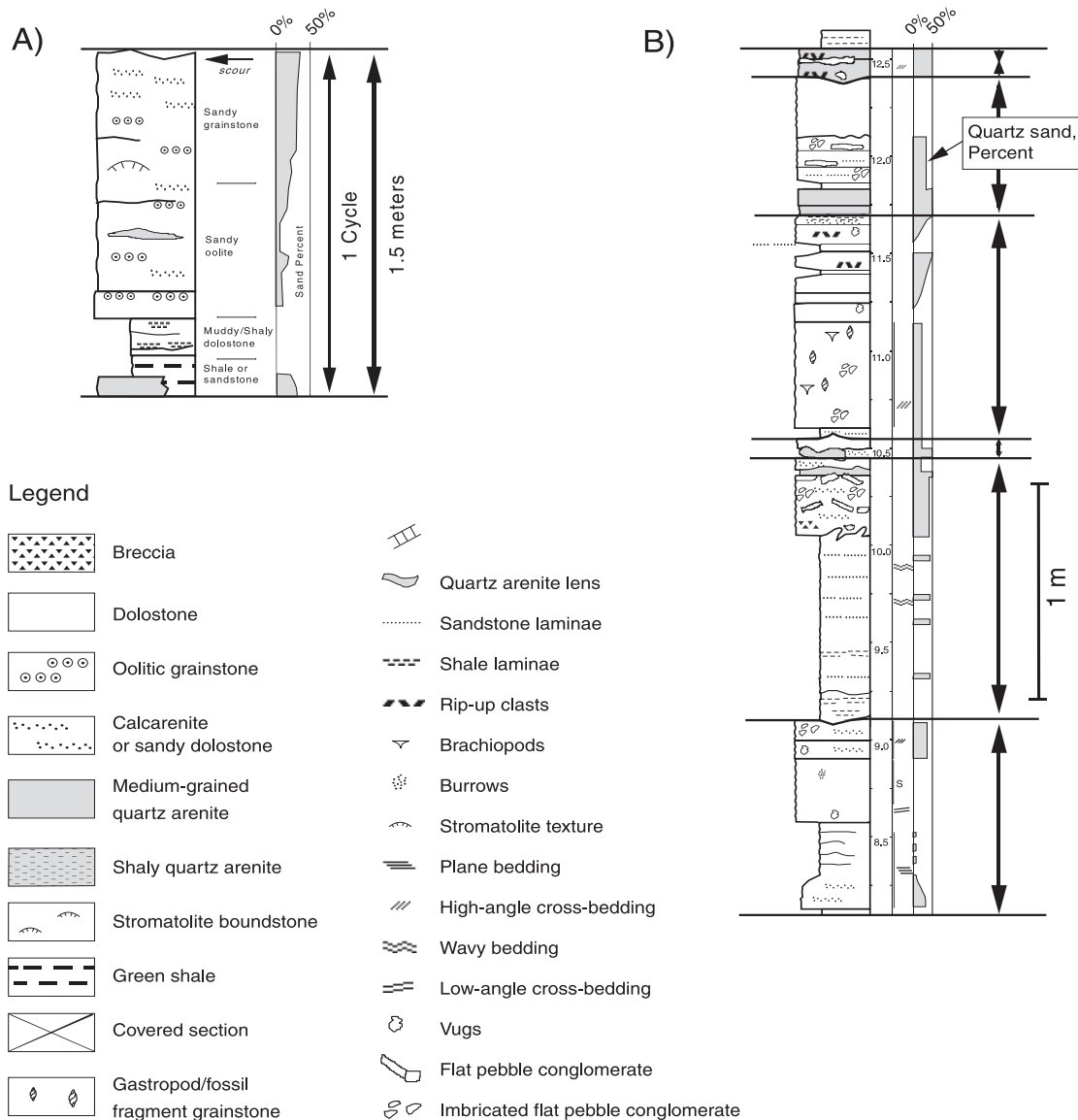


Figure 8. *Shallowing-upward cycles within the Shakopee Formation. A. Idealized cycle showing bounding erosional surfaces, shale and sandstone, argillaceous muddy carbonate, sandy oolite, stromatolites and sandstone lenses, and sandy grainstone. B. Cycle examples from Ripon Lime and Materials Quarry: Thick lines are cycle boundaries and individual cycle interval marked by arrows.*

and middle sections typically have wavy laminations, plane bedding, and low- to high-angle cross-bedding. The upper section of the cycle is characterized by mudcracks and increasing quartz sand up-section in the grainy carbonate facies. This description can be seen in the ideal cycle (fig. 8A) and cycle examples (fig. 8B). The cycles are laterally continuous only in places.

Similar meter-scale shoaling-upward cycles in

the Shakopee Formation in western Wisconsin and the Michigan Basin have been interpreted by Smith (1991) and Smith and others (1993, 1996) to have formed in low-energy intertidal environments that have prograding tidal flats and migrating tidal channels. The “muddy sequences” and “stromatolite sequences” of James (1984) and the cycles of Smith (1991) and Smith and others (1993, 1996) have basal grainy carbonate facies or pebble lag supporting the

tidal channel migration interpretation. In contrast, the Shakopee cycles in our study are characterized by basal sandstone and shale beds.

Two autocyclic models have been proposed by James (1984) to explain small-scale peritidal carbonate cycles in cratonic epeiric seas: the lateral progradation of a tidal-flat wedge model and the peritidal island facies model (fig. 7; Pratt and James, 1986). The peritidal island facies model originated from work in the St. George Group (Lower Ordovician) in western Newfoundland, Canada (Pratt and James, 1986). Due to the absence of laterally continuous cycles and the presence of shallowing-upward cycles, the peritidal island facies model is a better explanation than the prograding tidal-flat wedge model, although the prograding tidal-flat wedge model has not been disproven.

Sequence boundaries and sequences

Sequence boundaries

We characterized two bounding surfaces in quarries in Middle and Lower Ordovician strata in east-central Wisconsin. The two sequence boundaries are the intra-Shakopee unconformity and the post-Shakopee unconformity. The intra-Shakopee sequence boundary is an emergent surface indicating a relative fall in sea level. The post-Shakopee sequence boundary is a well established sequence boundary (Winchell, 1874; Chamberlin, 1877; Dott and others, 1986; Smith, 1991; Smith and others, 1993, 1996) representing the final regression of the Sauk epeiric sea in the study area. Both of the sequence boundaries are illustrated in Wheeler diagrams (figs. 3B and 4B).

Sequences

Smith and others (1993, 1996) interpreted the Shakopee Formation to be subdivided into three sequences (Sauk C2 2.1, 2.2, and 2.3, following Schutter, 1992, nomenclature). Smith and others (1993, 1996) interpreted the New Richmond Member (Sauk C2 2.1 and 2.2) to consist of a transgressive systems tract and a highstand systems tract and the Willow River Member (Sauk C2 2.3) to be only a highstand systems tract. The sequences in our study are not correlated to the sequence stratigraphic nomenclature of Schutter (1992) or Smith and others (1993, 1996) (fig. 2).

We identified two sequences in the Shakopee Formation in east-central Wisconsin: Sequence 1 is bounded on the bottom by the Oneota-Shakopee contact and on the top by the intra-Shakopee unconformity; sequence 2 is bounded at the bottom by the intra-Shakopee unconformity and on the top by the post-Shakopee unconformity. The upper part of sequence 1 is interpreted as the highstand systems tract; sequence 2 is interpreted to contain a transgressive systems tract

represented by the siliciclastic incised valley fill and a highstand systems tract represented by carbonate strata and blocks (fig. 4A, 4B, and 4C). The shape and thickness of sequence 2 are illustrated in the isopach map in figure 5C.

The transgressive systems tract is supported by marine siliciclastics and a partially truncating surface that separates the siliciclastics from the carbonates in the incised valley. Sarg (1988) speculated that this is a marine flooding surface. The highstand systems tract in each sequence is supported by shallowing-upward cycles, a facies mosaic, apparent aggradation due to consistent stacking of peritidal deposits, and preservation of peritidal sediments, which suggest no reworking by a wave reworking surface (Sarg, 1988). The Wheeler diagrams from two localities illustrate the sequence stratigraphic concept explained above (figs. 3B and 4B).

Interpretation of the stratal geometries

Faulting and stratal tilting

We interpreted the tilting of Lower Ordovician beds below unconformities to have resulted from the collapse of underlying cave systems (for example, Smith, 1991). The cave system would form from exposure and karstification associated with dissolution. Later, deposition of strata above the exposure surface would increase lithostatic pressure, causing cave roof collapse and normal faulting in the underlying strata and tilting of the overlying strata. This mechanism is hypothetical because cave collapse has not been documented in any of the field studies.

Deformation in incised valley fill

In the incised valley, convolution of siliciclastic deposits is associated with the collapse of overlying carbonate blocks. This collapse (fig. 4A and 4C) is explained by differential compaction of shale in relation to carbonates and/or de-watering of siliciclastics from overburden pressures created by lithified carbonates above. Peloids, intraclasts, and flat-pebble conglomerates suggest early lithification of the carbonate facies, resulting in a differential rate of lithification of carbonate facies to siliciclastic facies (Shinn, 1983). Differential rates of lithification are speculated to be the cause of differential compaction. The partial conformity of shale layers to the overlying carbonate blocks suggests a synchronous deformational origin of the convolute strata and dipping carbonate blocks (fig. 4A and 4C). We speculate that undulations in the Platville Formation above the incised valley fill were caused by post-Lower Ordovician compaction of the shale facies.

CONCLUSIONS

1) Facies in the study of the Lower Ordovician, Shakopee Formation, are alternating grainy dolostone, muddy dolostone, sandstone, shale, and stromatolitic–algal mat boundstone. Overall, the alternation is cyclic, representing variations in paleo-water depth within a restricted peritidal environment. The grainy dolostone and stromatolitic–algal boundstone facies were deposited in a subtidal to supratidal environment. The muddy dolostone, sandstone, and shale facies were deposited in a subtidal environment.

2) The previously undocumented intra-Shakopee unconformity is an emergent sequence boundary separating sequences 1 and 2. This sequence boundary corresponds to an incised valley filled with siliciclastic sediment and is regionally continuous. The surface truncates beds below and postdates normal faults. Strata overlying the incision consist of a shale drape and thick siliciclastic wedge.

3) The Shakopee Formation consists of two sequences. Sequence 1 consists of a highstand systems tract; sequence 2, a transgressive systems tract and a highstand systems tract. The highstand systems tract is composed of shallowing-upward cycles and peritidal dolostones in both sequences. The transgressive systems tract is composed of deformed siliciclastic deposits on top of the intra-Shakopee unconformity and in the incised valley. Above the incised valley fill the transgressive systems tract is overlain by a marine flooding surface and a highstand systems tract.

4) Associate strata to the intra-Shakopee unconformity are tilted and faulted, probably as a result of the overburden pressure of strata above paleocaves and differential compaction. Paleocaves associated with karstification from dissolution may have caused roof collapse. Differential lithification of carbonates in relation to siliciclastics caused differential compaction, resulting in convoluted siliciclastic deposits in the incised valley.

REFERENCES

- Ahlen, J.L., 1952, The regional stratigraphy of the Jordan Sandstone in west central Wisconsin: M.S. thesis, University of Wisconsin–Madison.
- Chamberlin, T.C., 1877, Geology of eastern Wisconsin, in *Geology of Wisconsin*, v. 2, part 2: Wisconsin Geological Survey, p. 268–287.
- Davis, R.A., 1966, Willow River Dolomite: Ordovician analogue of modern algal stromatolite environments: *Journal of Geology*, v. 74, p. 908–923.
- Dott, R.H., Jr., Byers, C.W., Fielder, G.W., Stenzel, S.R., Winfree, K.E., 1986, Aeolian to marine transition in Cambro-Ordovician cratonic sheet sandstones of the northern Mississippi Valley, U.S.A: *Sedimentology*, v. 33, p. 345–367.
- Dunham, R.J., 1962, Classification of carbonate rocks according to depositional texture, in *Classification of carbonate rocks: A symposium*: American Association of Petroleum Geologists Memoir 1, p. 108–121.
- Enos, P., 1983, Shelf environment, in Sholle, P.A., Bebout, D.G., Moore, C.H. [eds.], *Carbonate Depositional Environments*: American Association of Petroleum Geologists Memoir 33, p. 268–296.
- Ginsburg, R.N. [ed.], 1975, *Tidal Deposits*: Springer-Verlag, New York, p. 1–428.
- Ingram, R.L., 1954, Terminology for the thickness of stratification and parting units in sedimentary rocks: *Geological Society of America Bulletin*, v. 65, p. 935–938.
- James, N.P., 1984, Shallowing-upward sequences in carbonates, in Walker, R.G. [ed.], *Facies Models*: Geoscience Canada, Kitchener, Ontario, p. 213–228.
- Johnson, C.L., 1998, Sedimentology and sequence stratigraphy of a Lower Ordovician mixed siliciclastic–carbonate system, Shakopee Formation, east-central Wisconsin, senior thesis, University of Wisconsin–Madison, p. 68.
- Laporte, L.F., 1967, Carbonate deposition near mean sea-level and resultant facies mosaic; Manlius Formation (Lower Devonian) of New York State: *American Association of Petroleum Geologists Bulletin*, v. 51, p. 73–101.
- Logan, B.W., Rezak, R., Ginsburg, R.N., 1964, Classification and environmental significance for algal stromatolites: *Journal of Geology*, v. 72, p. 68–83.
- Mai, H., and Dott, R.H. Jr., 1985, A subsurface study of the St. Peter sandstone in southern and eastern Wisconsin: Wisconsin Geological and Natural History Survey Information Circular 47, 26 p.
- Pratt, B.R., and James, N.P., 1986, The St. George Group (Lower Ordovician) of western Newfoundland: Tidal flat island model for carbonate sedimentation in shallow epeiric seas: *Sedimentology*, v. 33, p. 313–343.

- Sarg, J.F., 1988, Carbonate sequence stratigraphy, in Wilgus, C.K., Hastings, B.S., Kendall, C.G. St. C., Posamentier, H.W., Ross, C.A., and Van Wagoner, J.C. [eds.], *Sea-Level Changes: An Integrated Approach*: Society of Economic and Petroleum Mineralogists Special Publication No. 42, p. 155–181.
- Schutter, S.R., 1992, Ordovician hydrocarbon distribution in North America and its relationship to eustatic cycles, in Webby, B.D., and Laurie, J.R. [eds.], *Global Perspectives on Ordovician Geology*: A.A. Balkema, Rotterdam, p. 421–432.
- Shinn, E.A., 1983, Tidal flat environment, in Sholle, P.A., Bebout, D.G., Moore, C.H., [eds.], *Carbonate Depositional Environments*: American Association of Petroleum Geologists Memoir 33, p. 172–210.
- Simo, J.A., Freiberg, P.G., Freiberg, K.S., 1996, Geologic Constraints on arsenic in groundwater with applications to groundwater modeling: University of Wisconsin–Madison Water Resources Center Groundwater Research Report 96-01.
- Sloss, L.L., 1963, Sequences in the cratonic interior of North America: *Geological Society of America Bulletin*, v. 74, p. 93–113.
- Smith, G.L., 1991, Sequence Stratigraphy and Diagenesis of the Lower Ordovician Prairie du Chien Group of the Wisconsin Arch and the Michigan Basin: Ph.D. thesis, University of Wisconsin, 265 p.
- Smith, G.L., Byers, C.W., and Dott, R.H., Jr., 1993, Sequence stratigraphy of the Lower Ordovician Prairie du Chien Group on the Wisconsin Arch and in the Michigan Basin: *American Association of Petroleum Geologists Bulletin*, v. 77, p. 49–67.
- Smith, G.L., Byers, C.W., and Dott, R.H., Jr., 1996, Sequence stratigraphy of the Prairie du Chien Group, Lower Ordovician, Midcontinent, U.S.A., in Wit-zke, B.J., Ludvigson, G.A., Day, J., [eds.], *Paleozoic Sequence Stratigraphy: Views from the North American Craton*: Geological Society of America Special Paper 306; p. 23–33.
- Starke, G.W., 1949, Persistent lithologic horizons of the Prairie du Chien Formation from the type section eastward to the crest of the Wisconsin Arch: M.S. thesis, University of Wisconsin, 29 p.
- Ulrich, E.O., 1911, Revision of the Paleozoic systems: *Geological Society of America Bulletin*, v. 22, p. 281–680.
- Ulrich, E.O., 1924, Notes on the new names in Table of Formations and on physical evidence of breaks between Paleozoic systems in Wisconsin: *Wisconsin Academy of Science Transactions*, v. 21, p. 71–107.
- Van Wagoner, J.V., Posamentier, H.W., Mitchum, R.M., Vail, P.R., Sarg, J.F., Loutit, T.S., and Hardenbol, J., 1988, An overview of the fundamentals of sequence stratigraphy and key definitions, in Wilgus, C.K., Hastings, B.S., Kendall, C.G. St. C., Posamentier, H.W., Ross, C.A., and Van Wagoner, J.C. [eds.], *Sea-Level Changes: An Integrated Approach*: Society of Economic and Petroleum Mineralogists Special Publication No. 42, p. 39–45.
- Winchell, N.H., 1874, Geology of the Minnesota Valley: Minnesota Geological and Natural History Survey Second Annual Report, p. 138–147.
- Wooster, L.C., 1882, Geology of the lower St. Croix district: *Geology of Wisconsin*, v. 4, p. 99–159.

TRACE-ELEMENT SIGNATURES AND TECTONIC AFFINITIES OF PROTEROZOIC A-TYPE GRANITES AND RHYOLITES IN CENTRAL WISCONSIN

Jennifer M. Wenner¹ and Mindy A. Lloyd²

ABSTRACT

New major-, trace- and rare-earth-element data for early Proterozoic A-type metaluminous granites and rhyolites exposed in east-central Wisconsin confirmed the genetic relationship of these rocks. Rhyolite exposed in Berlin, Wisconsin, has major- and trace-element chemistries and rare-earth-element patterns similar to that of the granite exposed at Redgranite, Wisconsin. Variation between the two suites is consistent with small amounts of fractional crystallization. We interpreted the Berlin rhyolite to represent the extrusive equivalent of the granite of Redgranite. One rhyolite sample, collected from a shear zone, has consistently lower values for rare-earth elements; this variation could represent variation in the degree of fractionation within the rhyolite or alteration that accompanied shearing.

New trace-element data also distinguished among the tectonic environments in which metaluminous granites and rhyolites of Wisconsin formed. Our data showed that the granite of Redgranite and the Berlin rhyolite have geochemical signatures that are consistent with extensional settings, and their metaluminous character supports generation by low-pressure melting of calc-alkaline crust. Comparison of Wisconsin rocks with other Proterozoic A-type granites confirmed that those of this study were likely generated during post-collisional extension of continental crust. The ages of the units (approximately 1,750 Ma) support the interpretation of these as post-orogenic granitic magmas. Therefore, we interpreted the Berlin rhyolite and the granite at Redgranite, Wisconsin, to represent post-collisional, A2-type rhyolites and granites generated during the collapse of crust that was thickened during the Penokean Orogeny.

INTRODUCTION

Numerous granite and rhyolite outcrops dispersed throughout east-central Wisconsin are important (if somewhat enigmatic) keys to understanding Wisconsin's Proterozoic history. In the early 1980s, Smith (1978, 1983) completed a geochemical study of these "inliers," attributing them to post-orogenic magmatism. His interpretation was based mainly on their ages in relation to the Penokean Orogeny. Uranium-lead isotope analyses of zircons from granite and rhyolite outcrops in Wisconsin suggest that the ages of these rocks fall in the most recent pulse of Geon 17 post-Penokean magmatism at approximately 1,750 Ma (Van Wyck, 1995; Van Schmus and others, 2001; Holm and others, 2005). In central and southern Wisconsin, rocks associated with this pulse are the rhyolite beneath the Baraboo quartzite, 1,754 ± 44 Ma; Baxter Hollow granite, 1,752 ± 15 Ma (Van Wyck, 1995); Observatory Hill rhyolite, 1,759 ± 2 Ma; and Montello granite, 1,746 ± 3 Ma (Van Schmus and others, 2001; Holm and others, 2005). These ages

indicate that they are younger than the calc-alkaline intrusive rocks associated with the main Penokean Orogeny (1,890–1,820 Ma, Sims and others, 1989) and older than the more extensive A-type magmatism of the Stettin syenite complex (1,565 ± 4 Ma, Van Wyck and others, 1994), Wausau syenite (1,520 Ma, Van Schmus, 1976) and the Wolf River batholith (1,470 Ma, Van Schmus and others, 1975; Dewane and Van Schmus, 2003) to the north. The Geon 17 igneous rocks are distinct from other Proterozoic igneous rocks and key to interpretation of the geologic history of Wisconsin.

Our study of the northernmost of the A-type granites of east-central Wisconsin continues the work of Smith (1978, 1983) and other workers (for example, Van Schmus, 1978, 1980; Anderson and others, 1980). Our intention was to characterize two suites of the Geon 17 A-type igneous rocks in central Wisconsin using trace- and rare-earth-element geochemistry. To understand their relationship, we used petrogenetic modeling to investigate the role of fractional crystalli-

¹ University of Wisconsin–Oshkosh, Geology Department, 800 Algoma Boulevard, Oshkosh, Wisconsin 54901;

² 2301 S. Millbend Drive, #1908, The Woodlands, Texas 77380. Corresponding author email: wenner@uwosh.edu

zation as a possible origin of geochemical differences between the two suites. We employed important trace-element ratios to infer the tectonic regime that was present during the early Proterozoic and compared A-type rocks of central Wisconsin to other Proterozoic A-type granites of known tectonic affinities. The new high-precision trace-element data presented in this paper helped us place the granites and rhyolites in a post-collisional (extensional) regime during the post-Penokean geologic history of central Wisconsin.

GEOLOGIC SETTING

The Penokean Orogeny was a major collisional event in the Early Proterozoic (1,870–1,820 Ma) of Wisconsin (Van Schmus, 1976, 1980; Maass, 1983; Sims and others, 1989). Voluminous calc-alkaline and alkaline plutonism and large-scale structural elements characterized this mountain-building event (Maass, 1983; Southwick and Morey, 1991; Holm and Lux, 1996; Van Wyck and Johnson, 1997). By 1,820 Ma, Penokean accretion terminated and was followed by an approximately 20 Ma period of magmatic quiescence in Wisconsin. Magmatism flared up again, beginning with a pulse at approximately 1,800 Ma; this pulse was followed by two other recognized post-Penokean pulses at 1,775 and 1,750 Ma (Van Schmus and others, 2001; Holm and others, 2005). During the three Geon 17 pulses, granites and rhyolites with A-type chemistries were generated and are preserved in central Wisconsin as isolated outcrops extending from Redgranite in the north to southern Sauk County (south of Baraboo; fig. 1). Recent workers in the Penokean and post-Penokean rocks of Minnesota suggested that Geon 17 rocks are associated with renewed subduction beneath Laurentia following Penokean accretion (Holm and others, 2005). Between 1,775 and 1,750 Ma, the angle of the subducting slab is thought to have steepened, altering horizontal stresses, changing the tectonic regime from compressional to extensional, and facilitating the collapse of overthickened Penokean crust (Holm and others, 2005).

In Wisconsin, magmatism associated with Penokean collapse ceased by approximately 1,750 Ma (Holm and others, 2005) and was followed by an extended period of cooling and exhumation of Penokean rocks and deposition of the Baraboo quartzite (Holm and others, 1998; Medaris and others, 2003). Extensive A-type magmatism was renewed in Wisconsin at approximately 1,565 Ma with the intrusion of the Stettin syenite (1,565 Ma, Van Wyck and others, 1994), the Wausau syenite (1,520 Ma, Van Schmus, 1976), and the more voluminous Geon 14 intrusions that

stretch from California to Scandinavia and include the Wolf River batholith in Wisconsin (Anderson, 1983). Although outside the scope of this paper, this later pulse of Proterozoic A-type magmatism represents an important chapter in the Proterozoic history of the entire North American continent and may have hydrothermally altered or reheated the post-Penokean igneous rocks addressed here.

The early Proterozoic granite of Redgranite (Smith, 1983; called Waushara granite by Weidman, 1898) and Berlin rhyolite (Buckley, 1898; Weidman, 1898) are two of the numerous Proterozoic A-type igneous rocks that crop out in east-central Wisconsin (fig. 1; Smith, 1978). Erosion has exposed such granites and rhyolites in central and eastern Wisconsin; they are elsewhere unconformably overlain by Cambrian sandstone and Pleistocene glacial deposits (Smith, 1983). Bedrock beneath the sandstone and glacial deposits, sampled in deep water wells, is similar in composition to those rocks exposed at the surface (Smith, 1978), and the dispersed outcrops have been interpreted to be genetically related: granites as part of the same composite pluton and rhyolites as the extrusive equivalents (fig. 1; Smith, 1983).

Previous workers (Smith, 1978, 1983; Van Schmus, 1978) interpreted Geon 17 rhyolites and granites in east-central Wisconsin to be co-magmatic on the basis of similar age and proximity to one another (fig. 1). Since the early 1980s, several studies of trace-element characteristics of A-type granites (for example, Pearce and others, 1984; Whalen and others, 1987; Eby, 1990, 1992) have refined our understanding of similar granites and their tectonic settings. However, few modern geochemical techniques have been used to correlate the trace-element geochemistry or tectonic setting of Geon 17 granites and rhyolites in central Wisconsin. Our study was designed to further correlate dispersed rhyolites and granites and to explore the tectonic environment in which they were emplaced. Characterization of the geochemical signatures of the Berlin rhyolite and the granite of Redgranite will expand our understanding of the early Proterozoic geologic history of Wisconsin.

METHODS

Hand-sized samples (RGQ01-2, RGQ01-3, RGQ01-5, and RGQ01-6) were collected from abandoned quarries at Redgranite and Berlin, Wisconsin. The Redgranite quarry is part of a park located in the center of the town of Redgranite, Wisconsin (lat: 44°02' 40"N, long: 89°05'55"W). Samples from Redgranite were chosen on the basis of freshness and spatial

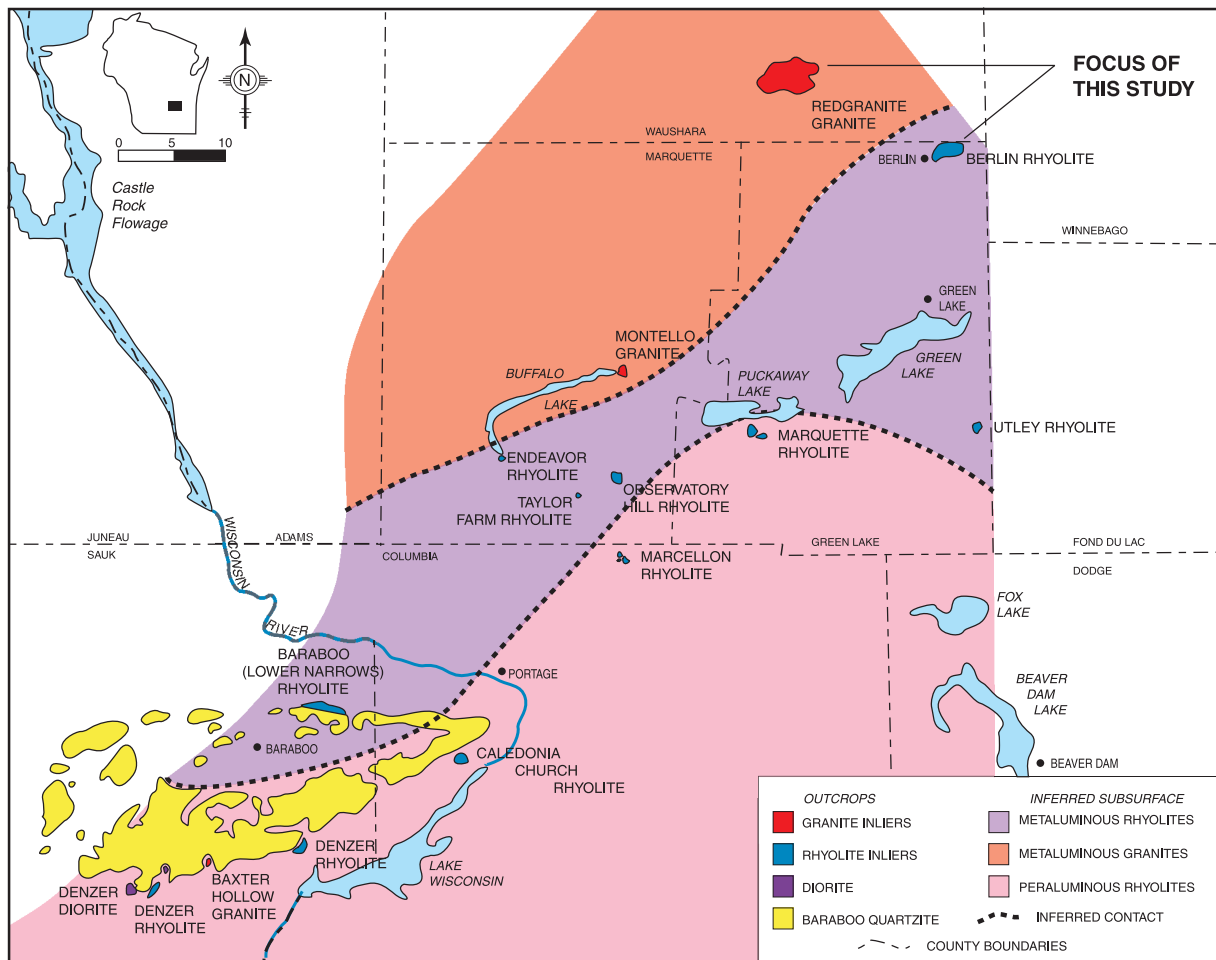


Figure 1. Map showing granite and rhyolite outcrops in central Wisconsin (after Smith, 1983). Also mapped are the inferred contacts of metaluminous granites and metaluminous and peraluminous rhyolites in the subsurface, outcrops of known related diorites, and the Baraboo quartzite. Locations from which we collected granite and rhyolite for this study are indicated in the northeastern part of the map.

distribution (taken at approximately 200 m intervals around the perimeter of the quarry). Recognized shear zones in the Redgranite quarry were avoided to minimize the effects of alteration and shear. Berlin rhyolite samples were collected from an abandoned quarry on the north–northwestern edge of Oakwood Cemetery along State Highway 91 in Berlin, Wisconsin (lat: 43°58'22"N, long: 88°55'55"W). Samples of the rhyolite were chosen as representative of the rock types exposed in this quarry and were part of a larger petrographic study to understand the effects of shearing (Hocker, 2002). Two fresh samples (BQS-12 and BQS-31) were collected at 20 to 30 m intervals along the north and east walls of the quarry to represent un-sheared, unaltered rhyolites. The third sample (BSH-2-1) from Berlin was collected from a narrow (9 to 18 cm) shear zone within the rhyolite (tens of meters

from other samples) to determine whether shearing and strain affected the geochemistry of the samples.

Redgranite and Berlin samples were analyzed by inductively coupled mass-spectrometry (ICP-MS) at Actlabs–Skyline in Tucson, Arizona, for major-, trace- and rare-earth-element geochemistry. Samples run for major- and selected trace elements were analyzed on a combination simultaneous sequential Thermo Jarrell-Ash ENVIRO II ICP or a Spectro Cirros ICP. All other trace- and rare-earth elements were spiked with an internal standard, and samples were analyzed using a Perkin Elmer SCIEX ELAN 6000 ICP-MS and proprietary sample-introduction methodologies. (Further information about geochemical preparation and analysis methods may be found on the Actlabs Web site: http://www.actlabs.com/methods_usa.htm.)

RESULTS

Hand-sample and thin-section analyses

The granite and rhyolite sampled for this study are part of the metaluminous suites defined by Smith (1983; fig. 1). Samples collected from Redgranite were texturally homogeneous, reddish-gray, fine-grained, and distinctly lacking in mafic minerals. We determined the modal mineralogy for the granite of Redgranite to be 30 to 40 percent quartz (0.2–1 mm), 45 to 55 percent perthitic alkali feldspar (0.2–5 mm), and 3 to 10 percent plagioclase (0.5–2 mm; table 1). Accessory minerals included primary apatite (1–2%; 0.05–0.1 mm), zircon–xenotime (1–2%; 0.1–0.2 mm), biotite (1–5%; 0.2–0.5 mm), and magnetite–ilmenite (1–3%; 0.3–0.5 mm) with secondary chlorite, sericite, hematite, and titanite composing the remainder of the rock (up to 4–6 modal percent; table 1). Quartz in Redgranite samples was significantly recrystallized (grains were small [0.2–1 mm] and showed irregular boundaries and undulatory extinction); alkali feldspar present in the groundmass was similar in size and morphology to recrystallized quartz and was also present as larger phenocrysts (2–5 mm) that showed perthitic texture. Grain boundaries on larger alkali feldspar grains also showed grain-boundary recrystallization. Biotite grains were significantly altered to chlorite, and magnetite–ilmenite grains generally had hematite and titanite rims in varying proportions (table 1). The alkali feldspar in the granite at Redgranite had a stippled appearance in plane-polarized light, suggesting that it was slightly altered to sericite–kaolinite (no more than 1–2% of each grain was altered).

The Berlin rhyolite (with the exception of sample BSH-2-1; see next paragraph) shows little visual variation in outcrop and is a reddish-brown ash-flow porphyry; we found similar proportions (10–15 modal percent each) of sub- to anhedral, pink, alkali feldspar phenocrysts (1–4 mm) and elongate “cigar-like” features (Smith, 1978; Tellock and Brinkmann, 1982) in a dark gray, quartzofeldspathic recrystallized groundmass. In thin section, the groundmass for the Berlin rhyolite consisted predominantly of fine-grained quartz (15–20 modal percent) and alkali feldspar (45–50 modal percent). Feldspar phenocrysts were sub- to anhedral in thin section, and grain-boundary migration recrystallization (Passchier and Trouw, 1996) was visible along the edges of the phenocrysts as fine, irregularly shaped quartz and feldspar grains. Few plagioclase grains (2–5 modal percent) were apparent; they were generally fine grained and recrystallized. In thin section, very fine-grained (0.05–0.5 mm) blue-green amphiboles (riebeckite?) defined a weak foliation and composed 5 to 10 modal percent of the rhyolite in

most samples. Anhedral opaque minerals (magnetite–ilmenite) were also present in small amounts (up to 1 mm; 1–4 modal percent) and were altered in places to titanite. Elongate cigar-like features were present throughout the rhyolite and appeared to be predominantly ribbons of recrystallized quartz and alkali feldspar. These features have been variably interpreted to represent lapilli (Smith, 1978; Tellock and Brinkmann, 1982) or the result of shearing (Hocker, 2002).

One Berlin rhyolite sample (BSH-2-1), collected from a narrow shear zone, was lighter in color and showed shear indicators (such as pressure shadows) in outcrop (Hocker, 2002). Shear-zone orientations in this locality are parallel or subparallel to layering and foliation (strike: 65°–70°; dip: 77°N to near vertical; Tellock and Brinkmann, 1982). Major minerals were similar to those in unsheared Berlin rhyolite; quartz and alkali feldspar were similar in size and composed 80 to 90 modal percent of the rock. In thin section, however, mineralogical differences included the near absence of blue-green amphiboles and the presence of biotite as an alteration product of amphibole and magnetite (table 1). Plagioclase was also much less abundant than in other Berlin samples, composing only 1 to 2 percent of the modal mineralogy. Elongated ribbons of quartz and K-feldspar were more abundant in this sample and they defined the foliation.

Geochemical analyses

Results of geochemical analyses for the granite of Redgranite and Berlin rhyolite samples are shown in table 2. In general, the results confirmed visual estimates of homogeneity for both suites. Standard deviations for major elements show variations of less than 1 weight percent of the total sample, with only SiO₂ in Redgranite varying by more than 1 percent (table 2). Trace-element values for Proterozoic Wisconsin granites and rhyolites generally vary no more than 20 percent from one another (table 2). Rare-earth elements vary by 0 to 10 percent. Trace-element values for sample BSH-2-1 are consistently lower than other Berlin samples, in a few cases varying as much as 35 percent (table 2).

Elemental variations between granite of Redgranite and Berlin rhyolite samples are also relatively small; sheared Berlin rhyolite shows the greatest variation. In general, values for immobile elements, such as the high-field strength elements and middle to heavy rare-earth elements, are similar between the two unaltered suites of samples. Large ion lithophile elements are the only values that vary significantly between the two suites (table 2). These observations are reinforced in rare-earth and extended trace-element spider diagrams for these samples (figs. 2 and

Table 1. Modal* and normative mineralogy of samples

Mineral	Modal mineralogy (volume %)						
	Redgranite samples				Berlin samples		
	RGQ01-2	RGQ01-3	RGQ01-5	RGQ01-6	BQS-31	BQS-12	BSH-2-1
Quartz (fine grained)	—	—	—	—	15–20	15–20	15–20
Quartz (coarse grained)	35–40	30–35	35–40	35–40	10–15	10–15	10–15
Alkali feldspar (fine grained)	—	—	—	—	45–50	45–50	45–50
Alkali feldspar (perthitic, coarse grained)	50–55	45–50	50–55	50–55	10–15	10–15	10–15
Plagioclase	3–5	8–10	3–5	5–7	2–4	3–5	1–2
Biotite	3–5	1–2	1–2	2–3	—	—	3–5 (alteration)
Sodic amphibole	—	—	—	—	7–10	5–7	2–4
Apatite	1–2	1–2	1–2	1–2	<1	<1	—
Magnetite/ilmenite	1–2	2–3	2–3	2–3	1–3	1–3	2–4
Chlorite (alteration)	1–2	2–3	2–3	2–3	<1	<1	<1
Hematite (alteration)	<1	<1	<1	1–2	1–2	1–3	2–4
Titanite (alteration)	<1	1–2	<1	<1	—	—	—
Zircon/xenotime	<1	1–2	<1	<1	—	—	—
Fluorite	1–2	1–2	1–2	1–2	—	—	—

Normative mineral	Normative mineralogy (wt %)						
	Redgranite samples				Berlin samples		
	RGQ01-2	RGQ01-3	RGQ01-5	RGQ01-6	BQS-31	BQS-12	BSH-2-1
Quartz	31.29	38.22	29.59	32.08	29.38	29.36	31.93
Orthoclase	29.08	29.73	32.27	32.44	27.42	26.30	26.59
Albite	27.59	23.78	27.84	27.92	35.74	37.57	35.96
Anorthite	1.80	0.44	0.89	0.87	0.00	0.05	0.03
Diopside	0.35	1.25	1.51	1.44	1.35	0.50	0.00
Hypersthene	7.40	5.12	5.50	4.21	3.91	4.17	4.37
Magnetite	1.14	0.87	0.95	0.75	0.19	0.68	0.68
Ilmenite	0.30	0.33	0.35	0.35	0.26	0.26	0.27
Apatite	0.04	0.04	0.04	0.04	0.02	0.04	0.02
Corundum	0.00	0.00	0.00	0.00	0.00	0.00	0.32
Acmite	0.00	0.00	0.00	0.00	0.95	0.00	0.00

*Modal mineralogy estimated visually by thin-section examination.

3), showing slight variation between Redgranite and unaltered Berlin samples; these Berlin samples generally exhibit consistently lower values for large ion lithophile and some of the rare-earth elements. The sheared Berlin sample exhibits significant variation in rare-earth elements from both unaltered suites (fig. 2), showing greater depletion in light and middle rare-earth elements than in heavy rare-earth elements.

Petrogenetic modeling

Petrogenetic models, like those of Anderson and Cullers (1978), use trace- and rare-earth elements and their distribution coefficients to distinguish processes that may have generated geochemical variations among samples. For our models, we used the distribution coefficients for rhyolites published in Rollinson (1993; data from Arth, 1976; Pearce and Norry, 1979; Nash

Table 2. Geochemical analyses for samples of granite of Redgranite and Berlin rhyolite

	Redgranite samples					Berlin samples					
	RGQ01-2	RGQ01-3	RGQ01-5	RGQ01-6	Mean	St Dev	BQS-31	BQS-12	BSH-2-1	Mean*	St Dev*
Major-element analyses (in wt %)											
SiO ₂	73.43	76.97	73.27	75.30	74.74	1.75	74.64	74.39	75.89	74.52	0.18
Al ₂ O ₃	11.35	10.23	11.65	11.69	11.23	0.68	11.97	12.14	12.2	12.06	0.12
Fe ₂ O ₃	5.74	4.38	4.80	3.80	4.68	0.82	3.33	3.42	3.41	3.38	0.06
MnO	0.06	0.05	0.05	0.05	0.05	0.01	0.06	0.04	0.02	0.05	0.01
MgO	0.08	0.09	0.08	0.08	0.08	0.01	0.04	0.04	0.04	0.04	0.00
CaO	0.47	0.40	0.55	0.53	0.49	0.07	0.32	0.15	0.02	0.24	0.12
Na ₂ O	3.26	2.81	3.29	3.30	3.17	0.24	4.35	4.44	4.25	4.40	0.06
K ₂ O	4.92	5.03	5.46	5.49	5.23	0.29	4.64	4.45	4.50	4.55	0.13
TiO ₂	0.16	0.18	0.18	0.18	0.18	0.01	0.14	0.14	0.14	0.14	0.00
P ₂ O ₅	0.02	0.02	0.02	0.02	0.02	0.00	0.01	0.02	0.01	0.02	0.01
LOI	-0.68	-0.65	-0.41	-0.19	-0.48	0.23	-0.15	-0.32	-0.18	-0.23	0.12
TOTAL	98.8	99.52	98.95	100.25			99.34	98.92	100.3		
Al ₂ O ₃	0.98	0.95	0.95	0.95			0.94	0.98	1.03		
CaO+Na₂O+K₂O											
Trace-element analyses (in ppm)											
Y	63	67	77	71	70	6.0	61	59	40	60	1.4
Sc	3	2	3	2	3	0.6	—	—	—	—	—
Be	3	4	5	5	4	1.0	4	3	2	4	0.7
Co	2	—	1	1	1	0.3	—	1	1	1	—
Cu	34	19	13	14	20	9.8	16	—	10	16	—
Zn	48	45	75	65	58	14.3	71	50	—	60	15.2
Ga	22	18	22	22	21	2.2	25	24	26	24	0.5
Ge	2	1	2	2	2	0.2	1	2	2	2	0.4
Rb	171	152	181	182	172	13.7	109	103	104	106	4.6
Sr	48	32	28	27	34	9.8	9	7	8	8	1.3
Y	64	65	75	73	69	5.8	61	59	43	60	1.8
Zr	274	300	339	307	305	26.8	374	359	397	366	10.9
Nb	36	33	39	36	36	2.4	28	25	29	27	2.1
Mo	3	—	4	3	3	0.5	6	—	—	6	—

	Redgranite samples					Berlin samples					
	RQ01-2	RQ01-3	RQ01-5	RQ01-6	Mean	St Dev	BQS-31	BQS-12	BSH-2-1	Mean*	St Dev*
Trace-element analyses (in ppm)											
Ag	—	0.8	0.6	—	0.7	0.1	—	—	—	—	—
Sn	10	10	8	12	10	1.5	10	5	9	7	4.069
Sb	3.4	1.9	1.8	1.0	2.0	1.0	—	0.7	0.6	0.7	—
Cs	2.3	1.4	2.1	2.5	2.1	0.5	0.6	—	0.6	0.6	—
Ba	397	359	392	408	389	21.2	106	103	109	104	2.03
Hf	9.4	9.7	11.6	9.9	10.2	1.0	10.2	9.9	10.2	10.0	0.25
Ta	3.1	2.8	3.4	3.0	3.1	0.3	2.0	2.0	2.0	2.0	0.00
W	1	2	2	2	2	0.7	—	—	—	—	—
Tl	1.0	0.9	1.6	1.4	1.3	0.3	0.5	0.5	0.9	0.5	0.03
Pb	92	56	93	52	73	22.3	11	20	22	15	6.11
Th	32.5	26.8	32.9	31.6	31.0	2.8	17.9	17.5	17.3	17.7	0.28
U	7.6	7.8	9.5	9.0	8.5	0.9	5.9	5.3	5.0	5.6	0.44
Rare-earth element analyses (in ppm)											
La	96.6	74.9	88.7	89.5	87.4	9.1	69.9	71.9	37.8	70.9	1.4
Ce	191.7	153.0	181.0	180.7	176.6	16.5	141.8	141.7	90.4	141.8	0.0
Pr	20.5	16.7	19.6	19.7	19.1	1.7	15.7	15.7	8.4	15.7	0.0
Nd	71.6	60.8	71.1	70.4	68.5	5.1	57.9	59.1	30.9	58.5	0.8
Sm	12.8	11.2	13.0	12.6	12.4	0.8	10.9	11.0	5.9	10.9	0.0
Eu	0.69	0.58	0.70	0.67	0.66	0.06	0.36	0.38	0.23	0.37	0.01
Gd	10.9	9.8	11.9	11.4	11.0	0.9	10.1	10.1	5.2	10.1	0.0
Tb	2.0	1.9	2.2	2.1	2.1	0.2	1.8	1.7	1.1	1.8	0.0
Dy	11.5	11.3	13.2	12.6	12.1	0.9	10.4	10.3	7.0	10.3	0.0
Ho	2.3	2.4	2.8	2.6	2.5	0.2	2.2	2.1	1.6	2.2	0.0
Er	6.8	7.1	8.3	7.7	7.5	0.6	6.4	6.3	5.1	6.4	0.1
Tm	1.11	1.14	1.38	1.28	1.23	0.12	1.03	1.00	0.88	1.02	0.02
Yb	7.0	7.1	8.6	7.8	7.6	0.7	6.4	6.5	5.9	6.5	0.0
Lu	1.02	1.06	1.24	1.16	1.12	0.10	0.98	0.97	0.89	0.97	0.01

*Mean and standard deviation calculated for unaltered/unsheared samples only.

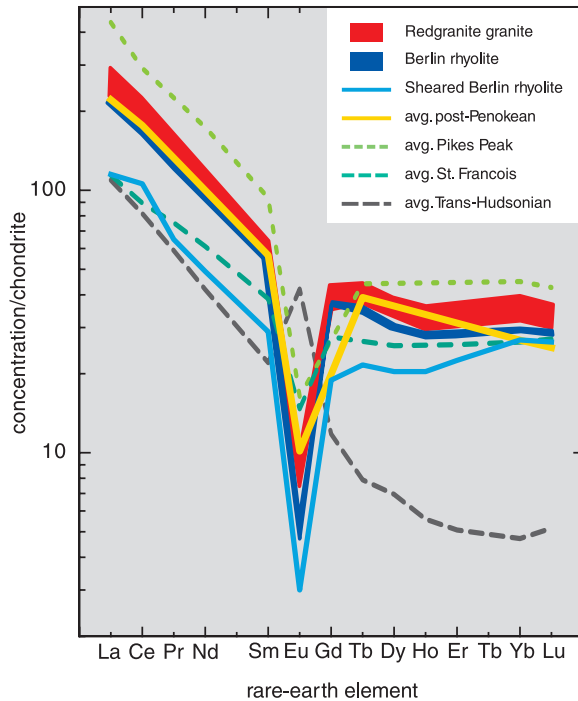


Figure 2. Rare-earth-element spider diagram showing similarities among samples from the same suite and between samples from the two suites collected for this study. The red field covers the range of data for the granite of Redgranite; the dark blue field covers the range of data for the Berlin rhyolite. Results for the Berlin rhyolite collected from a shear zone (sample BSH-2-1) are plotted separately (solid light blue line) for comparison and to illustrate the distinctiveness of this sample. Also plotted for comparison are published data for post-Penokean rocks (from Anderson and others, 1980), and three Proterozoic granitic–rhyolitic suites from a variety of tectonic settings, including continental rift (St. Francois, from Menuge and others, 2001), extensional–post-orogenic (Pikes Peak, from Smith and others, 1999) and continental arc rocks (Trans-Hudsonian, from Hollings and Ansdell, 2002). All samples are normalized to chondrite (Sun and McDonough, 1989).

and Crecraft, 1985). On the basis of mineralogical differences, we modeled fractionation of plagioclase, apatite, and biotite using the equation for Rayleigh fractionation (Rollinson, 1993):

$$\frac{C_L}{C_O} = F^{(D-1)}$$

where C_L is the concentration in the remaining liquid, C_O is the concentration in parent magma, F is the fraction of melt remaining, and D is the distribution coefficient. In figure 4 we present four models of fractionation, two using an average of the Redgranite samples as the source (C_O) and two using an average of the two Berlin rhyolite samples that are most similar. Each of the source rocks was modeled for two values of F : $F = 0.95$ and $F = 0.8$ (that is, 5–20% crystallization).

Published geochemical data for comparison

Average geochemistry for other post-Penokean granites in Wisconsin (Anderson and others, 1980), two A-type granitic–rhyolite suites from elsewhere in the United States (approximately 1.4 Ga, Pikes Peak, Colorado, Smith and others, 1999; approximately 1.1 Ga, St. Francois Mountains, Missouri, Menuge and others, 2001) and two suites of continental arc granites (approximately 1.8 Ga, Penokean orogen, Wisconsin, Van Wyck, 1995; approximately 1.8 Ga, Trans-Hudsonian orogen, Canada, Hollings and Ansdell, 2002) were used for comparison and were chosen on the basis

of their Proterozoic ages and tectonic settings. Average rare-earth and trace-element values (normalized to chondrite; Sun and McDonough, 1989) for these suites are shown in figures 2 and 3. In figures 5, 6, and 7, we include trace-element values for published A-type granites that have major-element chemistries similar to the granite of Redgranite and the Berlin rhyolite.

DISCUSSION

Comparison of rhyolite and granite chemistry

Trace- and rare-earth-element data for suites from the granite of Redgranite and unaltered Berlin rhyolite suggest that the rock suites are chemically similar. On trace- and rare-earth-element diagrams (figs. 2 and 3), the suites of granite and rhyolite from Wisconsin follow the same general trends, showing negative anomalies in trace elements, such as Ba, K, Sr, P, Eu, Sm, and Ti. Europium and Sr depletions for both suites may be interpreted to be the result of residual plagioclase or plagioclase fractionation in the source of these high-silica rocks; lower values in the Berlin rhyolite may represent fractionation of a magma similar to that of the rocks at Redgranite prior to eruption. Barium and K anomalies suggest variable fractionation of alkali feldspar or biotite in these suites. Phosphorus, Sm, and Ti anomalies may indicate apatite (P) and biotite or amphibole (Sm and Ti) fractionation–re-

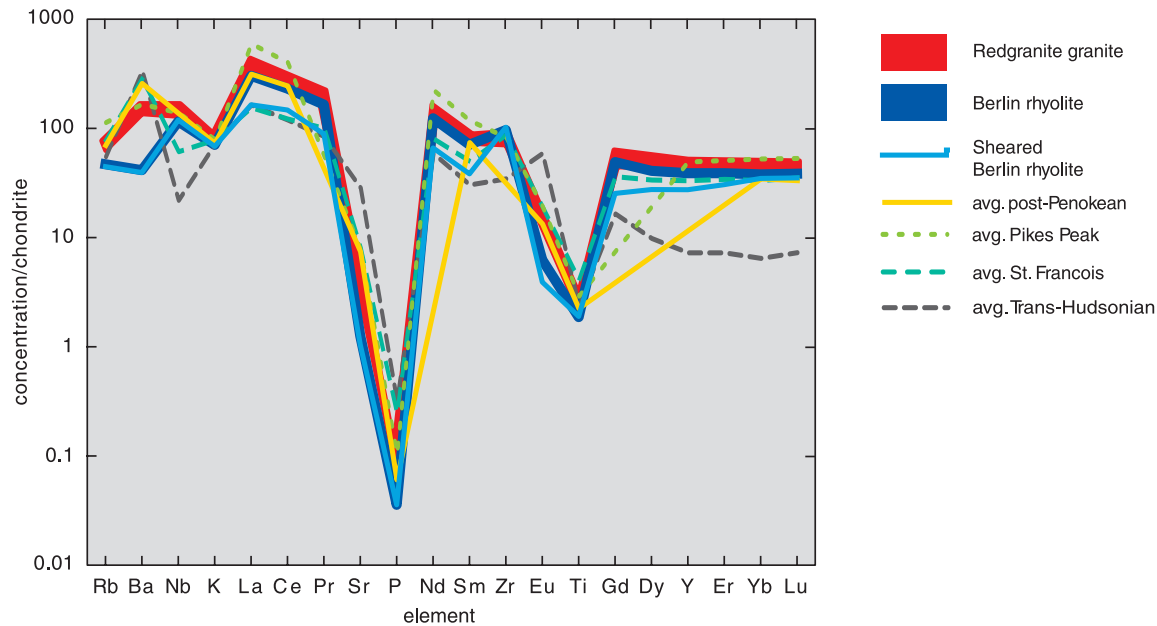


Figure 3. Extended trace-element spider diagram showing similarities and differences among suites collected for this study. Granite of Redgranite, Berlin rhyolite, and sheared Berlin rhyolite are plotted separately as in figure 2. Average trace-element values for Proterozoic granite–rhyolite suites from post-Penokean rocks (from Anderson and others, 1980) and a variety of tectonic settings, including continental rift (St. Francois, from Menuge and others, 2001), extensional–post-orogenic (Pikes Peak, from Smith and others, 1999) and continental arc rocks (Trans-Hudsonian, from Hollings and Ansdell, 2002) are plotted for comparison. All samples are normalized to chondrite (Sun and McDonough, 1989).

sidua in the source of Wisconsin granitoids.

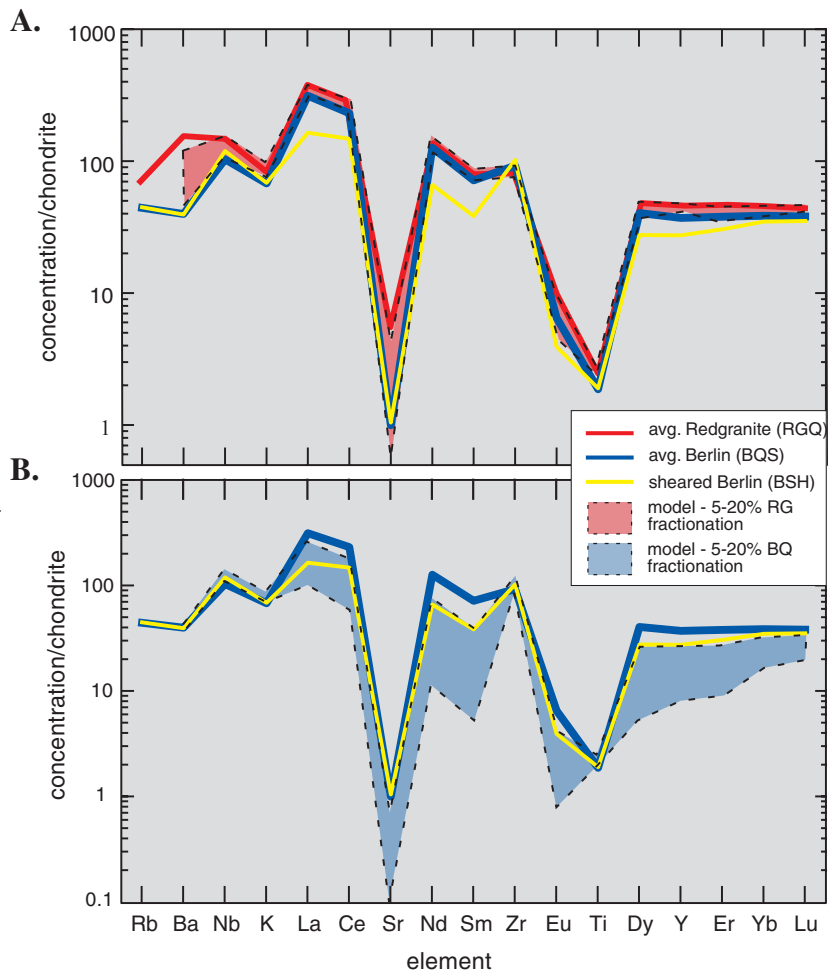
Large ion lithophile elements, such as Rb, Ba, Nb, and K, show marked differences between the two suites; Berlin rhyolite is depleted in these elements relative to Redgranite rocks. Rare-earth elements are also consistently lower in the rhyolite relative to the granite. Differences in Rb, Ba, and K can be explained by slight variations in the modal proportions of potassium-bearing minerals such as K-feldspar and biotite in both suites. Rare-earth-element compositions may be controlled by the fractionation of biotite or other accessory minerals that preferentially take up these elements, such as apatite, zircon, or allanite (Rollinson, 1993); a larger Eu anomaly suggests fractionation of plagioclase. In thin section, examination of unaltered rhyolite revealed a smaller fraction of plagioclase, apatite, and primary biotite than in the granite, supporting this interpretation.

To test the hypothesis that fractional crystallization of a single parent magma was the main mechanism by which variations in these magmas were generated, we performed petrogenetic modeling on average compositions of the granite of Redgranite and the Berlin rhyolite. Because these rocks are so similar in

major- and trace-element compositions, we modeled only slight fractionation (5% and 20%) of the granite to generate the compositional variations observed in Berlin rhyolite (fig. 4A). Variations in plagioclase and biotite contents are marked between the granite and rhyolite; also, the lack of apatite in the rhyolite suggests that it might be a fractionating phase. We modeled the fractionation of apatite, biotite, and plagioclase (5%, 25%, and 70% of the total fractionated solid, respectively; for example, Scaillet and others, 1995) on the basis of the mineralogy of the samples and on experimental data from high-silica granites (Piwinskii, 1968; Piwinskii and Wyllie, 1968; Scaillet and others, 1995). The trace-element values for the Berlin rhyolite fall within the modeled values for 5- to 20-percent fractionation of the granite of Redgranite (fig. 4A).

Similar rare-earth-element patterns between the granite and rhyolite samples suggested that the Berlin rhyolite is comagmatic with the granite of Redgranite and represents the granite's extrusive equivalent. Modeling indicated that slight differences in trace- and rare-earth-element values probably represent varying degrees of fractionation in the source magma prior

Figure 4. Results of trace-element modeling of fractionation. **A:** Models of compositions produced (orange field in dashed line) by 5- to 20-percent fractionation of average Redgranite granites (red line; RGQ samples). Fractionating minerals included plagioclase, biotite, and apatite (based on modal mineralogy). Note the overlap of Berlin samples (blue line) with the compositions generated particularly by 5-percent fractionation (upper dashed line), suggesting small amounts of fractionation of granite produce rhyolite. **B:** Models of compositions produced (blue field in dashed line) by 5- to 20-percent fractionation of average Berlin samples (blue line; unsheared Berlin rhyolite samples [BQS]). Fractionating minerals included biotite, amphibole, apatite, and plagioclase (based on differences in modal mineralogy). The models generate compositions similar to the sheared rhyolite sample (BSH) through small amounts of fractional crystallization.



to eruption and confirmed the hypothesis that Berlin rhyolite and Redgranite granites are related.

Origin of variations within the Berlin rhyolite

The rhyolite sample collected from the shear zone (BSH-2-1; Hocker, 2002) is chemically and mineralogically distinct from other rhyolites in this study. Although most trace-element concentrations are similar to unsheared Berlin rhyolite, the shear-zone sample has rare-earth-element values consistently lower than those of the Redgranite and the other Berlin samples collected for this study. Because the pattern is similar (fig. 2) and mobile elements such as Rb are not significantly depleted in the shear-zone sample relative to the other samples (fig. 3), it is difficult to interpret differences. We present two possibilities:

- Lower rare-earth-element values represent differing degrees of fractionation within Berlin rhyolite, with sample BSH-2-1 representing a more fractionated liquid.
- Fluids present during shearing have leached rare-

earth elements from accessory minerals along grain boundaries as they dissolve and recrystallize (for example, Condie and Sinha, 1996; Rolland and others, 2003).

The shear-zone sample from Berlin (BSH-2-1) is visually lighter and has mineralogy distinct from the other Berlin samples, and the shear zone is parallel to layering foliation (Tellock and Brinkmann, 1982). Layering in this area is close to vertical (dipping 77°–90°; Tellock and Brinkmann, 1982; Hocker, 2002); thus, lateral variations in composition may represent different ash flows. Consequently, we tested the hypothesis that this sample represents eruption of a slightly more fractionated rhyolite using trace-element modeling. Our modeling simulated fractionation of the average fresh compositions exposed at Berlin and is based on differences in modal mineralogy (table 1) and fractionating phases in experiments (Piwinski, 1968; Piwinski and Wyllie, 1968; Scaillet and others, 1995). It was designed to illustrate the effects of 5- to 20-percent fractionation of biotite (10%), amphibole

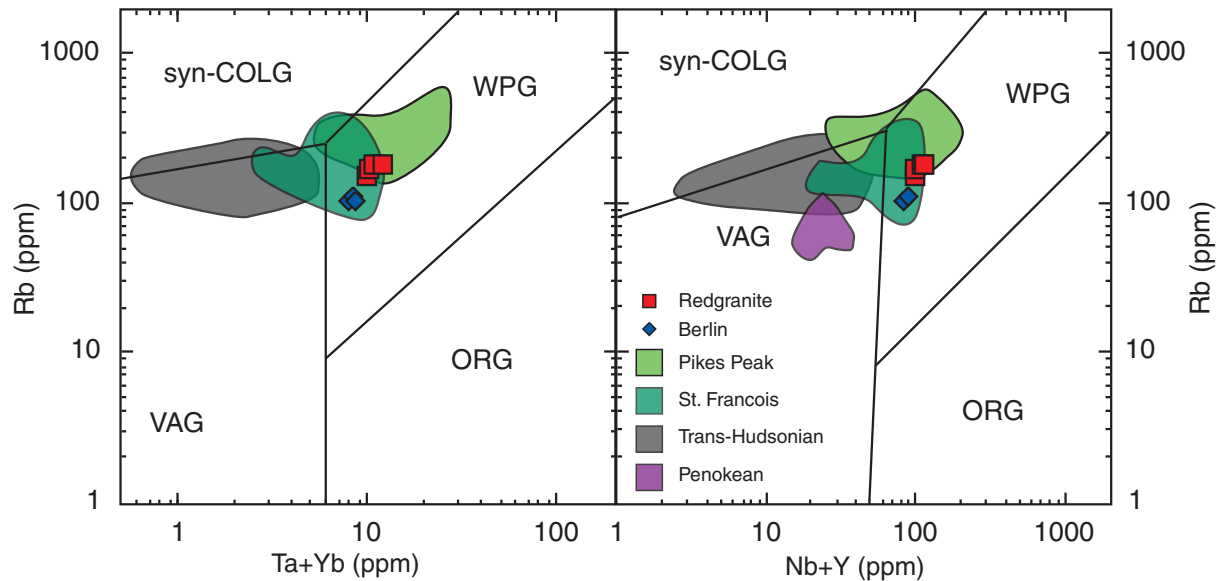


Figure 5. Tectonic discrimination diagrams for A-type granites after Pearce and others (1984). Symbols for rocks from this study are red squares (Redgranite) and blue diamonds (Berlin rhyolite). Fields for published Proterozoic A-type granites (Pikes Peak, from Smith and others, 1999; St. Francois Mountains, from Menuge and others, 2001; Trans-Hudsonian arc rocks, from Hollings and Ansdell, 2002; Penokean rocks, from Van Wyck, 1995) are plotted for comparison. Note that all data for this study fall in the within-plate granite (WPG) field and that trace elements for Wisconsin data are most like other Proterozoic post-orogenic granites: St. Francois and Pikes Peak. Field abbreviations: VAG: volcanic arc granite; syn-COLG: syncollisional granite; ORG: ocean-ridge granite; WPG: within-plate granite. Data symbols are larger than analytical error.

(15%), apatite (5%), and plagioclase (70%) (for example, Piwinski, 1968) from an average of the two unshered Berlin rhyolite samples (fig. 4B). Models of 5- to 20-percent fractionation of the modes listed above from unshered rhyolite compositions generate patterns that are sufficiently similar to the Berlin shear-zone sample (fig. 4B), which suggests that fractionation may have generated the variation and that outcrops sampled may represent a sequence of co-magmatic eruptions that recorded fractionation in the source magmas.

However, it cannot be overlooked that sample BSH-2-1 has experienced some deformation, demonstrated in shear sense indicators and significant recrystallization. Similarities in fluid mobile elements, such as Rb, between the sheared and fresh Berlin rhyolite samples suggest that hydrothermal alteration may not have played a significant role in changing the geochemistry of these rocks. Nonetheless, recent studies in quartzofelspathic rocks (Condie and Sinha, 1996; Rolland and others, 2003) suggested that fluids present during shearing may alter the rare-earth-element composition of similar rocks. Accessory minerals (such as zircon, xenotime, apatite, and possibly bio-

tite or amphibole) that are rich in rare-earth elements may be dissolved or leached along grain boundaries as a result of shearing (for example, Condie and Sinha, 1996; Rolland and others, 2003). The lower rare-earth-element values (more so in light rare-earth elements than in heavy rare-earth elements; fig. 2) in the sheared rhyolite sample are consistent with this interpretation. However, with only three samples, it is difficult to evaluate the validity of either fractionation or shearing as a mechanism to generate variations within the rhyolite. More detailed work on structures, spatial relationships, and mineralogical differences of these rocks needs to be completed to determine the dominant mechanism that produced chemical differences.

Source and tectonic affinities of granite and rhyolite

The characterization of these A-type rocks as metaluminous (fig. 1; table 2; Smith, 1978, 1983) indicates that these rocks may represent partially melted arc-related (calc-alkaline) rocks associated with post-orogenic collapse. Experimental melting of calc-alkaline granitoids at low pressures produces chemical compo-

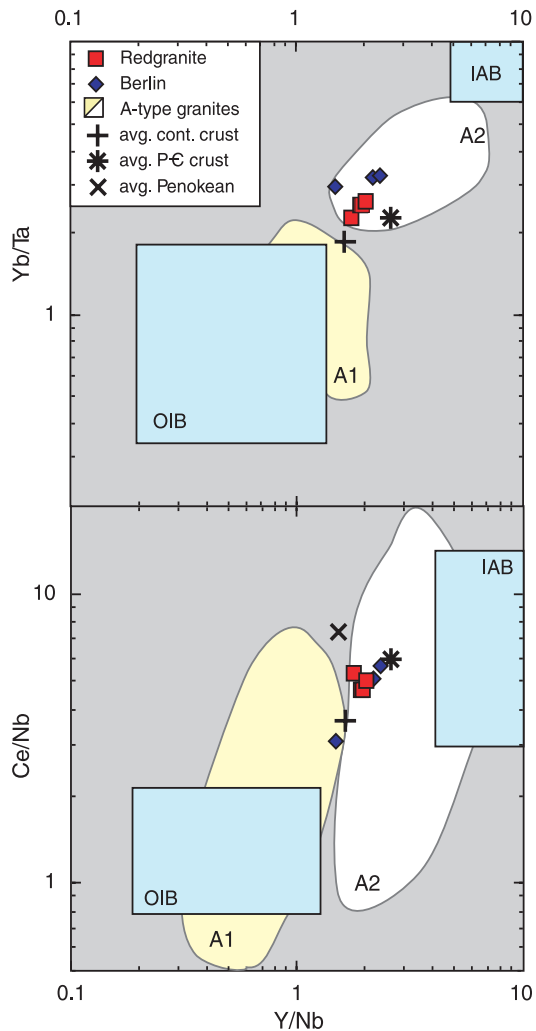


Figure 6. Plots designed to discriminate source (after Eby, 1990). Wisconsin rocks are represented by filled squares (granite of Redgranite) and filled diamonds (Berlin rhyolite). Also plotted are continental crust (black cross; from Taylor and McLennan, 1985), average Penokean crust (black X; from Van Wyck, 1995), and average Precambrian continental crust (black asterisk; from Rudnick and Fountain, 1995). Gray fields represent A1- and A2- (labeled) type granites of Eby (1990) and are used for comparison. Wisconsin data fall in A2 field, between ocean-island basalt (OIB) and island arc basalt (IAB) fields on plots of Y/Nb vs. Yb/Ta and Y/Nb vs. Ce/Nb , among average crustal values, and are very similar to average Precambrian crust. Data symbols are larger than analytical error.

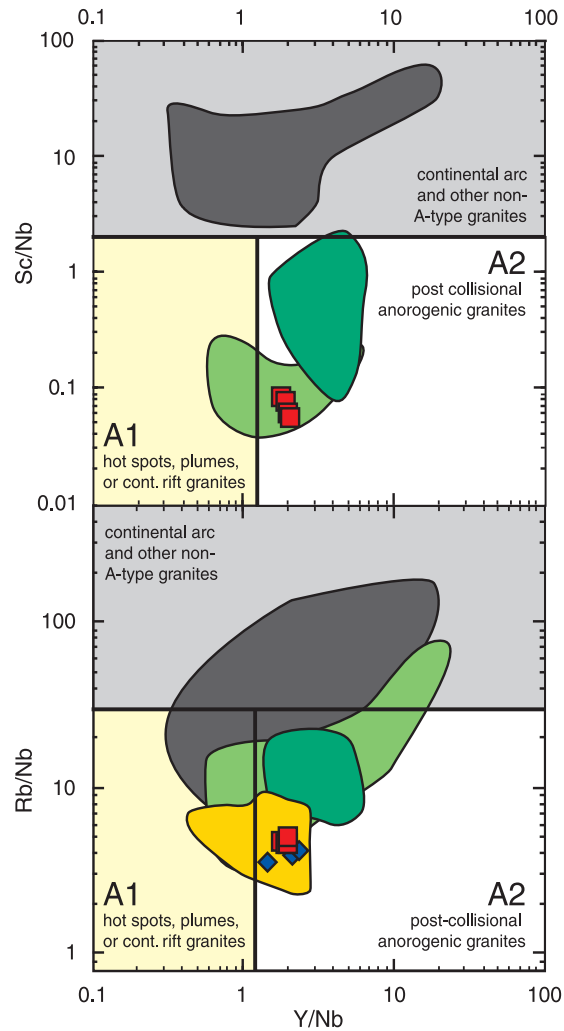


Figure 7. Diagram for discrimination between A-type granites after Eby (1992). On the diagram, solid line represents distinction between A1 and A2 granites: Y/Nb ratios of 1.2 (Eby, 1992). The A1 field (left) represents granites associated with hotspots, plumes, or continental rifts; the A2 field (right) represents granites associated with post-collisional or extensional settings (Eby, 1990, 1992). The long rectangular field represents granites associated with orogenic settings. Note that Wisconsin A-type granites are type A2 and are most like Pikes Peak (Smith and others, 1999). Data symbols are larger than analytical error.

- Redgranite
- ◆ Berlin
- Pikes Peak
- St. Francois
- Trans-Hudsonian
- post-Penokean

sitions similar to other metaluminous A-type granites (Patiño Douce, 1997). The generation of metaluminous A-type granite and rhyolite by low-pressure partial melting of arc-related granitoids is consistent with the geologic history of this part of Wisconsin and suggests that the rocks in this study may have been generated during the collapse of thickened Penokean crust.

To help understand the origin and tectonic setting for these A-type granites, we show them on several discrimination diagrams (figs. 5, 6, and 7). Diagrams that plot Rb against the sum of two incompatible elements (fig. 5) are designed to characterize the tectonic setting in which A-type granites may be emplaced (Pearce and others, 1984). Although some may argue that Rb can be relatively mobile during alteration, these diagrams have been reevaluated and still seem to give excellent results when used to discriminate tectonic setting of A-type granitoids (Förster and others, 1997). Two other diagrams (fig. 6) use trace-element ratios to distinguish between sources for two distinct A-type compositions—A1, a mixture of average crust (Taylor and McLennan, 1985; Rudnick and Fountain, 1995; Van Wyck, 1995) and mantle sources for ocean islands (OIB, fig. 6) and A2, a mixture of average crust and mantle sources for island arcs (IAB, fig. 6) (Eby, 1990). Ratios of Y, Sc, and Rb to Nb can also be used to distinguish among A-type rifting environments (fig. 7; Eby, 1992). On these diagrams (fig. 7), A1-type granitoids ($Y/Nb < 1.2$) were generated in hotspots, plumes, or continental rift zones; A2-type granitoids ($Y/Nb > 1.2$) are associated with post-collisional settings (Eby, 1990, 1992).

Low pressure melting during extension may be initiated by a number of mechanisms in a variety of tectonic settings (for example, hotspots, plumes, continental rift zones, ocean ridges, and post-collisional zones; Pearce and others, 1984). The addition of the new data about granite of Redgranite and Berlin rhyolite on these diagrams confirmed the hypothesis that low-pressure melting–extension contributed to the generation of A-type granites in east-central Wisconsin. On diagrams of Pearce and others (1984), A-type granitoids from Wisconsin fall in the within-plate-granite field (WPG, fig. 5) and thus can be associated with either plume–hotspot related or post-orogenic extension (Pearce and others, 1984).

The distinction between generation of A-type granites in hotspot and post-orogenic settings can be made by distinguishing source (fig. 6) and tectonic affinity (fig. 7). Data from Redgranite and Berlin rocks plot in the A2-type granitoid field (fig. 6)—commonly associated with melting of crust and arc-related basalts (IAB, fig. 6; thought to represent crust generated

during collision; Eby, 1990). Trace-element ratios from this study are very similar to average crustal compositions (Taylor and McLennan, 1985; Rudnick and Fountain, 1995; Van Wyck, 1995; fig. 6), suggesting that generation of A-type granites in Wisconsin involved extension and melting of a significant part of the pre-existing crust (Eby, 1990). Plots distinguishing tectonic setting for granitoids (fig. 7) further suggest the involvement of reworked thickened arc crust in the generation of the Wisconsin granites and rhyolites. Redgranite and Berlin samples collected for this study plot in the A2 field (fig. 7) and can be correlated with rifting in post-collisional tectonic settings (Eby, 1990, 1992).

The metaluminous character (table 1), similarity to average continental crust (fig. 6), and characterization of these rocks as the result of within-plate post-collisional extension (figs. 5 and 7) are consistent with the geologic history of eastern and central Wisconsin (for example, Holm and others, 2005). We interpreted the new data to indicate that low pressure melting of multiple crustal sources, particularly the extension of thickened crust that was generated during subduction and accretion associated with the Penokean Orogeny, contributed to the generation of these high-silica rocks.

Comparison of Wisconsin rocks to rocks of known tectonic affinities

Average trace- and rare-earth-element patterns and trace-element ratios for published A-type and arc suites (post-Penokean, Anderson and others, 1980; St. Francois, Menuge and others, 2001; Pikes Peak, Smith and others, 1999; Trans-Hudsonian, Hollings and Ansdell, 2002; and Penokean, limited data from Van Wyck, 1995) are plotted with geochemical analyses from this study in figures 2, 3, 5, and 7 to confirm our interpretation that these rocks formed in a post-collisional extensional regime. Normalized trace- and rare-earth-element values from this study overlap completely with average post-Penokean data (figs. 2 and 3), confirming previous characterization as post-Penokean. Discrimination diagrams also suggest correlation between granitoids from this study, published post-Penokean geochemistry, and other post-collisional granites (St. Francois and Pikes Peak; figs. 5 and 7). The rocks analyzed for this study show neither overlap with Penokean crustal values nor with other Proterozoic continental arc data (figs. 5, 6, and 7), confirming that these rocks were probably not directly associated with the Penokean Orogeny. Similarities in chemical composition between the granite of Redgranite, the Berlin rhyolite, other post-Penokean rocks and rocks

from Pikes Peak batholith (thought to be the result of post-orogenic activity; Smith and others, 1999) support the conclusion that the post-Penokean A-type granitoids are likely post-orogenic and associated with extension.

It is interesting to note that on figure 5 many post-collisional A-type granitoids straddle the line between the areas shown as within-plate granites and volcanic arc granites (WPG and VAG). Published data from other post-orogenic A-type rocks (for example, post-Penokean, Anderson and others, 1980; Van Wyck, 1995; Pikes Peak, Smith and others, 1999) also straddle the division between the A1- and A2-type rocks (fig. 7; Eby, 1992). The proximity of the data for this study to the VAG field and the overlap of other post-collisional suites on A-type discrimination diagrams (figs. 5 and 7) emphasize the complexity of the geochemistry associated with A-type igneous rocks. The close relationship of A-type geochemistry to WPG and VAG settings suggests that Penokean (arc) crust may have melted to generate the A-type granitoids of this study, imparting components of its geochemistry to the resulting rocks (Patiño Douce, 1997). Additionally, although the bulk of geochemistry for post-collisional A-type rocks fall in the A2 field, some data from A-type granitoids “spill over” into A1 field (fig. 7). The straddling of data across the dividing line for distinct rifting environments may also suggest a complex evolution of post-collisional A-type granitoids—transitioning from collapse and extension of thickened arc crust (A2-type granitoids) to continental rift (A1 type) settings (Rogers and Greenberg, 1990).

CONCLUSIONS

The geochemistry of the Berlin rhyolite and the granite of Redgranite suggests that they are likely comagmatic and derived from the same source. Slight variations in some trace elements suggest that the Berlin rhyolite represents a more fractionated phase of the granite of Redgranite. Trace-element modeling of fractionation of the granite of Redgranite suggests that 5- to 20-percent fractionation can generate compositions similar to that of unaltered Berlin rhyolite. We concluded that Berlin rhyolite is likely the extrusive equivalent of the granite exposed in Redgranite.

Within the sampled exposure of Berlin rhyolite, one sample showed consistently lower values for many of the rare-earth and other immobile elements. These geochemical variations can be explained by one of two mechanisms: (1) varying degrees of fractionation within multiple flows or (2) hydrothermal altera-

tion and/or shearing. Five- to 20-percent fractionation of unaltered Berlin rhyolite compositions can generate observed variations. However, because the sample with the most significant variation was taken in the proximity of a shear zone, it is also possible that shearing of high-silica rocks has produced significant decreases in rare-earth-element concentrations by alteration of rare-earth-element bearing minerals (for example, zircon, allanite, and so forth; Condie and Sinha, 1996; Rolland and others, 2003) and dissolution along grain boundaries (for example, Condie and Sinha, 1996). Although rare-earth-element bearing minerals are present in some of the samples, more work needs to be done to assess the contributions of alteration and/or fractionation to geochemical variations in the Berlin rhyolite.

The A-type granites in south and east-central Wisconsin likely had a complex tectonic history involving extension and melting (and possibly remelting) of crust. The metaluminous granitoids of Redgranite and Berlin rhyolite, like other metaluminous A-type granites, likely resulted from decompression melting of calc-alkaline rocks associated with collision (Patiño Douce, 1997). Tectonic discrimination diagrams support low pressure melting of thickened arc crust; the granite of Redgranite and Berlin rhyolite plot in the WPG (fig. 5; Pearce and others, 1984) and A2 (figs. 6 and 7; Eby, 1990, 1992) fields, commonly associated with post-orogenic or post-collisional extensional settings (Rogers and Greenberg, 1990). We concluded that melting during extension of thickened Penokean crust generated the A-type rocks of Redgranite and Berlin (Eby, 1990, 1992).

The Proterozoic history of central Wisconsin supports interpretation of these granitoids as post-orogenic and associated with collapse of crust thickened during Penokean accretion. Although subduction probably renewed immediately following the orogeny, the angle of the subducting slab steepened between 1,775 and 1,750 Ma (Holm and others, 2005). Slab rollback reduces horizontal stresses, and thus stresses in the overthickened Penokean crust may have shifted from dominantly compression to extension (Holm and others, 2005). Geon 17 granites and rhyolites of this area show a distinct change from the calc-alkalic (arc-like) activity of the Penokean Orogeny to post-collisional A-type volcanism and plutonism (Smith, 1983). It is likely that after the orogenic event associated with the Penokean, extension and rifting began to occur, generating the post-collisional A-type granite and rhyolite that crop out throughout south and east-central Wisconsin today.

ACKNOWLEDGMENTS

The authors acknowledge the academic and financial support of the Geology Department at the University of Wisconsin–Oshkosh. We are deeply indebted to them and the rest of the University of Wisconsin system for sponsoring the field conference for which this project was started. We also thank P.E. Brown (University of Wisconsin–Madison), L.G. Medaris, Jr. (emeritus, University of Wisconsin–Madison), and B.A. Brown (Wisconsin Geological and Natural History Survey) for making this a much better manuscript with their helpful reviews.

REFERENCES

- Anderson, J.L., 1983, Proterozoic anorogenic plutonism of North America, in Medaris, L.G., Jr., Mickelson, D.M., Byers, C.W., and Shanks, W.G., eds., Proterozoic geology: Selected papers from an international Proterozoic symposium: Geological Society of America Memoir 161, p. 133–154.
- Anderson, J.L., and Cullers, R.L., 1978, Geochemistry and evolution of the Wolf River Batholith, a Late Precambrian rapakivi massif in north Wisconsin, U.S.A.: *Precambrian Research*, v. 7, p. 287–324.
- Anderson, J.L., Cullers, R.L., and Van Schmus, W.R., 1980, Anorogenic metaluminous and peraluminous granite plutonism in the Mid-Proterozoic of Wisconsin, USA: *Contributions to Mineralogy and Petrology*, v. 74, p. 311–328.
- Arth, J.G., 1976, Behaviour of trace elements during magmatic processes—A summary of theoretical models and their applications: *Journal of Research of the U.S. Geological Survey*, v. 4, p. 41–47.
- Buckley, E.R., 1898, On the building and ornamental stones of Wisconsin: Wisconsin Geological and Natural History Survey Bulletin 4, 544 p.
- Condie, K.C., and Sinha, A.K., 1996, Rare earth and other trace element mobility during mylonitization: A comparison of the Brevard and Hope Valley shear zones in the Appalachian Mountains, USA: *Journal of Metamorphic Geology*, v. 14, p. 213–226.
- Dewane, T.J., and Van Schmus, W.R., 2003, Detailed U-Pb geochronology of the Wolf River batholith, north-central Wisconsin: Evidence for a short lived magmatic event ca. 1470 Ma: Geological Society of America Abstracts with Programs, v. 35, no. 2, p. 47.
- Eby, G.N., 1990, The A-type granitoids: A review of their occurrence and chemical characteristics and speculations on their petrogenesis: *Lithos*, v. 26, p. 115–134.
- Eby, G.N., 1992, Chemical subdivision of the A-type granitoids: Petrogenetic and tectonic implications: *Geology*, v. 20, no. 7, p. 641–644.
- Förster, H.-J., Tischendorf, G., and Trumbull, R.B., 1997, An evaluation of the Rb vs. (Y + Nb) discrimination diagram to infer tectonic setting of silicic igneous rocks: *Lithos*, v. 40, p. 261–293.
- Hocker, S., 2002, Textural studies of the Berlin rhyolites and implications for central Wisconsin geology, in 28th Wisconsin Undergraduate Geology Field Conference, Oshkosh, p. BE-1–BE-20.
- Hollings, P., and Ansdell, K., 2002, Paleoproterozoic arc magmatism imposed on an older back arc basin: Implications for the tectonic evolution of the Trans-Hudson orogen, Canada: *Geological Society of America Bulletin*, v. 114, p. 153–168.
- Holm, D.K., and Lux, D.R., 1996, Core complex model proposed for gneiss dome development during collapse of the Paleoproterozoic Penokean orogen, Minnesota: *Geology*, v. 24, p. 343–346.
- Holm, D.K., Schneider, D., and Coath, C., 1998, Age and deformation of Early Proterozoic quartzites in the southern Lake Superior region: Implications for extend of foreland deformation during final assembly of Laurentia: *Geology*, v. 26, p. 907–917.
- Holm, D.K., Van Schmus, W.R., MacNeill, L.C., Boerboom, T.J., Schweitzer, D., and Schneider, D., 2005, U-Pb zircon geochronology of Paleoproterozoic plutons from the northern midcontinent, USA: Evidence for subduction flip and continued convergence after Geon 18 orogenesis: *Geological Society of America Bulletin*, v. 117, p. 259–275.
- Maass, R.S., 1983, Early Proterozoic tectonic style in central Wisconsin, in Medaris, L.G., Jr., ed., Early Proterozoic geology of the Great Lakes Region: Geological Society of America Memoir 160, p. 85–95.
- Medaris, L.G., Jr., Singer, B.S., Dott, R.H., Jr., Naymark, A., Johnson, C.M., and Schott, R.C., 2003, Late Paleoproterozoic climate, tectonics and metamorphism in the southern Lake Superior region and Proto-North America: Evidence from the Baraboo interval quartzites: *Journal of Geology*, v. 111, p. 243–257.
- Menuge, J., Brewer, T., and Seeger, C., 2001, Petrogenesis of metaluminous A-type rhyolites from the St. Francois Mountains, Missouri and the Mesoproterozoic evolution of the southern Laurentian margin: *Precambrian Research*, v. 113, p. 269–291.
- Nash, W.P., and Crecraft, H.R., 1985, Partition coefficients for trace elements in silicic magmas: *Geochimica et Cosmochimica Acta*, v. 49, p. 2309–2322.

- Passchier, C.W., and Trouw, R.A.J., 1996, *Microtectonics*: Berlin, Springer-Verlag, 289 p.
- Patiño Douce, A.E., 1997, Generation of metaluminous A-type granites by low-pressure melting of calc-alkaline granitoids: *Geology*, v. 25, p. 743–746.
- Pearce, J.A., Harris, N.B.W., and Tindle, A.G., 1984, Trace element discrimination diagrams for the tectonic interpretation of granitic rocks: *Journal of Petrology*, v. 25, no. 4, p. 956–983.
- Pearce, J.A., and Norry, M.J., 1979, Petrogenetic implications of Ti, Zr, Y and Nb variations in volcanic rocks: *Contributions to Mineralogy and Petrology*, v. 69, p. 33–47.
- Piwinskii, A.J., 1968, Experimental studies of igneous rock series: Central Sierra Nevada batholith, California: *Journal of Geology*, v. 76, p. 548–570.
- Piwinskii, A.J., and Wyllie, P.J., 1968, Experimental studies of igneous rock series: A zoned pluton in the Wallowa batholith, Oregon: *Journal of Geology*, v. 76, p. 205–234.
- Rogers, J.J.W., and Greenberg, J.K., 1990, Late-orogenic, post-orogenic, and anorogenic granites: Distinction by major-element and trace-element chemistry and possible origins: *Journal of Geology*, v. 98, p. 291–309.
- Rolland, Yann, Cox, Stephen, Boullier, A.-M., Pennacchioni, Giorgio, and Mancktelow, Neil, 2003, Rare earth and trace element mobility in mid-crustal shear zones: Insights from the Mont Blanc Massif (Western Alps): *Earth and Planetary Science Letters*, v. 214, p. 203–219.
- Rollinson, H.R., 1993, *Using Geochemical Data: Evaluation, Presentation, Interpretation*: Essex, England, Longman Scientific and Technical, 352 p.
- Rudnick, R.L., and Fountain, D.M., 1995, Nature and composition of the continental crust: A lower crustal perspective: *Reviews of Geophysics*, v. 33, p. 267–309.
- Scaillet, Bruno, Pichavant, Michel, and Roux, Jacques, 1995, Experimental crystallization of leucogranite magmas: *Journal of Petrology*, v. 36, no. 3, p. 663–705.
- Sims, P.K., Van Schmus, W.R., Schultz, K.J., and Peterman, Z.E., 1989, Tectonostratigraphic evolution of the Early Proterozoic Wisconsin magmatic terranes of the Penokean orogen: *Canadian Journal of Earth Sciences*, v. 26, p. 2145–2158.
- Smith, D.R., Noblett, J., Wobus, R.A., Unruh, D., Douglass, J., Beane, R., Davis, C., Goldman, S., Kay, G., Gustavson, B., Saltoun, B., and Stewart, J., 1999, Petrology and geochemistry of late-stage intrusions of the A-type, mid-Proterozoic Pikes Peak batholith (Central Colorado, USA): Implications for petrogenetic models: *Precambrian Research*, v. 98, p. 271–305.
- Smith, E.I., 1978, Precambrian rhyolites and granites in south central Wisconsin—Field relations and chemistry: *Geological Society of America Bulletin*, v. 89, p. 875–890.
- Smith, E.I., 1983, Geochemistry and evolution of the early Proterozoic, post-Penokean rhyolites, granites, and related rocks of south-central Wisconsin, USA, in Medaris, L.G., Jr., ed., Early Proterozoic geology of the Great Lakes Region: Geological Society of America Memoir 160, p. 113–128.
- Southwick, D.L., and Morey, G.B., 1991, Tectonic imbrication and foredeep development in the Penokean orogen, east-central Minnesota—An interpretation based on regional geophysics and the result of test-drilling, in Simms, P.K., and Carter, L.M.H., eds., Contributions to Precambrian geology of Lake Superior Region: U.S. Geological Survey Bulletin 1904, p. C1–C17.
- Sun, S.S., and McDonough, W.F., 1989, Chemical and isotopic systematics of ocean basalts: implications for mantle composition and processes, in Saunders, A.D., and Norry, M.J., eds., Magmatism in the Ocean Basins, Geological Society Special Publication 42, p. 313–345.
- Taylor, S.R., and McLennan, S.M., 1985, *The Continental Crust: Its Composition and Evolution*: Oxford, Blackwell, 316 p.
- Tellock, P., and Brinkmann, R., 1982, Geology of Berlin Rhyolite, 14th Wisconsin Undergraduate Field Conference: University of Wisconsin–Oshkosh, p. 21–28.
- Van Schmus, W.R., 1976, Early and Middle Proterozoic history of the Great Lakes area, North America: *Royal Society of London Philosophical Transactions*, v. 280, p. 605–628.
- Van Schmus, W.R., 1978, Geochronology of the southern Wisconsin rhyolites and granites: *Geoscience Wisconsin*, v. 2, p. 19–24.
- Van Schmus, W.R., 1980, Chronology of igneous rocks associated with the Penokean Orogeny in Wisconsin: Geological Society of America Special Paper, v. 182, p. 159–168.
- Van Schmus, W.R., MacNeill, L.C., Holm, D.K., and Boerboom, T.J., 2001, New U–Pb ages from Minne-

- sota, Michigan and Wisconsin: Implications for late Paleoproterozoic crustal stabilization, Proceedings and abstracts for the 47th annual Institute on Lake Superior Geology, p. 100–101.
- Van Schmus, W.R., Thurman, E.M., and Peterman, Z.E., 1975, Geology and Rb–Sr chronology of Middle Precambrian rocks in eastern and central Wisconsin: *Geological Society of America Bulletin*, v. 86, p. 1255–1265.
- Van Wyck, Nicholas, 1995, Oxygen and carbon isotopic constraints on the development of eclogites, Holsnoy, Norway, and major and trace element, common Pb, Sm–Nd, and zircon geochronology constraints on petrogenesis and tectonic setting of pre- and early Proterozoic rocks in Wisconsin [Doctoral thesis]: University of Wisconsin–Madison, 287 p.
- Van Wyck, Nicholas, and Johnson, C.M., 1997, Common lead, Sm–Nd, and U–Pb constraints on petrogenesis, crustal architecture, and tectonic setting of the Penokean Orogeny (Paleoproterozoic) in Wisconsin: *Geological Society of America Bulletin*, v. 109, p. 799–808.
- Van Wyck, Nicholas, Medaris, L.G., Jr., and Johnson, C.M., 1994, The Wolf River A-type magmatic event in Wisconsin; U/Pb and Sm/Nd constraints on timing and petrogenesis, Proceedings and Abstracts from the 40th annual Institute on Lake Superior Geology, p. 81–82.
- Weidman, Samuel, 1898, A contribution to the geology of the Pre-Cambrian igneous rocks of the Fox River Valley, Wisconsin: Wisconsin Geological and Natural History Survey Bulletin 3, 63 p.
- Whalen, J.B., Currie, K.L., and Chappell, B.W., 1987, A-type granites: Geochemical characteristics, discrimination and petrogenesis: *Contributions to Mineralogy and Petrology*, v. 95, p. 407–419.

COUPLED MODELING OF GRAVITY AND AEROMAGNETIC DATA TO ESTIMATE SUBSURFACE BASEMENT TOPOGRAPHY IN SOUTHEASTERN WISCONSIN

John D. Skalbeck¹, James N. Couch¹, Ryan S. Helgesen¹, and Daniel S. Swosinski¹

ABSTRACT

We used coupled modeling of gravity and aeromagnetic data to estimate subsurface structure along seven northwest–southeast profiles perpendicular to the Waukesha Fault and one north–south profile (tie line). Study results showed the Waukesha Fault as a high-angle normal fault dipping southeast and having maximum vertical displacement of 560 m. The depth to Precambrian crystalline basement rock southeast of the fault (downthrown block) exceeds the total depth of water wells, with one exception, because of normal vertical displacement. Delineating the basement elevations in this area has implications for addressing geologic and groundwater-resource issues in southeastern Wisconsin. Data from well records constrained basement elevations for the profile parts northwest of the fault on the upthrown block and elevations of the top of the Cambrian Mount Simon Formation on the downthrown block. Only the southernmost profile contained data to constrain the basement elevations on the downthrown block; this profile was used to calibrate density and magnetic susceptibility values for the study. We used basement elevations from the profile models and well records to create a three-dimensional representation of the Precambrian basement surface, which appears complex on both sides of the fault. Comparison of the Precambrian basement surface from this study with a surface based on well record data alone illustrates the benefit of incorporating data from potential fields modeling for the delineation of subsurface structure.

INTRODUCTION

The lithologic units of the Precambrian basement in southeastern Wisconsin consist of granite, slate, and quartzite, which dip gently to the east from the Wisconsin Dome into the Michigan Basin. Mafic intrusions crosscut some of these units. The basement rocks are overlain by Cambrian and Ordovician sandstone and Ordovician and Silurian shale and dolomite. Pleistocene deposits of various thicknesses overlie these rocks. The northeast–trending Waukesha Fault, a prominent geologic structure in the area, has hydrogeologic significance. Jansen and others (2001) determined that the fault appears to be a dividing line for water quality of the sandstone aquifer. They found that levels of total dissolved solids generally increased to the east and with depth, but that no significant changes occurred on the upthrown (northwest) block of the fault; levels of total dissolved solids rose significantly on the downthrown (southeast) block. The fault offset and geometry are not well understood to date.

The only significant surface exposure, at the Waukesha Stone and Lime Quarry in Waukesha, reveals the fault strikes N 40° E with an apparent high-

angle southeast dip and normal displacement (Sverdrup and others, 1997). Sufficient well record data exist for the upthrown block to determine that the depth to the Precambrian basement ranges from approximately 250 to 600 m below ground surface (Smith, 1978; Feinstein and others, 2004); however, depth to basement on the downthrown block of this normal fault is not well established because of the lack of deep water wells. Thwaites (1940, 1957) inferred the depth to the Precambrian basement in this area as greater than 800 m, with maximum vertical displacement of 450 m across the fault. Eaton and others (1999) presented a contour map of the Precambrian basement surface for southeastern Wisconsin that showed approximately 300 m of vertical offset across the fault. Their map includes the depth to Precambrian basement on the downthrown side of the fault based on a single well record (Nicholas and others, 1987).

Geophysical investigations have added other estimates of the subsurface geometry in the area. A gravity survey in Waukesha County by Brukardt (1983) provided the basis for a Bouguer anomaly map over the fault that was interpreted as a high-angle (70°)

¹Department of Geosciences, University of Wisconsin–Parkside, Kenosha, Wisconsin 53141

normal fault dipping to southeast, with vertical displacement of at least 300 m. Moll (1987) performed an investigation of the Waukesha Fault that included 2.5-dimensional models of one north–south and two east–west profiles of ground magnetic data. Model results suggested normal offset of the downthrown fault block, ranging from 900 to 1,200 m, and the fault dip toward the southeast ranged from 20° to vertical. Lahr (1995) predicted depth to Precambrian rock by modeling gravity along two transects crossing the fault using basement density varying from 2.6 g/cm³ to 3.3 g/cm³. For a density of 2.9 g/cm³, depth to basement on the downthrown block was modeled at 905 m (vertical displacement of 500 m) and at 1,140 m (vertical displacement of 680 m), with fault dip to the southeast of 85° to 22° for the southern and northern transects, respectively. Sverdrup and others (1997) noted a steep gravity gradient coincident with the northeast-trending fault; gravity values on the upthrown fault block were approximately 10 mGal higher than values on the downthrown block. Gravity models along two profiles across the fault suggested a maximum vertical offset of 500 to 600 m and fault dip to the southeast of 80° for the southern profile and 10° to 20° for the northern profile. Eaton and others (1999) modeled the elevation of the magnetic basement in southeastern Wisconsin in an attempt to supplement scarce well data and concluded that the non-unique solution presented interpretation problems. Preliminary analysis of the Precambrian basement from aeromagnetic data (Mudrey and others, 2001) indicated this area is underlain by a complex Precambrian structural terrane and suggested the prominent northeast-trending aeromagnetic anomaly that corresponds to the Waukesha Fault defines a basement terrane boundary. Results of a detailed east–west gravity profile across the Waukesha Fault by Baxter and others (2002) yielded model estimates of vertical displacement of the Precambrian basement, ranging from 260 m to greater than 600 m, and fault geometry that varied significantly along strike.

Our study is the first to investigate the Precambrian basement topography adjacent to the Waukesha Fault using coupled (simultaneous) modeling of gravity and magnetic data, which minimizes the non-uniqueness problem inherent in potential fields modeling. In addition, we incorporated lithologic data from a single well record (Nicholas and others, 1987), which provided the depth to Precambrian basement on the downthrown side of the fault. The extensive lithologic data from the Wisconsin Geological and Natural History Survey wisLITH database (2004) provided constraint on the subsurface structure.

METHODS

We used existing gravity, aeromagnetic, elevation, density, magnetic susceptibility, and well record data to construct models along seven northwest–southeast profiles spaced 10 km apart across the Waukesha Fault and one north–south profile that serves as a “tie line” for the other profiles (fig. 1B). The gravity and aeromagnetic data are from compilations by the U.S. Geological Survey (fig. 1C and 1D; Daniels and Snyder, 2002) for the entire state of Wisconsin. They reduced the observed gravity values in relation to the IGSN-71 datum to the Bouguer anomaly using the 1967 gravity formula and a reduction density of 2.67 g/cm³; they then converted the data to a 1 km grid using minimum curvature techniques. Daniels and Snyder (2002) compiled the Wisconsin aeromagnetic map from 26 surveys with relative uniformity of flight-line spacing (0.5 mi or less) and processed the data to simulate flight altitude of 1,000 ft (305 m) above ground surface. They converted the data to a 250 m grid using a minimum curvature algorithm; we downloaded their grids and sampled along the study profiles at 500 m intervals.

We obtained ground-surface elevations along profiles at 500 m intervals from U.S. Geological Survey 7.5-minute series topographic maps. Well record data were obtained from the Wisconsin Geological and Natural History Survey (via the U.S. Geological Survey) as a digital database that was compiled for constructing the regional groundwater flow model of southeastern Wisconsin (Feinstein and others, 2004). Well records from a total of 41 wells that reach the Precambrian basement or the overlying Cambrian Mount Simon Formation were used in this study (table 1; fig. 1B) for vertical control of model blocks. Wells were projected perpendicular to the nearest profile. The log from a single U.S. Geological Survey test well in Zion, Illinois (Nicholas and others, 1987), includes the only depth to the Precambrian basement on the downthrown block of the Waukesha Fault, providing constraint on the subsurface structure along the southernmost profile (profile A–A'). Thus, the model for profile A–A' was constructed first to select appropriate density and magnetic susceptibility information for the study area. Initial density and magnetic susceptibility data were obtained from a state compilation (Dutch and others, 1994) and a number of local studies (Brukardt, 1983; Moll, 1987; Lahr, 1995; Sverdrup and others, 1997). Model block density and magnetic susceptibility values were adjusted to obtain the best fits between observed and calculated gravity and aeromagnetic anomalies along profile A–A' because the depth to the Precambrian basement is known on both sides of the

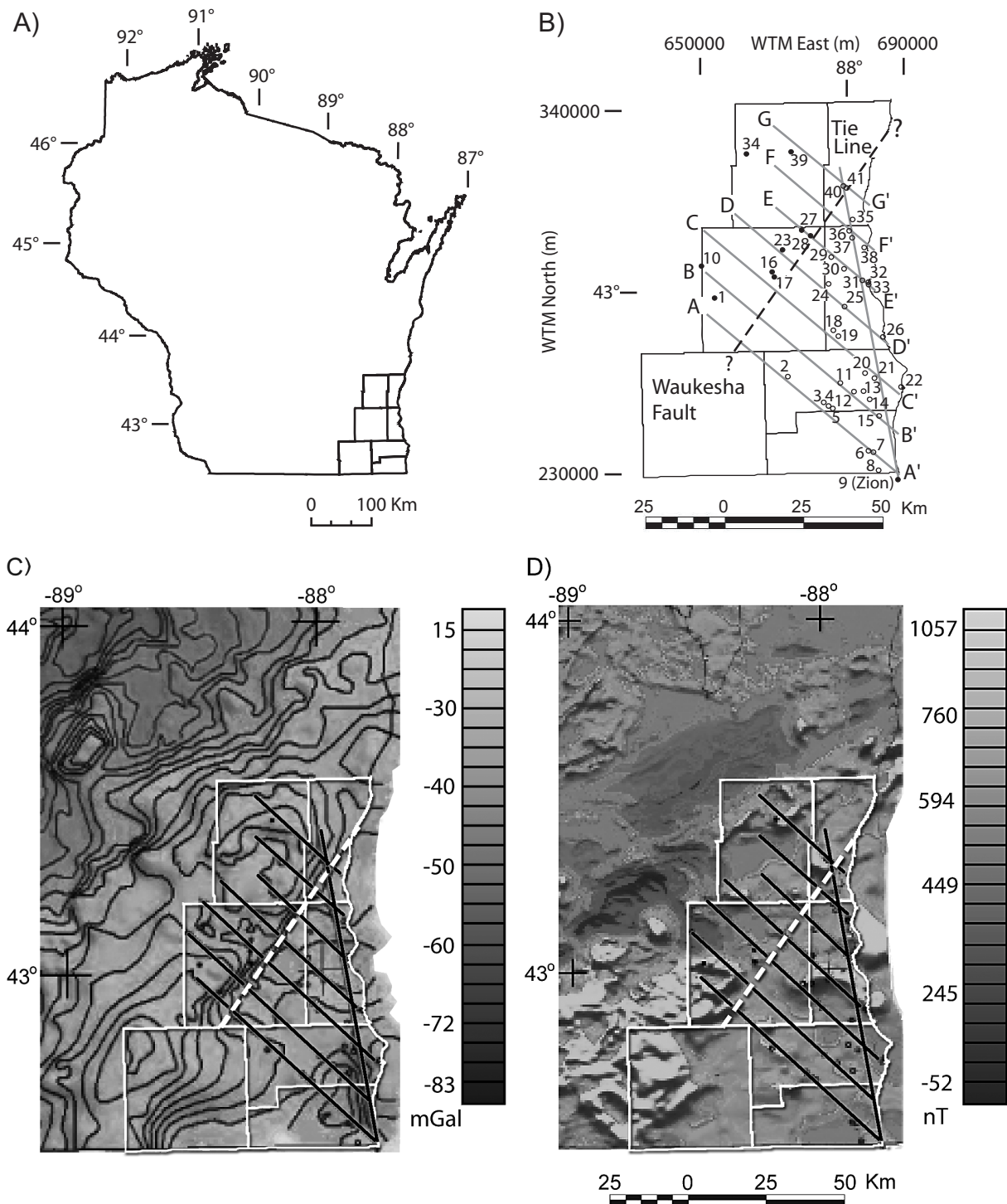


Figure 1. **A.** Seven-county study area location in southeast Wisconsin. **B.** Model profile lines and well locations used for vertical control; solid dots indicate wells that reach Precambrian basement, and open circles indicate wells that reach Cambrian Mount Simon Formation. Dashed line is Waukesha Fault. See table 1 for data associated with numbered locations. Complete Bouguer anomaly map (**C**) and residual aeromagnetic map (**D**) show data used for model profiles along with county boundaries, profile lines, and well locations. Bouguer anomaly and residual aeromagnetic maps were modified from Daniels and Snyder (2002).

Table 1. Well data (from Wisconsin Geological and Natural History Survey, 2004) used for vertical control in 2.75-dimensional forward models. NA: no data available.

Number on fig. 1	Profile line	wiscLITH well record	WTM-E ¹ (m)	WTM-N ² (m)	Surface elevation (m above mean sea level)	Glacial deposits bottom depth (m)	Mount Si-mon Fm. top depth (m)	Basement top depth (m)
1	A-A'	680862	644686	283489	263	96	223	331
2	A-A'	520351	666144	256748	252	30	334	
3	A-A'	520066	677062	248743	260	79	349	
4	A-A'	520376	678789	247635	248	49	343	
5	A-A'	520349	680091	246803	241	40	340	
6	A-A'	300274	691246	233692	223	52	401	
7	A-A'	300012	692748	233254	210	44	389	
8	A-A'	300301	694479	227429	220	54	438	
9	A-A'	Zion	698600	227300	180	36	500	1,047
10	B-B'	680020	640886	293445	269	52	223	235
11	B-B'	520354	682491	254858	217	40	352	
12	B-B'	520359	686799	252190	242	32	395	
13	B-B'	520017	692035	249808	220	48	453	
14	B-B'	520005	691689	249752	223	43	448	
15	B-B'	300006	694629	244471	195	30	366	
16	C-C'	680028	659494	289673	274	15	276	363
17	C-C'	680865	660658	287722	272	18	250	346
18	C-C'	410548	680300	271306	241	42	409	
19	C-C'	410400	681872	269383	233	42	373	
20	C-C'	520053	690244	257953	229	33	381	
21	C-C'	520350	693131	256262	220	40	355	
22	C-C'	520023	701819	253473	181	21	479	
23	D-D'	680180	664463	297673	287	9	287	393
24	D-D'	410321	678828	285770	223	23	314	
25	D-D'	410440	683864	278631	242	58	345	
26	D-D'	410332	695943	269224	206	58	404	
27	E-E'	670909	670428	304391	266	8	332	419
28	E-E'	680004	673081	302714	268	8	297	415
29	E-E'	410482	679709	293899	223	41	335	
30	E-E'	410286	683629	290350	238	46	415	
31	E-E'	410057	689358	286899	179	67	393	
32	E-E'	410052	690980	286141	178	58	372	
33	E-E'	410299	691189	285441	178	63	369	
34	F-F'	670920	654139	328150	303	17	NA	218
35	F-F'	460073	686386	305867	204	58	387	
36	F-F'	410431	685240	302265	205	163	384	
37	F-F'	410007	686259	300074	212	30	383	
38	F-F'	410341	689914	296861	196	56	395	
39	G-G'	670009	667386	325522	277	58	NA	284
40	G-G'	460016	683534	315985	242	4	343 (E) ³	
41	G-G'	460018	684347	315744	239	13	343 (E) ³	

¹ Wisconsin Transverse Mercator East

³ Wells only reach the top of the Eau Claire

² Wisconsin Transverse Mercator North

fault. A summary of this study's and published density and magnetic susceptibility data is given in table 2.

Coupled 2.75-dimensional forward modeling of gravity and aeromagnetic data was performed using the commercially available modeling program

GM-Sys[®] (by Northwest Geophysical Associates) based on Talwani and others (1959) and Talwani and Heirtzler (1964). Model block polygons were constructed to represent the subsurface geologic units along each profile. Model block strike lengths were

extended 10 km perpendicular to the profile. Density and magnetic properties within a given model block were assumed constant. Iterative adjustments to geologic block configuration, density, and magnetic properties were made to minimize the root mean square error (RMSE) between observed and calculated gravity and aeromagnetic anomalies. Because GM-Sys calculates the modeled gravity and aeromagnetic anomalies simultaneously in real time, the modeler endeavors to achieve the smallest RMSE possible for both techniques by adjusting block shapes after settling on acceptable density and magnetic properties.

Experience from previous coupled modeling of aeromagnetic and gravity data (Skalbeck, 2001; Skalbeck and others, 2005) suggested that models were judged acceptable when the percentage of RMSE (%RMSE [RMSE/anomaly range]) was below 5 percent for gravity and below 10 percent for aeromagnetic data. A summary of model best-fit statistics for each profile is given in table 3.

RESULTS AND DISCUSSION

2.75-dimensional models of selected profiles

Some mafic bodies that were not documented in the

well record data used in this study were included in the geologic model for the profiles to match observed aeromagnetic anomalies. Initial models were constructed without these bodies, but no reasonable combination of physical properties and model configuration could be found to simultaneously match gravity and aeromagnetic data. Moll (1987) included subsurface mafic bodies to yield reasonable model anomalies for profiles across the Waukesha Fault, and Sverdrup and others (1997) had included gabbro in models to account for gravity and magnetic highs attributed to mafic rock at depth. We found that mafic bodies were needed in this study to achieve acceptable fit between model and observed anomalies.

Due to the higher density and magnetic susceptibility values and to the greater volume of the model blocks representing Precambrian basement and mafic bodies in relation to overlying sedimentary and glacial deposits, the crystalline rocks contribute most of the model anomalies. Qualitative sensitivity analysis indicated that the Precambrian basement and mafic bodies significantly influence the gravity and aeromagnetic anomalies. Adjustments in physical property values and model configuration of the crystalline model

Table 2. Density and magnetic susceptibility data from previous work and this study; cgs: centimeter-gram-second; NA: not available or applicable.

Geologic unit	Model symbol	Density (g/cm ³)					Magnetic susceptibility (x 10 ⁻⁶ cgs)		
		Brukardt (1983)	Dutch and others (1994)	Lahr (1995)	Sverdrup and others (1997)	This study	Dutch (1994)	Moll ¹ (1987)	This study
Lake Michigan		NA	NA	NA	1.00	1.00	NA	NA	0
Glacial		1.80	1.80	1.80	1.80	1.80	NA	NA	0
Silurian		2.70	2.29 – 2.86	2.77	2.67	2.77	49–76	0	75
Maquoketa		2.70	2.54 – 2.74	2.63	NA	2.63	79–108	0	100
Sinnipee		NA	2.51 – 2.84	2.72	NA	2.72	80–113	0	100
St. Peter		2.67	2.19 – 2.66	2.33	2.60	2.45	32–126	0	100
Trempealeau		2.67	2.82	2.45	NA	2.82	16–125	0	100
Wonewoc		2.67	NA	NA	NA	2.67	NA	0	100
Eau Claire		2.67	2.67	2.45	NA	2.67	16 – 125	0	100
Mount Simon		2.67	2.58	2.45	2.60	2.58	16–125	0	100
Precambrian basement		3.00	2.63–2.74	2.60–3.30	2.69	2.77 – 3.02	44–3489	200	1000
Mafic bodies ²		NA	NA	2.71–3.04	3.00	3.00 – 3.05	91 – 2713	6000	3000
Fault zone		NA	NA	NA	NA	2.22 – 2.82	NA	NA	100–1000

¹ Moll (1987) modeled sedimentary formations as a single unit.

² Remanent magnetism properties include magnetic intensity 2000 x 10⁻⁶cgs

Table 3. Model best fit statistics for Waukesha Fault area, southeastern Wisconsin. RMSE: root mean square error; %RMSE: RMSE/anomaly; mGal: milligal; nT: nanoTesla.

Profile	Complete Bouguer residual gravity				Residual aeromagnetism			
	Range (mGal)	Anomaly (mGal)	RMSE (mGal)	%RMSE	Range (nT)	Anomaly (nT)	RMSE (nT)	%RMSE
Line A–A'	-31.9 – -52.1	20.2	0.69	3.4	354–1742.8	1389	127.6	9.2
Line B–B'	-32.8 – -49.7	16.9	0.36	2.1	-94–1675	1769	106.7	6.0
Line C–C'	-39.3 – -49.1	9.8	0.23	2.3	71–951	880	55.5	6.3
Line D–D'	-37.0 – -48.1	11.1	0.52	4.7	264–1229	965	94.1	9.8
Line E–E'	-35.5 – -50.5	15.0	0.49	3.3	445–1341	896	73.0	8.1
Line F–F'	-32.5 – -44.9	12.4	0.42	3.4	338–1040	702	54.8	7.8
Line G–G'	-31.8 – -45.4	13.6	0.33	2.4	426–1141	715	69.5	9.7
Tie line	-35.6 – -50.3	14.7	0.39	2.7	391–1107.2	716	67.8	9.5
Target value for %RMSE				5.0	10.0			

blocks have significantly greater effect on model anomalies than changes with the sedimentary and glacial deposits model blocks.

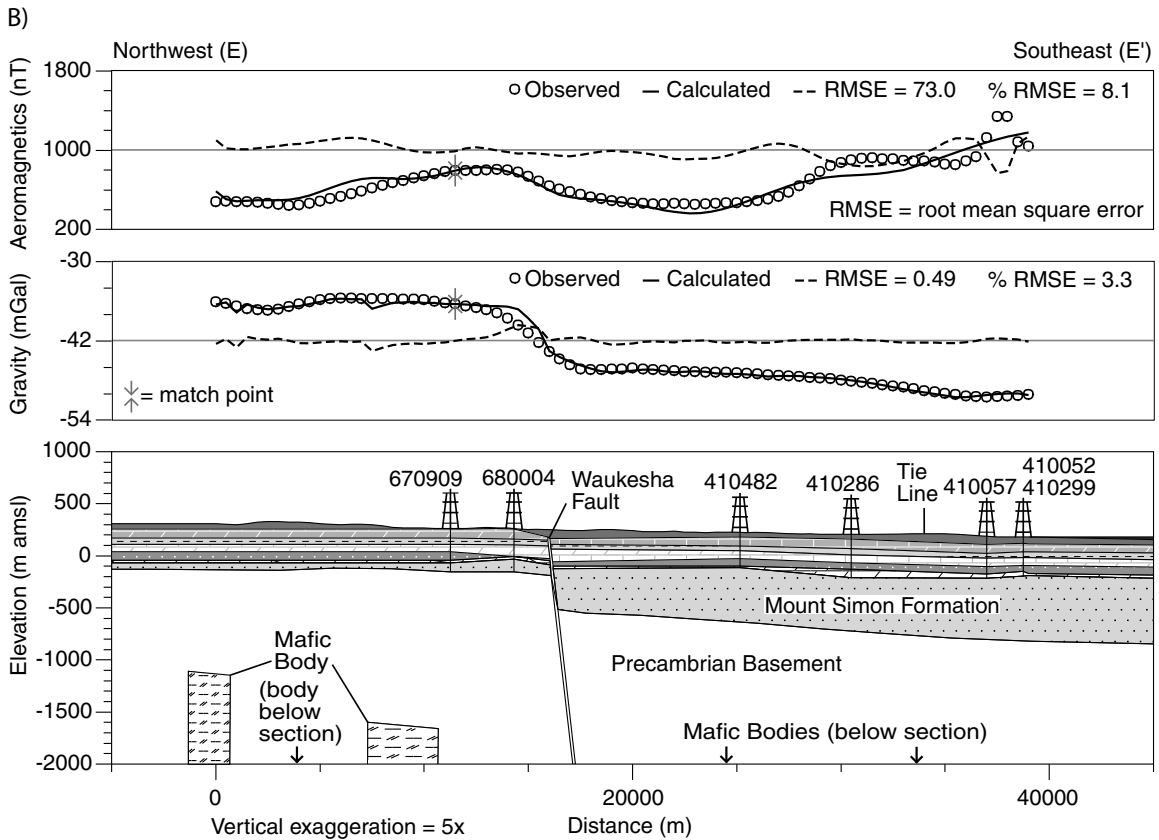
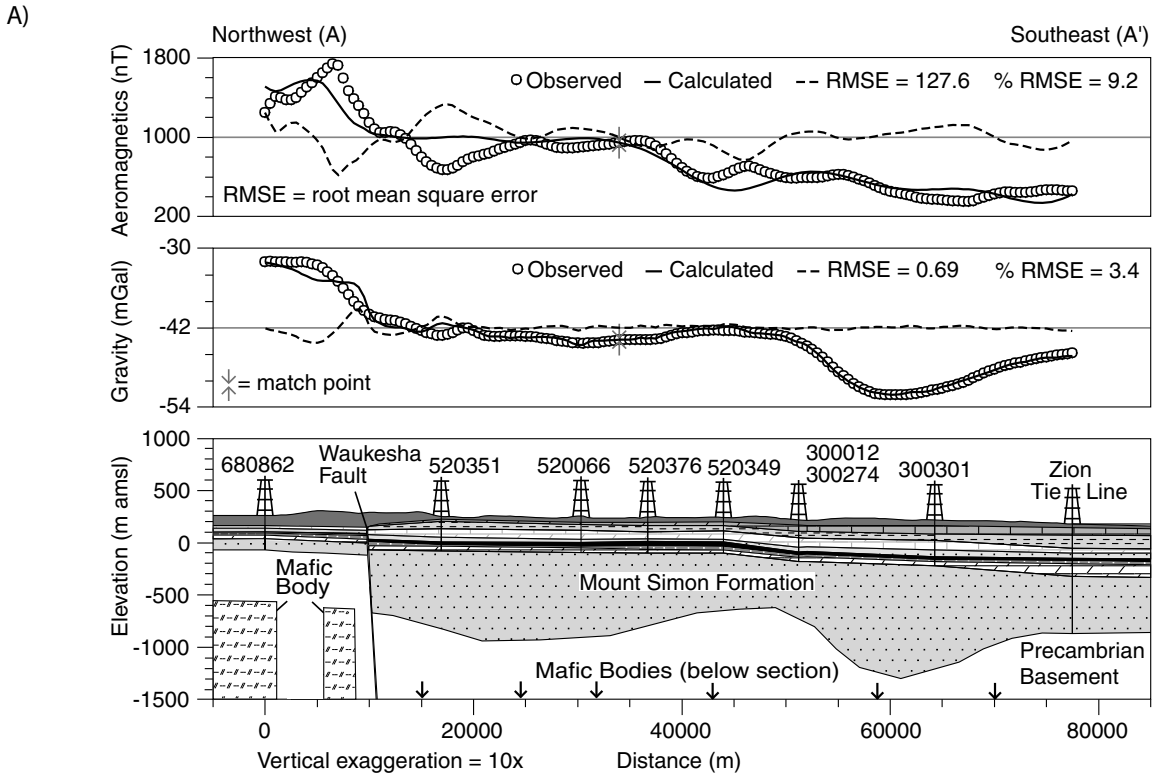
Figure 2 shows two of the eight modeled profiles (profiles A–A' and E–E'). Note the difference in scale and vertical exaggeration between the two profiles. Profile A–A' (fig. 2A) crosses the Waukesha Fault at the southernmost extent of the study area and represents the best constrained model. Good model fits for gravity (%RMSE = 3.4) and aeromagnetic data (%RMSE = 9.2) were obtained for this profile. Excellent vertical geologic control data were provided from nine wells, including the only well (Zion) within the study area that reaches the Precambrian basement on the downthrown (southeast) block of the fault. The Waukesha Fault is represented as a 100 m wide zone that dips 60° toward the southeast. The part of the fault adjacent to sedimentary units has a density of 2.22 g/cm³ and magnetic susceptibility of 100 x 10⁻⁶ centimeter-gram-second (cgs); the part ad-

acent to Precambrian basement units has a density of 2.82 g/cm³ and magnetic susceptibility of 1,000 x 10⁻⁶ cgs (table 2). Modeling results from Skalbeck (2001) suggested that rocks within major fault zones may have altered density and magnetic properties relative to the host rocks. This model configuration of the fault is maintained consistently throughout the study area. Lake Michigan does not appear on either of the profiles, but was modeled using density of 1.0 g/cm³ and magnetic susceptibility of 0 x 10⁻⁶ cgs. The density and susceptibility values for glacial, sedimentary, and Precambrian basement and mafic intrusive units are also provided in table 2.

Depth control on both blocks of the fault is good for the glacial unit through the Eau Claire Formation. The Mount Simon Formation is well constrained on the upthrown fault block, but the bottom of this unit (top of Precambrian basement) is estimated from the model results on the downthrown block. Depth to the Precambrian

► **Figure 2. A.** Profile A–A', showing 2.75-dimensional model for southern extent of study area. **B.** Profile E–E', showing 2.75-dimensional model for northern part of study area. The upper section of each profile shows the aeromagnetic data; the center section, the gravity data. In each section, open circles represent the observed data; the solid line indicates the model-calculated anomaly. The dashed line represents the deviation between the observed and calculated data, and distance from the horizontal gray line indicates greater error. Cumulative error of the model is indicated by the RMSE value. The lower section of each profile illustrates the geologic model; the horizontal distance is relative to the northwest end of the profile, and elevation is above or below mean sea level. Geologic unit categories were modified from the groundwater model layers used by Feinstein and others (2004). nT: nanoTesla.





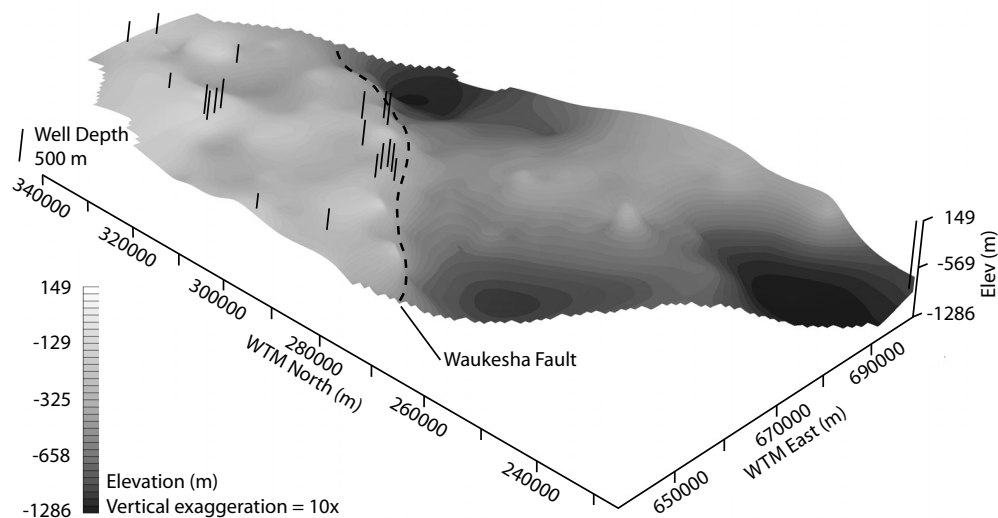


Figure 3. Precambrian basement elevation surface obtained from model profile and well record elevations. View from southwest ($S 45^{\circ}E$) at 30° above horizon. Wells represented by vertical bars; length of bars indicates depth to basement. Elevations are above or below mean sea level.

an basement on the upthrown block was documented at 331 m below ground surface (bgs) in wisLITH well record 680862 and was modeled at approximately 890 m on the downthrown block adjacent to the fault. This model yielded a normal vertical displacement of approximately 560 m; most of the displacement was within the Cambrian Mount Simon Formation. Well data indicated vertical displacement of 120 to 130 m for the Cambrian Eau Claire, Wonewoc, and Trempealeau Formations and 30 m for the Ordovician Sinnipee and St. Peter Formations. The maximum depth to basement within the study area was modeled at 1,520 m bgs along this profile near wisLITH well 300301. The model indicates a significant depression in the basement surface; this area has local relief of 470 m, in contrast to the documented depth at the Zion well and of 660 m for the modeled ridge beneath wisLITH well 300274. A second depression between wisLITH wells 520351 and 520066, modeled with a maximum depth of 1,200 m bgs, shows relief of 270 to 315 m for the fault and model ridge, respectively. Two mafic bodies with densities of 3.01 g/cm^3 , magnetic susceptibility of $3,000 \times 10^{-6} \text{ cgs}$, and remanent magnetism with reverse polarity (declination = 270° , inclination = -45° , intensity of $2,000 \times 10^{-6} \text{ cgs}$) were modeled on the upthrown fault block at depths of 900 and 1,000 m bgs. Six mafic bodies on the downthrown fault block (not shown in fig. 2A because of the depth) were modeled at depths of 4,000 to 5,000 m with the same magnetic properties, but with densities of 3.00 to 3.03 g/cm^3 .

Profile E–E' (fig. 2B) crosses the northern part of the Waukesha Fault, where a good fit for gravity (%RMSE = 3.3) and for aeromagnetic data (%RMSE = 8.1) was obtained for this model. Data from seven wells provided vertical geologic control for the profile. Two wells on the upthrown fault block document the depth to Precambrian basement at 415 and 419 m bgs, but the four wells on the downthrown fault block do not reach the basement. Model results yielded normal vertical displacement of 340 m of the Precambrian basement. Unlike the undulating surface modeled in profile A–A', the modeled basement surface in profile E–E' gently slopes to the east. The depth to basement adjacent to the fault is modeled at 765 m bgs and at 1,000 m bgs beneath wisLITH well 410299, which is approximately 20,000 m south-east of the fault. Two mafic bodies with densities of 3.00 and 3.01 g/cm^3 , magnetic susceptibility of $3,000 \times 10^{-6} \text{ cgs}$, and reverse polarity remanent magnetism (declination = 270° , inclination = -45° , intensity of $2,000 \times 10^{-6} \text{ cgs}$) were modeled on the upthrown fault block at depths of 1,400 and 1,900 m bgs. Another mafic body on the upthrown fault block was modeled at a depth of 3,000 m (not shown in fig. 3B because of the depth) with the same magnetic properties, but with density of 3.02 g/cm^3 . On the downthrown block, two mafic bodies were modeled at depths of 3,000 and 4,000 m (not shown in fig. 3B because of the depth) with the same magnetic properties, but with densities of 3.01 and 3.02 g/cm^3 .

Table 4. Well data used for Precambrian basement elevation surface.

wiscLITH well record	WTM-E ¹ (m)	WTM-N ² (m)	Surface elevation (m above mean sea level)	Basement top depth (m)	Basement top elevation (m above or below mean sea level)
Wells used for vertical control on profiles and for basement surface elevation					
680862	644686	283489	263	331	-68
Zion	698600	227300	180	1047	-867
680020	640886	293445	269	235	34
680028	659494	289673	274	363	-89
680865	660658	287722	272	346	-74
680180	664463	297673	287	393	-106
670909	670428	304391	266	419	-153
680004	673081	302714	268	415	-147
670920	654139	328150	303	218	85
670009	667386	325522	277	284	-7
Wells used for basement surface elevation					
680027	661765	291564	259	401	-142
680723	663014	290982	324	431	-106
680758	671878	300936	344	489	-145
680888	664846	298300	364	467	-102
681233	662342	290038	336	438	-102
670006	653879	317482	473	390	84
670008	663293	340505	292	318	-25
670012	651668	316710	594	450	144
670013	652244	317752	597	453	145
670034	655188	317877	604	455	149

¹ Wisconsin Transverse Mercator East

² Wisconsin Transverse Mercator North

Precambrian basement topography

Figure 3 illustrates the model top of the Precambrian basement elevation obtained from the 2.75-dimensional coupled model of gravity and aeromagnetic elevations along eight profiles, extracted at 500 m intervals, and elevations from 20 wells (table 4). The top of basement elevations ranges from 149 m above mean sea level in the northern part of the study area (Wisconsin Transverse Mercator [WTM] North 320000 m, WTM East 650000 m) to 1,286 m below mean sea level in the southeast part of the study area (WTM North 240000 m, WTM East 690000 m). We interpreted the prominent southwest–northeast trending drop in basement surface elevation as the Waukesha Fault scarp dipping steeply toward the southeast. The model suggests that the trend of the scarp is primarily linear with some minor curvature along strike. The model basement surface shows some moderate undulations on the upthrown block and major undulations on the downthrown block. An elevated area

was modeled on the downthrown block centered near WTM North 250000 m and WTM East 660000 m. This may represent a small upthrown fault sub-block within the primary downthrown block or may be a result of deep erosion of two nearly parallel valleys.

For comparison, figure 4A shows the Precambrian basement elevation surface from this study as a contour map; figure 4B is the contour map from Eaton and others (1999) based on well record data. Delineation of the Waukesha Fault and the surface of the upthrown (northwest) fault block are similar. The lack of detail for the downthrown (southeast) fault block surface is obvious in the Eaton and others (1999) map because the surface is based on a single elevation point from the Zion well. Our map illustrates the additional resolution of the Precambrian basement surface for the downthrown block that has been added on the basis of the coupled modeling of gravity and aeromagnetic data. Because the Precambrian basement serves as the base of the overlying

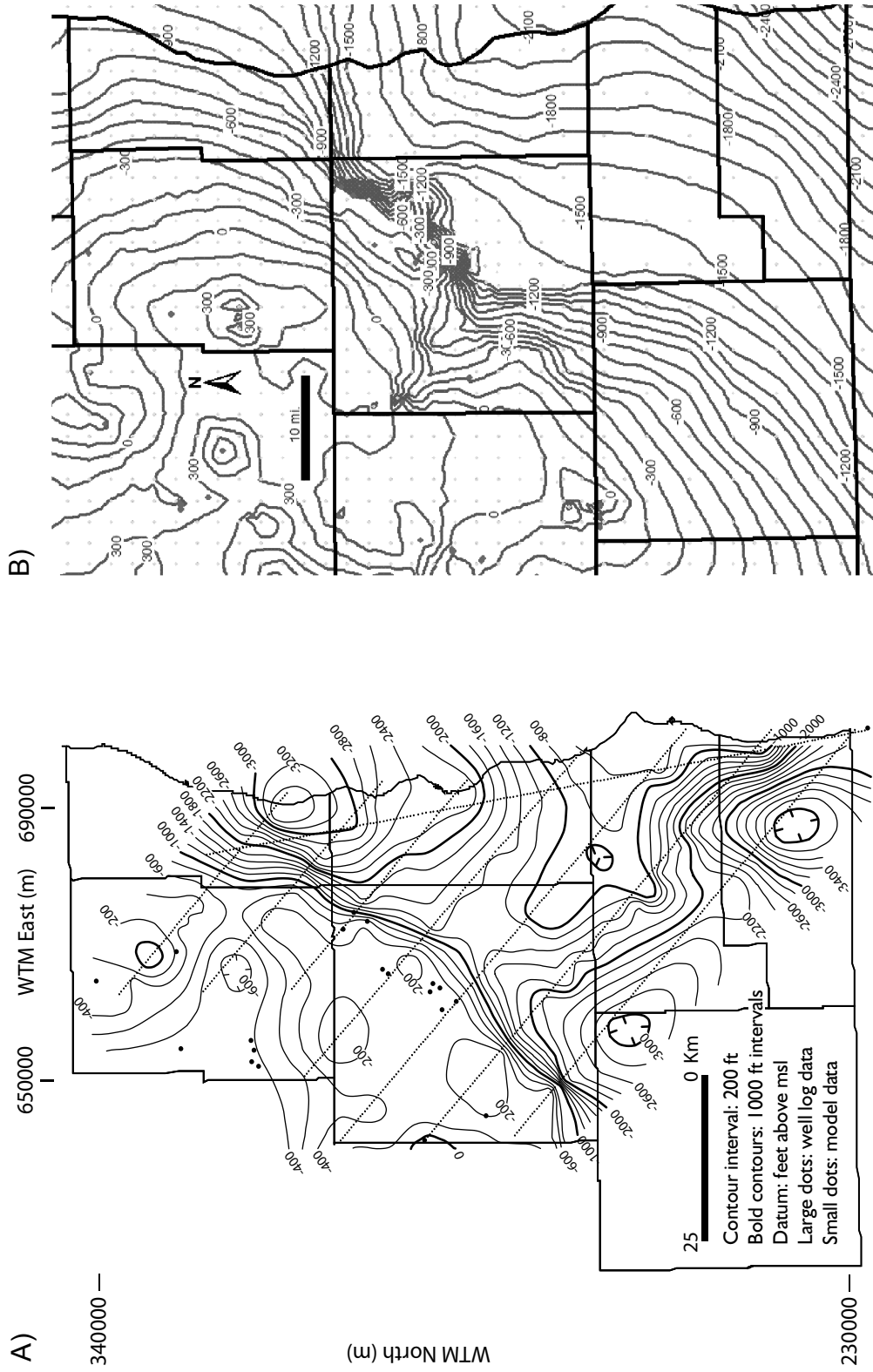


Figure 4. Contour maps of Precambrian basement elevation surface from (A) this study and (B) modified from Eaton and others (1999). (Elevations on our map [A] are shown in feet instead of meters to facilitate comparison with the previously published map [B] and are above or below mean sea level.)

Mount Simon Formation, which is the lower part of an important sandstone aquifer system in southeast Wisconsin, the added detail of the basement surface from this study could provide critical information for future study of this system.

CONCLUSIONS

The Waukesha Fault was modeled in this study as a high-angle normal fault dipping to the southeast; however, the gravity error associated with the location of the fault suggests that a shallower dip angle is possible. Model topography of the Precambrian basement elevation surface appears undulated on both sides of the fault, with more relief on the downthrown fault block. Reasonable estimates of the elevations of the top of the basement southeast of the fault have been obtained from this study. The well record data used in this study support the model results of Sverdrup and others (1997), showing vertical displacement of 30 m in Silurian rocks. Our model results for maximum vertical displacement of the Precambrian basement of 560 m along profile A–A' are also in close agreement with Sverdrup and others (1997) results of between 500 and 600 m of vertical displacement. Although the Waukesha Fault was modeled as a geologic unit with constant dip of 60° for each of the profile models, the Precambrian basement model topography gradient on the downthrown fault block along some profile models appears to gradually shallow. Thus, the model structure could alternatively be interpreted as a listric-type fault.

Coupled modeling of gravity and aeromagnetic data provides non-unique solutions because numerous different model geometries and assigned density and magnetic properties can produce fields that closely match the observed anomalies. For example, decreasing the model's density contrast between sedimentary rock and crystalline basement, and increasing the depth to basement could produce a computed field similar to the previous configuration. Input of published density and magnetic susceptibility data and subsurface geology from well records greatly constrains possible interpretations of the subsurface structure in southeast Wisconsin; however, other interpretations of the structure do exist.

Results from this study provide an excellent data set for the Precambrian basement configuration. Researchers working on groundwater-management issues (such as arsenic contamination, excessive draw-down, increasing salinity, and so forth) in southeast Wisconsin may find the results of this study useful. In addition, these results may be of interest to research-

ers working on structural and tectonic models for the region. Coupled modeling of gravity and aeromagnetic data can be applied to other research topics across Wisconsin. For example, researchers have long known of the undulating nature of the top of Precambrian basement in the Fond du Lac area from well records, but have not been able to construct a reasonable three-dimensional model of this surface due to the paucity of point data. Because of the excellent statewide compilation of gravity and aeromagnetic data for Wisconsin, a well constrained three-dimensional model of Precambrian basement topography is obtainable not only for the Fond du Lac area, but for almost anywhere in the state.

ACKNOWLEDGMENTS

Funding was provided by the Wisconsin Groundwater Research Program through the University of Wisconsin Water Resources Institute, grant number R/UW-HDG-007 (WR03R003). We give special thanks to David J. Hart of the Wisconsin Geological and Natural History for providing the suggestion to pursue the study and Daniel T. Feinstein of the U.S. Geological Survey for providing the well record database and many helpful discussions. Thanks also to undergraduate students Jamie Lambert, Adrian Koski, and Stephan Kurdas for their important contributions. Lastly, we appreciate the helpful comments and suggested changes of the reviewers William Kean, David J. Hart, David L. LePain, and Thomas J. Evans.

REFERENCES

- Baxter, T.A., Boscov-Parfitt, S., Breitzmann, S.S., Schmitz, P.J., Shultis, A.I., Temme, T.W., Lahr, M.J., Sverdrup, K.A., and Cronin, V.S., 2002, Detailed gravity profile across the Waukesha Fault, SE Wisconsin: Final Program of North-Central Section (36th) and Southeastern Section (51st), Geological Society of America Joint Annual Meeting, April 3–5, 2002. Available online at <http://gsa.confex.com/gsa/2002NC/finalprogram/abstract_31558.htm>.
- Brukardt, S.A., 1983, Gravity survey of Waukesha County: Master's thesis, University of Wisconsin–Milwaukee, 131 p.
- Daniels, D.L., and Snyder S.L., 2002, Wisconsin aeromagnetic and gravity maps and data: A Web site for distribution of data: U.S. Geological Survey Open-File Report 02-493. Available online at <<http://pubs.usgs.gov/of/2002/of02-493/>>.

- Dutch, S.I., Boyle, R.C., Jones, S.K., and Vandebush, S.M., 1994, Density and magnetic susceptibility of Wisconsin rock: *Geoscience Wisconsin*, v. 15, p. 1–18.
- Eaton, T.T., Bradbury, K.R., and Evans, T.J., 1999, Characterization of the hydrostratigraphy of the deep sandstone aquifer in southeastern Wisconsin: Wisconsin Geological and Natural History Survey Open-File Report 1999-02, 30 p.
- Feinstein, D.T., Hart, D.J., Eaton, T.T., Krohelski, J.T., and Bradbury, K.R., 2004, Simulation of regional groundwater flow in southeastern Wisconsin: Wisconsin Geological and Natural History Survey Open-File Report 2004-01, 134 p.
- Jansen, J., Taylor, R.W., and Powell, T., 2001, A regional TEM survey to map saline water in the Cambrian–Ordovician sandstone aquifer of southeastern Wisconsin in Proceedings of The Symposium on the Application of Geophysics to Engineering and Environmental Problems CD-ROM: Environmental and Engineering Geophysical Society, file GW1_3.
- Lahr, M.J., 1995, Detailed gravity profiles of the Waukesha Fault, southeastern Wisconsin: Master's thesis, University of Wisconsin–Milwaukee, 405 p.
- Moll, J.G., 1987, A magnetic investigation of the Waukesha Fault, Wisconsin: Master's thesis, University of Wisconsin–Milwaukee, 94 p.
- Mudrey, M.G., Jr., Brown, B.A., and Daniels, D.L., 2001, Preliminary analysis of aeromagnetic data in southern Wisconsin: The role of Precambrian basement in Paleozoic evolution: Wisconsin Geological and Natural History Open-File Report 2001-03, 3 p. with 1 CD-ROM.
- Nicholas, J.R., Sherrill, M.G., and Young, H.L., 1987, Hydrogeology of the Cambrian–Ordovician aquifer system at a test well in northeastern Illinois: U.S. Geological Survey Water Resources Investigations Open-File Report 84-4165, 30 p.
- Schaper, D.J., and Kean, W.F., 1999, Multiple magnetic directions in a Proterozoic dike near Waterloo, Wisconsin [abs]: American Geophysical Union, *EOS Transactions*, v. 80, no. 46, p. F289.
- Skalbeck, J.D., 2001, Geophysical modeling and geochemical analysis for hydrogeologic assessment of the Steamboat Hills area, Nevada: Ph.D. dissertation, University of Nevada, Reno, 213 p.
- Skalbeck, J.D., Karlin, R.E., Shevenell, L., and Widmer, M.C., 2005, Gravity and aeromagnetic modeling of alluvial basins in the southern Truckee Meadows adjacent to the Steamboat Hills geothermal area, Washoe County, Nevada: *Geophysics*, v. 70, no. 3, p. 1–9.
- Smith, E.I., 1978, Introduction to Precambrian rocks of south-central Wisconsin: *Geoscience Wisconsin*, v. 2, p. 1–14.
- Sverdrup, K.A., Kean, W.F., Herb, S., Burkardt, S.A., and Friedel, S.J., 1997, Gravity signature of the Waukesha Fault in southeastern Wisconsin: *Geoscience Wisconsin*, v. 16, p. 47–54.
- Talwani, M., and Heirtzler, J.R., 1964, Computations of magnetic anomalies caused by two-dimensional bodies of arbitrary shape, in Parks, G.A., ed., Computers in the mineral industry, Part I: *Stanford University Publications in Geological Sciences*, v. 9, p. 464–480.
- Talwani, M., Worzel, J.L., and Landisman, M., 1959, Rapid gravity computations for two-dimensional bodies with application to the Mendocino Submarine fracture zone: *Journal of Geophysical Research*, v. 64, p. 49–59.
- Thwaites, F.T., 1940, Buried pre-Cambrian of Wisconsin: *Wisconsin Academy of Sciences, Arts and Letters Transactions*, v. 32, p. 233–242.
- Thwaites, F.T., 1957, Map of buried pre-Cambrian of Wisconsin: Wisconsin Geological and Natural History Survey, 1 sheet, scale 1:2,500,000.
- Wisconsin Geological and Natural History Survey, 2004, *wiscLITH*: A digital lithologic and stratigraphic database of Wisconsin geology: Wisconsin Geological and Natural History Survey Open-File Report 2003-05, version 2.0, 1 CD-ROM.